**Springer Theses**
Recognizing Outstanding Ph.D. Research

Martin Lorenz Stein

# NMR-Bioassay Guided Isolation of the Natural 20S Proteasome Inhibitors from Photorhabdus Luminescens

## A Novel NMR-Tool for Natural Product Detection

Springer

# Springer Theses

Recognizing Outstanding Ph.D. Research

For further volumes:
http://www.springer.com/series/8790

## Aims and Scope

The series "Springer Theses" brings together a selection of the very best Ph.D. theses from around the world and across the physical sciences. Nominated and endorsed by two recognized specialists, each published volume has been selected for its scientific excellence and the high impact of its contents for the pertinent field of research. For greater accessibility to non-specialists, the published versions include an extended introduction, as well as a foreword by the student's supervisor explaining the special relevance of the work for the field. As a whole, the series will provide a valuable resource both for newcomers to the research fields described, and for other scientists seeking detailed background information on special questions. Finally, it provides an accredited documentation of the valuable contributions made by today's younger generation of scientists.

## Theses are accepted into the series by invited nomination only and must fulfill all of the following criteria

- They must be written in good English.
- The topic should fall within the confines of Chemistry, Physics, Earth Sciences, Engineering and related interdisciplinary fields such as Materials, Nanoscience, Chemical Engineering, Complex Systems and Biophysics.
- The work reported in the thesis must represent a significant scientific advance.
- If the thesis includes previously published material, permission to reproduce this must be gained from the respective copyright holder.
- They must have been examined and passed during the 12 months prior to nomination.
- Each thesis should include a foreword by the supervisor outlining the significance of its content.
- The theses should have a clearly defined structure including an introduction accessible to scientists not expert in that particular field.

Martin Lorenz Stein

# NMR-Bioassay Guided Isolation of the Natural 20S Proteasome Inhibitors from Photorhabdus Luminescens

## A Novel NMR-Tool for Natural Product Detection

Doctoral Thesis accepted by
Technical University of Munich, Germany

Springer

*Author*
Dr. Martin Lorenz Stein
Faculty of Chemistry
Department of Biochemistry
Technical University of Munich
Garching
Germany

*Supervisor*
Prof. Michael Groll
Department of Biochemistry
Center for Integrated Protein Science at the Department of Chemistry
Technical University of Munich
Garching
Germany

ISSN 2190-5053 ISSN 2190-5061 (electronic)
ISBN 978-3-319-07913-4 ISBN 978-3-319-07914-1 (eBook)
DOI 10.1007/978-3-319-07914-1
Springer Cham Heidelberg New York Dordrecht London

Library of Congress Control Number: 2014941117

© Springer International Publishing Switzerland 2014
This work is subject to copyright. All rights are reserved by the Publisher, whether the whole or part of the material is concerned, specifically the rights of translation, reprinting, reuse of illustrations, recitation, broadcasting, reproduction on microfilms or in any other physical way, and transmission or information storage and retrieval, electronic adaptation, computer software, or by similar or dissimilar methodology now known or hereafter developed. Exempted from this legal reservation are brief excerpts in connection with reviews or scholarly analysis or material supplied specifically for the purpose of being entered and executed on a computer system, for exclusive use by the purchaser of the work. Duplication of this publication or parts thereof is permitted only under the provisions of the Copyright Law of the Publisher's location, in its current version, and permission for use must always be obtained from Springer. Permissions for use may be obtained through RightsLink at the Copyright Clearance Center. Violations are liable to prosecution under the respective Copyright Law.
The use of general descriptive names, registered names, trademarks, service marks, etc. in this publication does not imply, even in the absence of a specific statement, that such names are exempt from the relevant protective laws and regulations and therefore free for general use.
While the advice and information in this book are believed to be true and accurate at the date of publication, neither the authors nor the editors nor the publisher can accept any legal responsibility for any errors or omissions that may be made. The publisher makes no warranty, express or implied, with respect to the material contained herein.

Printed on acid-free paper

Springer is part of Springer Science+Business Media (www.springer.com)

## Parts of this thesis have been published in the following journal articles:

Modulating the reactivity of the proteasome using a chimeric enone inhibitor based on the natural products carmaphycin and syringolin.
Trivella D, Pereira A, Stein ML, Byrum T, Kasai Y, Valeriote F, Tantillo D, Groll M Gerwick W, (**2014**) Moore B. Chem. Biol. *In press*

Systematic comparison of peptidic proteasome inhibitors highlights the α-ketoamide electrophile as an auspicious reversible lead motive.
Stein ML, Cui H, Beck P, Dubiella C, Voss C, Krüger S, Schmidt B, Groll M, (**2014**) Angew. Chem. Int. Ed. 3;53(6):1679–83

Applied techniques for mining natural proteasome inhibitors.
Stein ML, Groll M (**2014**), Biochem. Biophys. Acta. 1843(1):26–38

One-shot NMR analysis of microbial secretions identifies highly potent proteasome inhibitor.
Stein ML, Beck P, Kaiser M, Dudler R, Becker CF, Groll M (**2012**). Proc. Natl. Acad. Sci. 109, 18367–71

Activity enhancement of the synthetic syrbactin proteasome inhibitor hybrid and biological evaluation in tumor cells.
Archer CR, Groll ML, Stein ML, Schellenberg B, Clerc J, Kaiser M, Kondratyuk TP, Pezzuto JM, Dudler R, Bachmann AS (**2012**). Biochemistry. 51, 6880–8

Elucidation of the α-keto-aldehyde binding mechanism: a lead structure motif for proteasome inhibition.
Gräwert MA, Gallastegui N, Stein ML, Schmidt B, Kloetzel PM, Huber R, Groll M. Angew. Chem. Int. Ed. (**2011**) 10;50(2):542–4.

The work in this thesis was conducted from August 2010 fo December 2013 under the supervision of Prof. Dr. Michael Groll, Chair of Biochemistry, TUM.

*To my family*

# Supervisor's Foreword

The ubiquitin-proteasome system is of fundamental importance to many cellular pathways and is nowadays an established target for the treatment of malignant blood tumors in the pharmaceutical industry. Furthermore, the development of the first immunoproteasome-specific inhibitors has recently disclosed the vast field of immunosuppressive therapies. The numerous future applications of proteasome inhibitors, however, decisively depend on the identification of highly selective small molecule elicitors that modulate the proteolytic reactions of the various proteasomal active sites. The release of carfilzomib, the first natural-product-based-compound, has impressively demonstrated the advantages of these evolutionarily optimized compounds by a vastly reduced record of side effects compared to the first FDA-approved and fully synthetic inhibitor bortezomib. The identification of further lead structures is therefore of vital importance to answer the urging need for new compounds in the oncological and immunological sectors.

The outstanding Ph.D. thesis of Dr. Martin Lorenz Stein describes the establishment of a novel methodology to detect such bioactive natural products from the highly heterogeneous matrices present in raw organic extracts or culture broths. Compared with previously applied screening techniques, the developed tool is highly robust and produces unambiguous and reproducible readout. Moreover, due to the standard preparation of the peptidic substrate and the straightforward execution of the method, it is accessible to a broad scientific community. These features allow both the analysis of samples produced by standard protocols as well as the screening of individual environmental growth conditions during fermentation. Due to the silencing of many biosynthesis assembly lines of natural products in microorganisms, this is vital to determine a suitable molecular trigger to initiate biosynthesis and secretion of highly toxic, but likewise interesting secondary metabolites. The present work depicts the identification and isolation of applicable syrbactin proteasome inhibitors from the bacterium *Photorhabdus luminescens*. Noteworthy, it was shown that the secretion of these natural products is strictly regulated and thus only gets induced by a defined and adequate environmental habitat, dependent on the partially symbiotic life cycle of the producing bacteria. However, even after inducing the pathogenic phase, the syrbactins are produced in trace amounts, which is typical for toxic secondary metabolites. As a consequence, the isolation of the secondary metabolites was

only feasible by the application of the newly developed NMR-technique both in the screening and isolation approaches.

With regard to the rich assortment of natural proteasome inhibitors available nowadays, the new tool will pave the way to identify even more and diverse molecules in future screening approaches. It has again proven its strengths in the first subsequent studies in our lab by the identification of promising organisms for further investigations. Hereby, it forms the basis of all analytical steps during our robot-assisted automated screenings and is applied for the bioassay-guided isolation of the active compounds. Hence, the transferability of the assay principle to many other target enzymes will certainly stimulate the research on natural products and their distinct implementations in the near future.

Garching, March 2014 Prof. Michael Groll

# Acknowledgments

First of all, I would like to thank my supervisor, Prof. Michael Groll, for giving me the opportunity to write my Ph.D. thesis at his chair and for his tremendous support during these 3 years. The highly interesting topics together with his fierce enthusiasm for even the slightest progress made me bear even the times when my projects did not proceed as desired. His positive leadership has encouraged me to enjoy even challenging experiments and helped the whole team to strive even harder. Eventually, his ingenious ideas and perseverance let me achieve the high goals during this thesis.

I am also especially grateful for the support of Prof. Robert Dudler, University of Zürich, and Prof. Christian F. W. Becker, University of Wien. Both did not only supply crucial material for the establishment of the NMR assay, but constructively supported my project during all stages.

Furthermore, I would like to acknowledge PD. Dr. Wolfgang Heinemeyer for his advice and support in yeast genetics. He is a true expert and I would argue that there are not many scientists in this field who match his practical and theoretical competence. Due to his experience and calm character he was always one of my first contact persons for difficult questions.

I strongly want to thank Richard Feicht for his tremendous effort in proteasome isolation and his advice to all questions concerning protein purification. I have never met anyone with comparable and sometimes seemingly supernatural skills with regard to native protein purifications. His steady supply with crystals and material has facilitated the work of everyone in the team working on the proteasome

A special thank you goes to all members of the Groll group. I have always enjoyed the friendly atmosphere in our lab and often laughed heartily about the funny moments during our everyday work. Our synchrotron trips, which were often extraordinarily exhausting, were only bearable due to our mutual personal and professional appreciation that in some cases developed into friendships. I will never forget the legendary moments during our shifts.

Last but not least, I would like to thank my family for enabling my studies and their interest and personal support for my work. I doubt that I would have achieved this high goal without them.

# Contents

# Abbreviations

| | |
|---|---|
| AAA | ATPases associated with diverse cellular activities |
| ACN | Acetonitrile |
| AMC | 7-Amino-4-methyl-coumarin |
| APS | Ammonium persulfate |
| BODIPY | Boron-dipyrromethene |
| BSA | Bull serum albumin |
| CD8 | Cluster of differentiation 8 |
| Cdk | Cyclin dependent kinase |
| ChTL | Chymotrypsin-like |
| CL | Caspase-like |
| COSY | Correlated spectroscopy |
| cCP | Constitutive 20S proteasome |
| CP | Core particle |
| DCM | Dichloromethylene |
| DIPEA | *N,N*-Diisopropylethylamine |
| DMEM | Dulbecco's Modified Eagle Medium |
| DMF | *N,N*-Dimethylformamide |
| DMSO | Dimethyl sulfoxide |
| ECL | Electrochimiluminescence |
| EDTA | Ethylenediaminetetraacetic acid |
| ESI | Electron spray ionization |
| FBS | Fetal Bovine Serum |
| Fmoc | Fluorenylmethyloxycarbonyl |
| GADPH | Glycerinaldehyd-3-phosphat Dehydrogenase |
| HCTU | O-(1H-6-Chlorobenzotriazole-1-yl)-1, 1, 3, 3-tetramethyluronium hexafluorophosphate |
| HMBC | Heteronuclear multiple bond correlation spectroscopy |
| HPLC | High-performance liquid chromatography |
| HSQC | Heteronuclear single bond correlation spectroscopy |
| iCP | 20S immunoproteasome |
| MeOH | Methanol |
| MDa | Mega Dalton |
| MHC-I | Major histocompatibility complex I |

| | |
|---|---|
| MPD | 2-methyl-2, 4-pentanediol |
| NMR | Nuclear magnetic resonance (spectroscopy) |
| PAGE | Polyacrylamide gel electrophoresis |
| PBS | Phosphate buffered saline |
| PDB | Potatoe dextrose broth |
| pNA | Para-naphtylamine |
| PTFE | Polytetrafluoroethylene |
| RP-C18 | Reversed Phase capped with linear C18 alkyl chains |
| SDS | Sodium dodecyl sulfate |
| tCP | 20S thymo proteasome |
| TEMED | Tetra methylethylenediamine |
| TB | Terrific broth |
| TBS | Tris buffered saline |
| TFA | Trifluoro acetic acid |
| TL | Trypsin-like |
| Tris | Tris(hydroxymethyl)aminomethane |
| Trt | Triphenylmethyl |
| TWEEN 20 | Polysorbate 20 |
| Ub | Ubiquitin |
| WT | Wild type |

# Chapter 1
# Introduction

## 1.1 The Ubiquitin-Proteasome-System

The ubiquitin-proteasome system (UPS) is responsible for the directed disposal of unfolded, misfolded and short-lived proteins in eukaryotic cells and is therefore a key player in protein homeostasis. Moreover, it participates in crucial biological pathways by the degradation of signaling factors such as cyclins or the tumor suppressor p53. Eventually, not only the degradation of substrate proteins, but also the generation of peptide fragments is exploited in vertebrates for MHC-I epitope presentation and subsequent T-cell activation. Due to the involvement in these vital processes, the UPS is linked to diseases as diverse as cancer, autoimmunity or neurodegeneration and has been in the limelight of pharmaceutical industry for the last decade. Being an evolutionarily conserved target, many bacteria and fungi have developed secondary metabolites that attenuate the activity of their host's or competitor's UPS. Due to their gradual optimization over millions of years, these compounds are highly potent and versatile in terms of binding mechanism, target specificity and bioavailability, which makes them a treasure trove for the rational design of new agents. Although several classes of natural proteasome inhibitors have been discovered, the identification of novel lead structures is an ongoing challenge especially with regard to the discrepancy between the exploited applications of the commercially available drugs and their potential scope for various indications.

### *1.1.1 Ubiquitinylation*

Similar to small molecule metabolites, proteins are in a permanent dynamic equilibrium that is determined by their ribosomal synthesis rate and their degradation by proteases such as cathepsins or the proteasome [1, 2]. Thus, the rates for their (re-)formation and destruction can be used as a control system for various processes just like transcriptional and translational regulation, which is exemplified

M. L. Stein, *NMR-Bioassay Guided Isolation of the Natural 20S Proteasome Inhibitors from Photorhabdus Luminescens*, Springer Theses, DOI: 10.1007/978-3-319-07914-1_1,
© Springer International Publishing Switzerland 2014

by the periodically fluctuating levels of cyclins during the cell cycle [3]. Generally, the intracellular stability of a random protein in pro- and eukaryotes can be evaluated by the so-called N-end rule [4]. It defines degradation signals, whose detrimental effects accumulate to curtail a protein's half-life time. Apart from hydrophobic patches, distinct N-terminal amino acids such as lysine and arginine lead to an accelerated recognition by the respective degradation system [5].

In eukaryotic cells, the ubiquitin-proteasome system (UPS) represents the main non-lysosomal pathway for the selective decomposition of proteins [3]. It is structured into two successive processes, the covalent ubiquitinylation of target proteins and their subsequent break down by the 26S proteasome to defined cleavage products [6].

Ubiquitin (Ub), a comparatively small 8.5 kDa protein, can be posttranslationally attached by an isopeptide bond to the ε-amine moiety of surface-exposed lysine residues via its free glycine C-terminus [7]. Further Ub molecules can then be linked in a similar way to any of its seven lysine residues, thereby generating a great variety of polyubiquitinylated products [8]. Although often referred to as a black spot that dooms a protein to degradation, only K-48 linked Ub chains of at least 4 molecules definitely lead to proteasomal digestion, while other configurations have been shown to rather convey a translocational information or contribute to signaling [9, 10]. The overall ubiquitinylation of the proteome is therefore an exceptionally dynamic process that has been compared in its complexity and versatility with other post-translational modification like phosphorylation or glycosylation [8]. It is controlled by a highly specific system of ubiquitin ligases on the one hand and deubiquitinating enzymes on the other, thereby representing an entire posttranslational level of regulation [4, 11].

The biochemical reaction of ubiquitinylation includes three different classes of enzymes denominated as E1 (Ub-activating enzymes), E2 (Ub-conjugating enzymes) and E3 (Ub-ligating enzymes), which successively activate, transmit, and tag the Ub molecule to a substrate protein (Fig. 1.1) [11]. Resembling a pyramid scheme reaction setup, there exist only two rather promiscuous E1 enzymes in the human proteome that interact with around 50 E2 proteins, which in turn bind to approximately 1,000 E3 ligases [13, 14]. Due to the high degree of substrate specificity of the latter, their number also reflects the vast amount of proteins that are thus labeled for proteolytic degradation.

In detail, Ub is ATP-dependently activated by the E1 enzyme to form a thermodynamically rich Ub-E1 thioester intermediate [19]. Subsequently, E1 hands over its Ub moiety to an E2 protein [20], where it is again covalently bound as a thioester. Eventually, the substrate protein is recognized by the Ub ligase, which transfers the Ub molecule from E2 to the target protein [18]. Repeated cycles of this process finally yield isopeptide-bridged polyubiquitin chains that can be recognized by the 19S regulatory particle of the 26S proteasome [21].

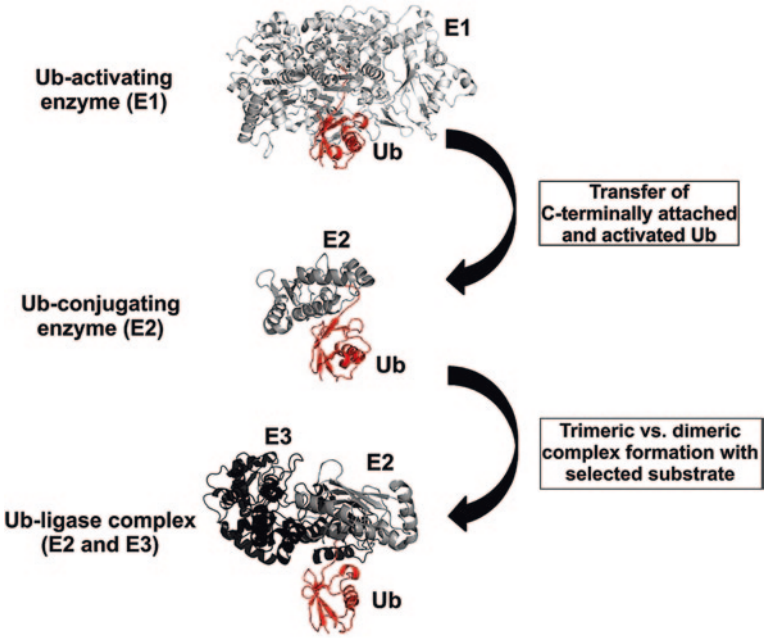


**Fig. 1.1** Ubiquitinylation involves three enzymes in a cascade-like reaction setup, which activate (E1, *upper*) [15], hand over (E2) [16] and ligate (E3) [17] an Ub molecule to a growing chain attached at a suitable substrate molecule. Substrate recognition can be achieved by a E3 alone or in complex with the E2 enzyme [18]. Figure adapted from Stein and Groll [12]

### *1.1.2 The 26S Proteasome*

This huge 2.6 MDa heteroprotein complex is composed of the catalytically active 20S proteasome (core particle; CP) and the 19S regulatory particle (RP) [22, 23]. After the detection of suitably Ub-tagged substrates, the RP removes the Ub molecules and simultaneously unfolds and threads the substrate into the proteolytic chamber of the CP [23, 24]. Although the inherent flexibility of the RP has hampered attempts of crystallization to date, recent biochemical, bioinformatical and largely electron microscopical analyses have contributed to understand the subunit location, the precise function and dynamics of this macromolecular machinery [21, 25, 26]. Gating the entry into the proteolytic CP, the RPs are perched on both lateral sides of the barrel-shaped 20S proteasome (Fig. 1.2). Due to their ability to hydrolyze ATP, the 19 different proteins that build up the RP were classified into Regulatory particle ATPases (Rpt) and Regulatory particle non-ATPases (Rpn)

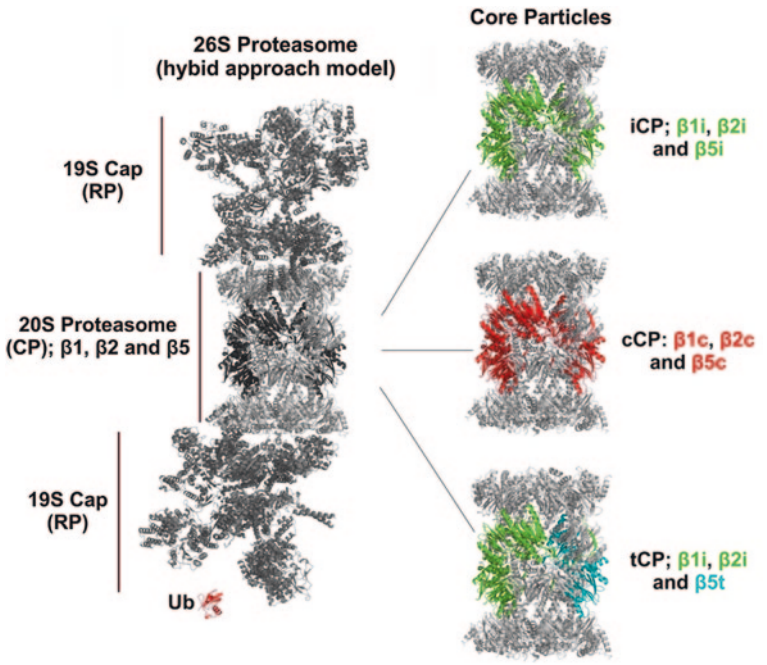


**Fig. 1.2** The 26S proteasome with an approximate molecular weight of 2.6 MDa is huge compared to the small Ub tag (*red*) of marked substrate proteins. Vertebrates have developed subspecies of the central catalytic machinery residing in the CP. In these particles, the proteolytic subunits are exchanged to reshuffle the cleavage activities and hence adapt to the physiological requirements. Electron microscopical model received from Morris [26]. Figure adapted from Stein and Groll [12]

subunits [27]. Furthermore, they were historically assigned to the modules "base" and "lid" due to biochemical association studies and their assumed location in the macroscopic subunits present in low resolution electron microscopy data [27]. However, the lid has meanwhile been shown to not be located top of the RP but rather on its side [28], with contact areas even to the CP subunits. Making the base and lid categories even more superfluous, subunits that had been assigned to the base, such as Rpn10 or Rpn13, are situated at the far side of the RP [25, 27, 29].

These two Ub-binding receptors are responsible for the selective docking of suitably tagged substrate proteins [30–32]. After this initial recognition step, the substrate is deubiquitinylated by the catalytically active zink-metallaprotease Rpn11 [33], which resides in the palm of the horseshoe-like setup formed by the subunits Rpn 3, 5–7, 9 and 12 [34]. Explaining the minimum Ub chain length, structural data have shown that only four Ub molecules are able to span the distance between the receptor proteins and Rpn11, which is required to prevent dissociation of the substrate from the RP [21]. Moreover, comparison of Rpn11, as well as the residual lid subunits, in the free and the bound state in complex with the remaining RP subunits revealed the regulatory mechanism of Rpn11, which is

only activated by structural rearrangements in the matured form of the RP, thereby protecting the cell from futile deubiquitinylation activity in the cytosol [29].

Subsequently, the six AAA+ ATPases Rpt1-6 [35, 36], which are arranged in a pseudohexameric spiral staircase above the outer subunits of the CP, exert tethering forces on the substrate protein [26]. Recent electron microscopical studies in complex with a substrate protein suggest that the Rpt subunits already engage with flexible and unstructured regions of the substrate before the Ub chain is cleaved off [21]. However, only after deubiquitinylation, which restores the Ub molecules for attachment to other client proteins, the Rpt subunits can gradually unfold and translocate the substrate into the hydrolytic chamber of the CP [21].

### *1.1.3 The Core Particle*

The 20S proteasome represents the downstream end of the UPS that performs the hydrolytic digestion of unfolded protein substrates to defined cleavage products [12, 37, 38]. Unlike the highly dynamic 19S cap, the CP is a rigid body that is framed by either the RP or other adapter proteins such as PA28 and Blm10, which tune its catalytic activity (Fig. 1.2) [39–41]. Its cylinder-shaped overall structure is composed of four heptameric rings following a $C_2$-symmetrical $\alpha_{1-7}\beta_{1-7}\beta_{1-7}\alpha_{1-7}$ arrangement [42].

As high resolution data is available for both the prokaryotic and eukaryotic CP, the molecular details including the regulatory and catalytic mechanisms of this molecular shredder have been elucidated [42, 44]. The α-subunits that form the outer rings hold both structural and functional roles during assembly and in the maturated particle [22]. Apart from forming the interface for binding to adapter proteins, they seal the central longitudinal pore through the CP by a thin interdigitating network composed of their N-termini, thus protecting the cell from detrimental self-digestion [24, 44]. As the proteolytic activity is completely unspecific with regard to the substrate proteins, it must be strictly compartmented in vivo. Therefore, the gate is only unlocked if a regulator such as the RP docks onto the outer α-ring and in consequence takes over the regulatory function [24]. Hereby, three Rpt subunits containing a C-terminus with a discrete recognition sequence bind into pockets between the adjacent α-subunits α1–α2, α3–α4 and α5–α6 to trigger the movement of a lever-like structure that lifts the N-terminus of the respective α-subunit, thus breaking the network over the central pore [44, 45].

On the other hand, the β-subunits within the equatorial rings exert the catalytic activities within the CP [46]. Whereas in prokaryotic organisms all α- and β-subunits are equal in structure, primary sequence and function [42], they have evolved in nucleated cells to individual proteins in order to reflect the advanced requirements in terms of signaling and sequence specificity [43, 47]. In consequence, the human proteasome contains only three proteolytically active subunits called β1, β2 and β5 that are endowed with distinct proteolytic specificities denominated as caspase-like (CL), trypsin-like (TL) and chymotrypsin-like

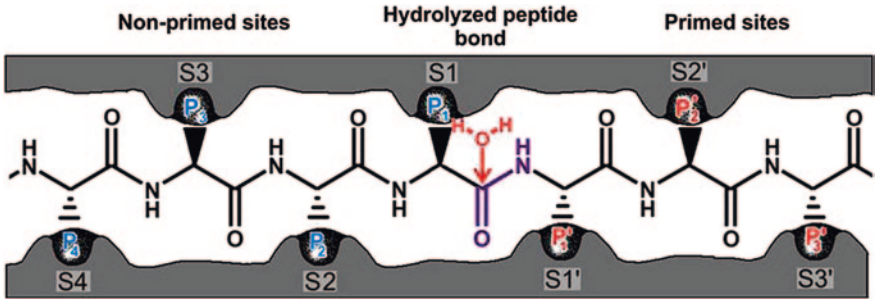


**Fig. 1.3** Schematic substrate binding channel of the active proteasomal β-subunits. The hydrolyzed peptide bond (*violet*) is initially activated by Thr-1 to form an acyl-enzyme intermediate, which in turn is attacked by an electrophilic water molecule. Adapted from Stein [52]

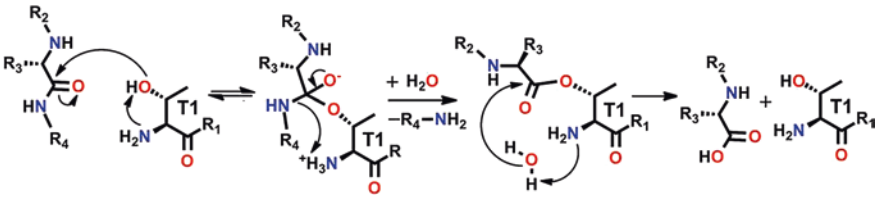


**Fig. 1.4** Catalytic peptide cleavage by the proteasomal active sites. By a nucleophilic attack of Thr-1O$^{\gamma}$ on the scissile peptide bond, an acyl-enzyme intermediate is formed. Subsequently, the ester is hydrolyzed by an activated water molecule to release the N-terminal peptide fragment

(ChTL), respectively, due to the chemical nature of the amino acids after which they preferentially cut a primary sequence [46, 48]. However, this assignment is misleading because not the first amino acid (P1, Fig. 1.3), but also the P3 and even the P4 sites have been shown to specifically interact with the binding pockets (S1–S4) within the substrate channels [49–51]. Moreover, with regard to the endoproteolytic character of the proteasome, also the binding pockets beyond the cleavage site (primed sites, S1′–S2′) have been suggested to contribute to binding and cleavage specificity [51].

However, the interactions between a suitable primary peptide sequence and the proteasomal binding channel eventually result in an elongated mean residence time of the substrate [53]. In turn, the Thr-1 residue attacks the scissile peptide bond via its electrophilic hydroxyl moiety that is activated by the basicity of the free amino terminus, thus forming a negatively charged tetrahedral transition state that is stabilized by the oxyanion hole formed by Gly-47N (Fig. 1.4) [43, 54].

Following the breakage of the peptide bond, the C-terminal fragment of the substrate is released to generate an acyl-enzyme intermediate. Subsequently, an activated water molecule that is prearranged in the Bürgi-Dunitz trajectory hydrolyzes the planar ester to yield the free carboxylic acid [55, 56]. With regard to the role of the free proteasomal N-termini of the active subunits, the CP is assigned to the class of N-terminal nucleophilic (Ntn) hydrolases [57].

Apart from the diversification of subunits in eukaryotes, vertebrates have even developed tissue-specific sets of β-subunits with distinct sequence specificities to adapt to the complex physiological signaling pathways present in higher organisms [53]. They are incorporated into nascent CPs, which are consequently named constitutive (cCP), immuno- (iCP) or thymus (tCP) core particles with allusion to their assigned function or the tissue in which they are produced [58, 59] (Fig. 1.2). Whereas the cCP is present in all cells and majorly responsible for protein homeostasis and the participation of the UPS in intracellular pathways, the iCP, which contains the β1i, β2i and β5i subunits in exchange for their constitutive counterparts, is produced in immune-related cell types such as lymphocytes and also in immunologically stimulated tissue [60, 61]. Due to the structure elucidation of the murine cCP and the iCP in 2012, the overall shift in the catalytic properties could be disclosed, thus offering the opportunity to specifically address the constitutive and the immunological branch of the UPS by selective inhibitors [62]. Overall structural comparison of both particles revealed that their folding and arrangement of the catalytic subunits match almost perfectly. Also, the β2c and β2i subunits conserve the specificity for basic amino acids while still allowing for a broad substrate tolerance and feature nearly identical substrate binding channels [62]. Therefore, the exchange of β2c with β2i stays elusive both with regard to the structural and functional consequences. In contrast, the cleavage preference of β1 is dramatically changed from acidic residues in β1c to small branched amino acids [63]. As MHC-I complexes have been shown to prefer hydrophobic C-termini, this immediately leads to an increased cell surface presentation pattern [64, 65].

Compared to the cCP and the iCP, very little is known about the tCP that is exclusively produced in the cortical thymus and linked to the development of various autoimmune diseases [66, 67]. Apart from β1i and β2i, it harbors another specific β5t subunit that confers a hydrophilic character to the substrate-binding channel due to structural simulations [62]. In agreement with initial experiments, the activity of the subunit is hence strongly attenuated, which is supposed to lead to a decrease of MHC-I presentation [58]. As β5t knockout mice display impaired development of T-cells in the thymus, the subunit has been suggested to play a pivotal role in positive $CD8^+$ T-cell selection [58]. By decreasing the stimulus for these cells, T-cells are proposed to slowly adapt to self-antigens instead of crossing the threshold that eventually leads to immune response. Contrary to β5t, the immunoproteasomal β5i has been shown to exhibit a larger P1 binding pocket compared to β5c, thus leading to a shift in the cleavage preference from small to large hydrophobic residues and hereby again to an enhanced MHC-I presentation [62, 68].

In conclusion, after the diversification of the β1i and β5i subunits, they have again passed through a process of convergent evolution to extend the pool of suitable antigenic epitopes [53]. The differentiation and specialization of the UPS in different cell types with regard to regulators, subunit composition and substrate specificity reflects the increased complexity in higher eukaryotic organisms. In turn, this might be exploitable by medicinal chemistry to selectively target certain pathways or specifically address either the constitutive or the immunological branch of the UPS [53]. Although studies have suggested that several players

within the UPS are equally "drugable", the CP is today in the focus of pharmaceutical industry [69]. This is not only due to the straightforward addressable enzymatic activity, but also to its direct involvement in inflammatory pathways, cell cycle control and immune response. For probably the same reasons, as well as the evolutionarily conserved character of the pathway, many microorganisms such as bacteria and fungi produce small molecules that attenuate their competitors' or host's UPS [70]. Due to their gradual optimization over millions of years, they often display extraordinary properties in terms of binding strength, selectivity and bioavailability. Hence, they pose a perfect starting point for the rational design of the second generation of proteasome inhibitors after the admission of the synthetic compound bortezomib (Velcade) by the FDA for the treatment of multiple myeloma and mantle cell lymphoma in 2003 [71].

## 1.2 Principles and Applications of Synthetic Proteasome Inhibitors

The inhibition of the UPS has been proven in numerous studies to be an effective rationale for the treatment of oncological diseases. However, the molecular reasons that ultimately lead to apoptosis and cell cycle arrest in cancerous tissue are difficult to determine due to the entanglement of the proteasome in so many crucial cellular processes.

The primary indication for which bortezomib received its admission was the altered transcription pattern due to the suppression of the inflammatory NF-κB signaling cascade [71]. Another consequence of UPS blockage is the accumulation of proapoptotic factors such as the Bcl-2 family as well as p53, which play a crucial role for triggering apoptotic processes [72]. Also, the prevented degradation of cyclins and the accumulation of Cdk inhibitors like p21 during the cell cycle have been shown to lead to impaired cell proliferation, which is especially detrimental for fast growing transformed cells [73, 74]. Eventually, the accelerated metabolism and the chromosomal aberrations of these cells are also associated with an augmented turnover and production of aberrant proteins [75]. As a consequence, they are more affected by proteasome inhibition than benign cells, resulting in ER-associated stress that triggers the unfolded protein response and consecutively leads to apoptosis [76]. Although it is not clear if a single or a combination of the described effects leads to the desired result, proteasome inhibitors are able to exploit the generated therapeutic window to selectively address malign tumors.

To date, a dazzling amount of synthetic inhibitors have been postulated that block the different proteasomal subunits and in turn the pathways in which the UPS is involved [77]. Generally, they are composed of a peptide backbone endowed with a C-terminal electrophile by which they react with the active Thr-1 residue (Fig. 1.5). As aldehydes had been known as potent inhibitors of nucleophilic proteases before, the tripeptide derivatives Calpain Inhibitor I (Ac-Leu-Leu-Nle-al) and MG132 (Z-Leu-Leu-Leu-al) were also among the first commercially available compounds to

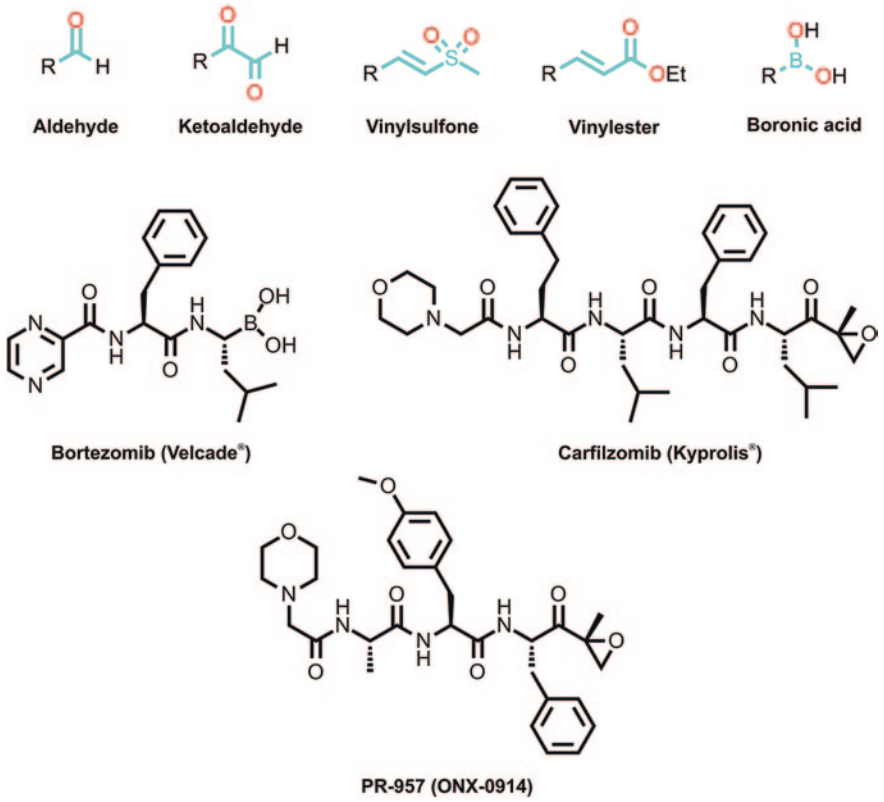


**Fig. 1.5** Described and validated electrophilic warheads of peptidic proteasome inhibitors. Bortezomib was the first prescriptive UPS inhibitor admitted by the FDA. Carfilzomib and PR-957 represent the next generation of proteasome inhibitors that rely on lead motives derived from natural secondary metabolites

block the proteasomal activities [78, 79]. However, the high reactivity of the aldehyde functional group leads to undesired cross reactivity with other enzymes [80], oxidation to the corresponding acid [81] as well as addition reactions with somatic nucleophiles. Hence, aldehyde compounds have stayed of limited interest for pharmaceutical industry. As a consequence, this class of inhibitors was further refined to yield the bivalent α-ketoaldehydes [82]. In contrast to monovalent electrophiles, they both react with the Thr-1O$^{\gamma}$ and the free N-terminus, thus reversibly generating a six-membered heterocycle [82]. Hereby, α-ketoaldehydes are able to discriminate against other serine, cysteine and metallaproteases and thus considerably increase the specificity of the monovalent pharmacophore.

In contrast to aldehyde inhibitors, vinyl sulfones react irreversibly with Thr-1O$^{\gamma}$ via their activated Michael-system to produce a stable ether product [50, 83]. Compared to other pharmacophores, they are rather unreactive and inert against decomposition by hydrolysis.

Although vinyl esters have been described as well, their even lower electrophilicity sets them far behind other inhibitor classes with regard to their exerted binding strength [84]. Relative to the commercially available compounds, even the inhibitory potential of vinyl sulfones is strongly diminished and despite belonging to the first established proteasome inhibitors, they are thus limited to laboratory applications.

Although aldehydes and vinyl sulfones failed to advance to clinical trials, their biochemical evaluation and structural characterization eventually lead to the development of the blockbuster drug bortezomib (Velcade®). With an annual sales volume of 2 billion dollars, it belongs to the 20 most valuable drugs distributed and has been proven to considerably prolong survival of treated patients. The dipeptide derivative carries a highly electrophilic boronic acid as C-terminal warhead, which binds to the Thr-1O$^{\gamma}$ moiety and thereby forms a covalent tetrahedral adduct that is also able to mimic the oxyanion during peptide cleavage [85]. Besides its anti-cancerous properties, bortezomib has been shown to be effective in studies with human allograft rejections, thus also highlighting the potential of a selective immunoproteasome specific agent and the important role of the UPS in the genesis of the immune response [86, 87]. On the other hand, bortezomib unexpectedly showed to be ineffective especially against solid tumors [88]. This might be caused by the high reactivity and instability of the boronic acid, which lead to extremely short half-life times in the blood stream [89]. In addition to the limited tissue penetration and the low bioavailability [90–92], administration of bortezomib often results in an upregulation of proteasome levels as well as adaptive resistances after prolonged treatment [93]. Furthermore, its application suffers from the promiscuous character of both the pharmacophore and the peptide backbone, which is linked to a vast record of side effects ranging from polyneuropathy over thrombocytopenia to gastrointestinal disorders [90]. As it has been shown that the proteasome harbors binding pockets up to the S4 position [50], the dipeptide certainly does not exploit the full potential with regard to target specificity. Combined with the high reactivity of the boronic acid, this leads to substantial off-target effects especially towards other proteases with the most prominent being cathepsin G, dipeptidyl peptidase II and HtrA2/Omi [94]. Notably, inhibition of the mitochondrial serine protease HtrA2/Omi has been shown to be responsible for the detrimental neurodegenerative effects [94].

Taking account of all these drawbacks of the otherwise highly potent drug has raised the need for proteasome inhibitors with improved pharmacological properties. The admission of carfilzomib (Kyprolis®) in 2012 for the same indications as bortezomib has heralded the era of second generation compounds [95]. Being based on novel and orthogonal lead structures, these drugs have been identified by searching the rich assortment of natural proteasome inhibitors [70], which have been designed not only towards highest inhibition values, but also towards biostability, selectivity and cell permeability. Similar to α-ketoaldehydes, carfilzomib addresses both nucleophilic centers of the proteasomal Thr-1 by its bifunctional α′, β′-epoxyketone warhead, thereby irreversibly generating a six-membered morpholino heterocylce [96]. Due to the bivalent character of the pharmacophore, carfilzomib inherently exhibits a high degree of selectivity for the few members of

the Ntn-hydrolase family, which directly translates to decreased off-target reactivity and a tremendously improved record of side-effects [94].

Another derivative using the α′, β′-epoxyketone pharmacophore, which is currently in the limelight of medicinal research, is the first-in-class immunoproteasome specific inhibitor PR-957 [97]. Recently, the molecular background for the particle specificity of PR-957 could be elucidated [62]. Complex structure analysis with murine cCP and iCP demonstrated that the size of the S1 pocket in the β5i subunit is bigger and thus able to accommodate larger hydrophobic residues than its constitutive counterpart [62]. This now enabled the rational design of iCP selective inhibitors and opened the door to the pharmaceutical exploitation of this branch of the UPS [53]. Despite the advantages of the epoxyketone warhead over the boronic acid, its application still suffers from the highly reactive nature of the epoxide moiety, which leads to fast hydrolysis in aqueous solution [98].

## 1.3 Natural Proteasome Inhibitors

Both carfilzomib and PR-957 are endowed with a lead motive derived from the natural product epoxomicin (Fig. 1.6) that was isolated from an *Actinomyces* bacterium [99, 100]. Pronouncing its biological impact and inhibitory potency, the epoxyketone moiety was adapted over the species barrier in cyanobacteria and *Streptomyces* strains, from which the analogous compounds carmaphycin A and eponemycin were isolated, respectively [101, 102]. Despite varying habitae and arguably different target organisms, these species have conserved the electrophilic warhead as the crucial determinant of the small molecule.

Apart from epoxyketones and rather unspecific peptide aldehydes, many distinct inhibitor classes have been identified (Fig. 1.6) [70]. Lactones range among the most prominent examples of antibiotics and consequently also represent a considerable share of the identified natural CP inhibitors [103, 104]. They possess a constrained β-lactone moiety, which undergoes a nucleophilic ring-opening reaction with Thr-1O$^{\gamma}$ to generate a covalent acyl-enzyme adduct [43]. Yet, this reaction is slowly reversible in the case of belactosin C as the ester can be hydrolyzed similar to the intermediates in peptide turnover by an activated water molecule.

In omuralide, the reverse reaction is suppressed because the β-lactone-γ-lactam bicyclic scaffold localizes a free hydroxyl group at the very position of the water molecule, thereby displacing it from its activated state in the Bürgi-Dunitz trajectory [43, 85]. Beside a high degree of target specificity, omuralide was shown to cause neurite outgrowth and cell cycle arrest by inhibition of cyclin turnover [104].

Therefore, omuralide was among the first proteasome inhibitors to which a distinct biological function could be assigned, which put CP-modulating agents on the agenda of pharmaceutical industry with regard to cancer treatment. The approach utilized by omuralide is brought to perfection in the completely irreversible inhibitor salinosporamide A (Marizomib) [105], where the produced hydroxyl group reacts further with a 2-chloroethyl tail in an $S_N2$ reaction to yield a cyclic

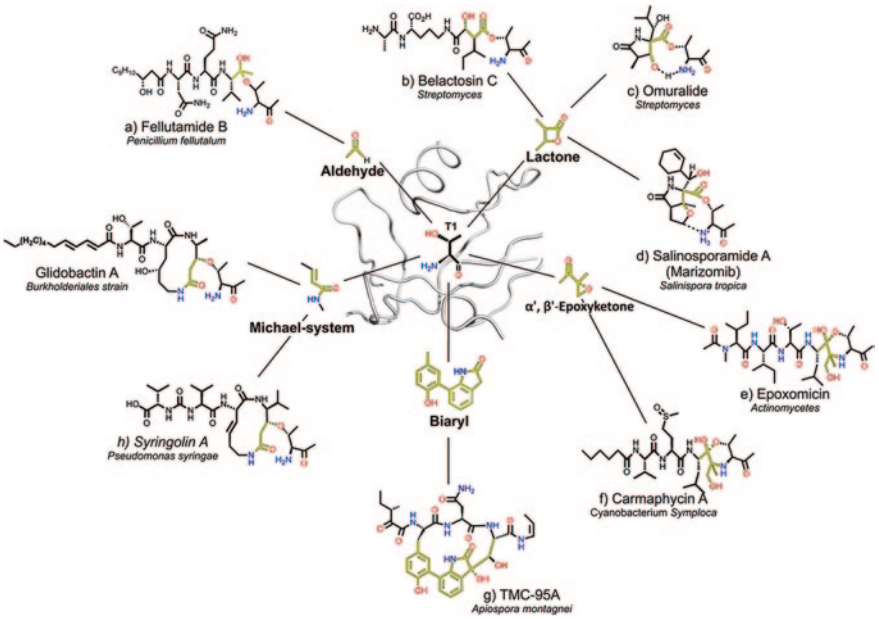


**Fig. 1.6** Natural proteasome inhibitors of the 20S proteasome. **a** The linear peptide aldehyde fellutamide B and **b** the β-lactone belactosin C were among the first identified natural proteasome inhibitors. **c** Omuralide and **d** salinosporamide A suppress the reactivation of the enzymatic functions by dislocating the nucleophilic water molecule via a hydroxyl and a tetrahydrofuran moiety, respectively. **e–f** The bifunctional α′, β′-epoxyketone warhead of epoxomicin and carmaphycin A is exploited in the prescriptive drug carfilzomib and the immunoproteasome inhibitor PR-957. The electrophilic pharmacophore reacts both with Thr-1O$^{\gamma}$ and Thr-1N to form an irreversible morpholino ring derivative. **g** TMC-95A is the only non-covalent natural product inhibitor identified to date. The rigid biaryl-bridged peptide scaffold carries many decorations and chiral centers that shape the compound's three dimensional structure, thus balancing the enthalpic loss by enhanced entropic properties. **h** Syringolin A and **g** glidobactin A are the eponymous compounds for the group of syrbactins. The constrained 14-membered macrolactam ring contains an electrophilic Michael system that generates an irreversible ether with the catalytically active Thr-1O$^{\gamma}$. Figure adopted from Stein and Groll [12]

tetrahydrofuran ether product, thereby rigidly precluding the nucleophilic water molecule [56]. Due to the high potency in vivo and in vitro as well as the elaborated binding mechanism, salinosporamide A is in clinical trials for treatment of multiple myeloma as the first non-peptidic UPS inhibitor [106].

Contrasting all synthetic and natural agents described so far, the cyclic peptide TMC-95A, which was isolated from cultures of the fungi *Apiospora montagnei,* is assigned to the group of reversible and non-covalent CP inhibitors [107, 108]. Despite the lack of an enthalpic contribution by forming connecting bonds to the proteasomal subunits, its binding strength is in the range of the highly reactive boronic acid and epoxyketone derivatives [109, 110]. This is not only caused by a tight network of interactions with the binding channels, but also by the entropically favorable rigidity of the cyclic scaffold [111]. Due to their dynamic binding equilibrium,

reversible inhibitors are hypothesized to penetrate into solid tumors, which makes TMC-95A an interesting candidate for pharmaceutical research. Yet, its highly demanding stereochemistry has complicated attempts to synthesize the compound [110, 112–114]. In turn, the complex structure of TMC-95A was broken down to its crucial functional determinants that were identified by in vitro and complex structure analyses with the CP [115]. However, none of the generated derivatives was able to surpass or even reach the inhibitory potential displayed by the natural product [109, 115, 116]. Moreover, TMC-95A has stayed the only representative of this intriguing class of natural inhibitors, which is partially due to the predominance of covalent compounds but also to the lack of appropriate assay techniques for their detection.

## 1.4 Proteasome Inhibitors as Virulence Factors from Pathogenic Origin

The syrbactins were the last group of secondary metabolites discovered to inhibit the proteasome to date [117]. Named after their two most prominent representatives syringolin A (SylA) [118] and glidobactin A (GlbA) [119], they share the common motive of a twelve-membered macrolactam cycle featuring a constrained Michael system as electrophilic pharmacophore. By reacting with Thr-1O$^{\gamma}$, they form an irreversible ether product similar to linear vinyl esters and vinyl sulfones [117]. Yet, whereas the $IC_{50}$ values of the synthetic compounds are in the micromolar range, syrbactins reach low nanomolar values [117]. Analogous to TMC-95A, the rigid macrolactam cycle is entropically favored compared to linear peptidic compounds as these loose considerable degrees of freedom versus their state in solution [117]. Moreover, analyses of X-ray crystallographic structures in complex with the CP suggest that the rigid cycle of the macrolactam scaffold prepositions the electrophilic β-carbon of the Michael system in close proximity to the nucleophilic hydroxyl moiety, thereby lowering the activation energy on the reaction trajectory and activating the rather inert Michael system [117]. However, as the Michael system displays reduced chemical reactivity that lags far behind the boronic acid or the epoxyketone, syrbactins have been shown to be strictly target-specific and in turn exhibit only decreased detrimental side effects.

Interestingly, whereas the lead motive is conserved in SylA and GlbA, both compounds differ considerably in their decoration pattern. By illustrating an optimized interaction network with the proteasomal substrate binding channel, GlbA holds enhanced potency compared to SylA and in fact even ranges among the most potent proteasome inhibitors in general [117]. Noteworthy, the differing functional groups and layout of the molecules turned out to only reflect their respective biological purpose for which the toxins are produced.

SylA was the first natural proteasome inhibitor to which a defined virulence function could be assigned. The compound, which was isolated from cultures of the bacterium *Pseudomonas syringae,* which causes the brown spot disease on crop plants, is secreted during the infection process, thereby weakening the immune response system and debilitating the host organism [117].

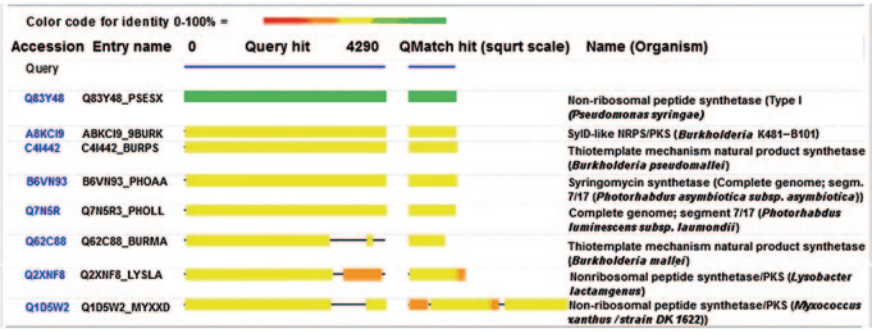


**Fig. 1.7** BLAST search result of the SylD gene within the SylA nonribosomal-synthase cluster. Apart from the *Burkholderiales* strain K481-B101, many other *Burkholderia* and *Photorhabdus* species possess equivalent gene clusters. Interestingly, *B. mallei* harbors an intron within its SylD gene, which might be responsible for the decreased human pathogenicity of the bacterium compared to *B. pseudomallei*

Subsequent to the discovery of SylA, comparison of the genes responsible for its synthesis by performing BLAST searches led to the identification of a whole array of bacteria with similar virulence clusters (Fig. 1.7) [120]. Besides the *Burkholderiales* strain K481-B101 from which GlbA had been isolated, the search yielded hits among various species within the *Burkholderia* and the *Photorhabdus* genera, which therefore also have been suggested to produce syrbactin compounds. The former even comprise human pathogenic agents like *B. pseudomallei*, the causative agent of melioidosis that has been categorized as a potential biological weapon of mass destruction [121]. Interestingly, the closely related but less virulent *B. mallei* contains an inactivating transposon-mediated rearrangement in the respective gene cluster, thereby emphasizing the importance of the small molecule and generally of the UPS during infection (Fig. 1.7) [117, 120]. With regard to the high potency of GlbA and the incidence of syrbactin compounds in general, it is likely that they join carfilzomib and marizomib as second generation proteasome inhibitors in the future.

The described assortment of natural substance classes that have been utilized to modulate the UPS of host organisms or nutrition competitors give a first glimpse into the treasure trove of small molecule elicitors harbored by nature. Still, the newly disclosed fields of iCP and tCP inhibition together with the vast unexploited potential of proteasome blockage for countless cancer diseases fuel the search for alternative substances.

However, although four out of ten best-selling drugs in the US are derived from natural compounds, research in this field suffers from a severe dilemma nowadays. Despite rising expenditures that often exceed economic sufficiency criteria, the number of newly discovered substances steadily decreases, which lead to the shutdown of many industrial screening programs [122]. Yet, due to the accessibility of the genomes of many organisms, it has become clear that only a small proportion of produced secondary metabolites have been isolated [123]. This can be attributed to

the silencing of the corresponding gene clusters under common culture conditions [124, 125]. Especially proteasome inhibitors, which belong to the cytotoxic warfare equipment of pathogenic organisms, are only produced after being triggered by suitable external conditions. This environmental sensing is not only due to the sumptuous production of the toxin, but also to ensure that it is specifically utilized during a defined stage of the life-cycle [126] in order to avoid self-detrimental consequences.

## 1.5 Overview of Currently Applied Methods for Proteasomal Inhibitor Detection

Due to the strict biosynthetic regulation of toxins, it is crucial to apply appropriate techniques to elucidate the molecular triggers that lead to their secretion. Subsequently, the downstream isolation can be achieved by routine extraction and column purification strategies. Many assay techniques have been described to evaluate the proteasomal activity [12, 127]. However, they all act within certain boundaries that limit their implementation especially in crude extracts and culture broths.

One of the most frequent methods utilized today is based on unnatural peptide substrates that carry an internally quenched C-terminal chromophor such as 7-amino-4-methl-coumarin (AMC) or para-naphtylamine (pNA) (Fig. 1.8). Their amino acid scaffold is adapted to the different proteasomal activities, which cleave off the chromogenic headgroups. In turn, these develop their absorptive or fluorescent properties [12, 127], thereby allowing the direct quantification of the enzymatic substrate turn-over. Because of their straightforward performance, UV-VIS based assays range among the most prominent techniques for high-throughput screenings of small molecule libraries [128]. However, they also hold a major drawback that leads to a high rate of artifacts especially in screens of biological samples. Due to their UV-VIS based nature, they are prone to all kinds of optical interferences including quenching and autofluorescence by colorful substances. As most microorganisms tend to produce pigments and phenolic macromolecules after prolonged incubation times [124, 129–132], the background of this technique is usually too high to reliably detect inhibitors in heterogeneous matrices.

Another common approach to evaluate the proteasomal activity is the quantification of intracellularly accumulated proteasome substrates upon treatment of mammalian cells with an inhibitory compound. The read-out can be achieved by standard western-blot analysis of either ubiquitinated proteins in general [133, 134] or distinct proteasomal substrates such as IκB or p53 [135–137]. The methodology is capable to detect both reversible and irreversible inhibitors of the UPS. It also benefits from the co-evaluation of cell permeability as well as the commercial availability of all components. Moreover, accumulation assays of select signaling substrates allows for the evaluation of affected cellular pathways, thereby connecting UPS inhibition with a defined biological effect such as the suppression of inflammatory cytokines caused by the blockage of the iCP [97, 138]. Despite their significance for in vivo characterizations, the application of these assays for screenings is largely hampered

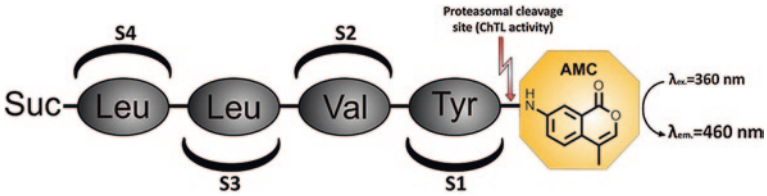


**Fig. 1.8** The most commonly applied proteasome assays use a non-natural substrate that contains a subunit-specific amino acid scaffold with a chromogenic headgroup, which is internally quenched by the attachment to the peptide. Upon cleavage by one of the proteasomal activities, the dye develops its absorptive or fluorescent properties

by their difficult and tedious execution. The cells have to be incubated with each sample for at least one day, submitted to hypotonic as well as frictional lysis and the extract must be standardized to a defined protein concentration. In turn, the blot needs to be co-stained against reliable housekeeping factors to finally enable an only qualitative result. In addition, the semi-quantitative data obtained by western-blots further require that the concentrations of the analyzed marker proteins must differ substantially in order to yield an unambiguous readout. Also, the approach suffers from its lack of specificity for single proteasomal active sites or even the entire UPS, as also upstream effects such as stress responses or the manifold interdependencies within signal transduction pathways can have a significant influence on the assay result [139–142]. Eventually, the detection limits in cell culture techniques are far higher than in enzymatic assays. However, as the titer of toxic secondary metabolites is very low to prevent noxious effects for the producing organism, these experiments are not suitable for the screening of fermentation conditions for proteasome inhibiting compounds. Yet, they represent valuable tools to complement other methodologies for the investigation of isolated compounds.

A more specific and direct approach that utilizes site-directed-affinity-probes (SSAP) accounts for many of the draw-backs of intracellular substrate accumulation assays (Fig. 1.9) [129, 143–145]. It relies on the specific interaction of an established inhibitor with the CP. The compound, which desirably binds equally to all active proteasomal subunits, is linked to a fluorescent dye. The inhibitor moiety of the probe covalently binds to the proteolytic sites, thereby labeling them with the chromophor [127]. After submission to an SDS-PAGE, the respective subunits can be visualized in a fluorescent gel scanning device (Fig. 1.9).

However, if the proteasome is previously treated with a sample that also contains proteasome-inhibiting species, the active sites are blocked from the chromogenic label and in turn the fluorescence signal is suppressed. Due to the linear dependency, the inhibition of each subunit can be separately quantified [145–147]. Furthermore, it is capable to distinguish between different proteasome particles in cells that produce iCP or tCP beside the constitutive 20S particles, thereby enabling the assessment of the selectivity of the inhibitory molecule. More importantly, the technique is not influenced by quenching or autofluorescence by components present in the complex sample matrix [127, 146]. On the other hand, the SSAP technique suffers

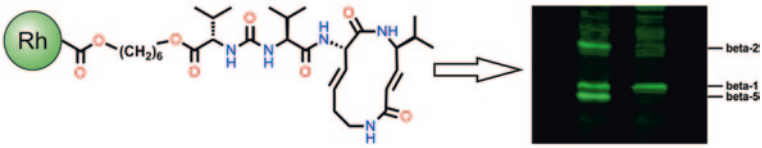


**Fig. 1.9** Site-directed-affinity-probe (SSAP) methods exploit the specific interaction of an inhibitor that is covalently linked to a chromophor. In this case, SylA is coupled to rhodamine via an alkyle linker moiety. Upon binding to the active proteasomal subunits, these can be visualized by SDS-gel separation and subsequent fluorescence detection (*left lane*). However, if an inhibiting sample is added to the proteasome before staining, blocked subunits cannot be tagged with the dye and in turn vanish on the developed gel (*right lane*). Figure adapted from Stein and Groll [12]

from the difficult preparation of the probe molecules. Being derived from previously established inhibitors, their synthesis can only be accomplished by specialized laboratories with organic chemistry facilities. Eventually, in order to stay attached to the proteasomal subunits, the probe must react irreversibly [99, 143]. Thus, it inevitably displaces all reversible ligands and precludes their detection, which is a serious draw-back of the approach. This is further exemplified by TMC-95A, which is still the only non-covalent proteasome inhibitor discovered to date. With regard to the suggested advantages over irreversible compounds, this is a grievous drawback of the otherwise solid methodology. In conclusion, all described techniques are valuable tools to characterize proteasome inhibitors both in vitro and in vivo. Yet, they are hardly suitable for high-throughput natural product screens and especially not for an application in crude extracts and culture broths.

## References

1. A. Hershko, A. Ciechanover, Annu. Rev. Biochem. **51**, 335–364 (1982)
2. J.D. Etlinger, A.L. Goldberg, Proc. Natl. Acad. Sci. USA **74**, 54–58 (1977)
3. A. Hershko, A. Ciechanover, Annu. Rev. Biochem. **67**, 425–479 (1998)
4. A. Varshavsky, Protein Sci. **20**, 1298–1345 (2011)
5. A. Varshavsky, Trends Biochem. Sci. **30**, 283–286 (2005)
6. A. Hershko, A. Ciechanover, Annu. Rev. Biochem. **61**, 761–807 (1992)
7. O. Kerscher, R. Felberbaum, M. Hochstrasser, Annu. Rev. Cell Dev. Biol. **22**, 159–180 (2006)
8. D. Komander, Biochem. Soc. Trans. **37**, 937–953 (2009)
9. J.S. Thrower, L. Hoffman, M. Rechsteiner, C.M. Pickart, EMBO J. **19**, 94–102 (2000)
10. C.M. Pickart, FASEB J. **11**, 1055–1066 (1997)
11. M. Hochstrasser, Cell **124**, 27–34 (2006)
12. M.L. Stein, M. Groll, *Biochim. Biophys. Acta* (2013)
13. B. Zhao, K. Bhuripanyo, J. Schneider, K. Zhang, H. Schindelin, D. Boone, J. Yin, *ACS Chem. Biol.* (2012)
14. P. Kaiser, L. Huang, *Genome Biol.* **6**, 233 (2005)
15. I. Lee, H. Schindelin, Cell **134**, 268–278 (2008)
16. K.S. Hamilton, M.J. Ellison, K.R. Barber, R.S. Williams, J.T. Huzil, S. McKenna, C. Ptak, M. Glover, G.S. Shaw, Structure **9**, 897–904 (2001)

17. H.B. Kamadurai, J. Souphron, D.C. Scott, D.M. Duda, D.J. Miller, D. Stringer, R.C. Piper, B.A. Schulman, Mol. Cell **36**, 1095–1102 (2009)
18. A. Hershko, A. Ciechanover, H. Heller, A.L. Haas, I.A. Rose, Proc. Natl. Acad. Sci. USA **77**, 1783–1786 (1980)
19. A. Hershko, H. Heller, S. Elias, A. Ciechanover, J. Biol. Chem. **258**, 8206–8214 (1983)
20. C.M. Pickart, I.A. Rose, J. Biol. Chem. **260**, 1573–1581 (1985)
21. M.E. Matyskiela, G.C. Lander, A. Martin, Nat. Struct. Mol. Biol. **20**, 781–788 (2013)
22. N. Gallastegui, M. Groll, Trends Biochem. Sci. **35**, 634–642 (2010)
23. R.J. Tomko Jr, M. Hochstrasser, Annu. Rev. Biochem. **82**, 415–445 (2013)
24. M. Groll, M. Bajorek, A. Köhler, L. Moroder, D. Rubin, R. Huber, M. Glickman, D. Finley, Nat. Struct. Biol. **7**, 1062–1067 (2000)
25. G.C. Lander, E. Estrin, M.E. Matyskiela, C. Bashore, E. Nogales, A. Martin, Nature **482**, 186–191 (2012)
26. P.C. da Fonseca, J. He, E.P. Morris, Mol. Cell **46**, 54–66 (2012)
27. M.H. Glickman, D.M. Rubin, O. Coux, I. Wefes, G. Pfeifer, Z. Cjeka, W. Baumeister, V.A. Fried, D. Finley, Cell **94**, 615–623 (1998)
28. K. Lasker, F. Förster, S. Bohn, T. Walzthoeni, E. Villa, P. Unverdorben, F. Beck, R. Aebersold, A. Sali, W. Baumeister, Proc. Natl. Acad. Sci. USA **109**, 1380–1387 (2012)
29. G.C. Lander, A. Martin, E. Nogales, Curr. Opin. Struct. Biol. **23**, 243–251 (2013)
30. Q. Deveraux, V. Ustrell, C. Pickart, M. Rechsteiner, J. Biol. Chem **269**, 7059–7061 (1994)
31. K. Husnjak, S. Elsasser, N. Zhang, X. Chen, L. Randles, Y. Shi, K. Hofmann, K.J. Walters, D. Finley, I. Dikic, Nature **453**, 481–488 (2008)
32. P. Schreiner, X. Chen, K. Husnjak, L. Randles, N. Zhang, S. Elsasser, D. Finley, I. Dikic, K.J. Walters, M. Groll, Nature **453**, 548–552 (2008)
33. R. Verma, L. Aravind, R. Oania, W.H. McDonald, J.R. Yates, E.V. Koonin, R.J. Deshaies, Science **298**, 611–615 (2002)
34. G.R. Pathare, I. Nagy, S. Bohn, P. Unverdorben, A. Hubert, R. Körner, S. Nickell, K. Lasker, A. Sali, T. Tamura, T. Nishioka, F. Förster, W. Baumeister, A. Bracher, Proc. Natl. Acad. Sci. USA **109**, 149–154 (2012)
35. D.M. Smith, N. Benaroudj, A. Goldberg, J. Struct. Biol. **156**, 72–83 (2006)
36. S. Djuranovic, M.D. Hartmann, M. Habeck, A. Ursinus, P. Zwickl, J. Martin, A.N. Lupas, K. Zeth, Mol. Cell **34**, 580–590 (2009)
37. A.K. Nussbaum, T.P. Dick, W. Keilholz, M. Schirle, S. Stevanović, K. Dietz, W. Heinemeyer, M. Groll, D.H. Wolf, R. Huber, H.G. Rammensee, H. Schild, Proc. Natl. Acad. Sci. USA **95**, 12504–12509 (1998)
38. T.P. Dick, A.K. Nussbaum, M. Deeg, W. Heinemeyer, M. Groll, M. Schirle, W. Keilholz, S. Stevanović, D.H. Wolf, R. Huber, H.G. Rammensee, H. Schild, J. Biol. Chem. **273**, 25637–25646 (1998)
39. W. Dubiel, G. Pratt, K. Ferrell, M. Rechsteiner, J. Biol. Chem. **267**, 22369–22377 (1992)
40. P. Ma, C.A. Slaughter, G.N. DeMartino, J. Biol. Chem. **267**, 10515–10523 (1992)
41. C.V. Ustrell, L. Hoffman, G. Pratt, M. Rechsteiner, EMBO J. **21**, 3516–3525 (2002)
42. J. Löwe, D. Stock, B. Jap, P. Zwickl, W. Baumeister, R. Huber, Science **268**, 533–539 (1995)
43. M. Groll, L. Ditzel, J. Löwe, D. Stock, M. Bochtler, H. Bartunik, R. Huber, Nature **386**, 463–471 (1997)
44. F.G. Whitby, E.I. Masters, L. Kramer, J.R. Knowlton, Y. Yao, C.C. Wang, C.P. Hill, Nature **408**, 115–120 (2000)
45. G. Tian, S. Park, M.J. Lee, B. Huck, F. McAllister, C.P. Hill, S.P. Gygi, D. Finley, Nat. Struct. Mol. Biol. **18**, 1259–1267 (2011)
46. W. Heinemeyer, M. Fischer, T. Krimmer, U. Stachon, D.H. Wolf, J. Biol. Chem. **272**, 25200–25209 (1997)
47. L.V. Pham, A.T. Tamayo, L.C. Yoshimura, P. Lo, R.J. Ford, J. Immunol. **171**, 88–95 (2003)
48. M. Orlowski, Biochemistry **29**, 10289–10297 (1990)
49. T. Nazif, M. Bogyo, Proc. Natl. Acad. Sci. USA **98**, 2967–2972 (2001)

50. M. Groll, T. Nazif, R. Huber, M. Bogyo, Chem. Biol. **9**, 655–662 (2002)
51. M. Groll, O. Larionov, R. Huber, A. de Meijere, Proc. Natl. Acad. Sci. USA **103**, 4576–4579 (2006)
52. M. Stein, Master thesis (2010)
53. E.M. Huber, M. Groll, Angew. Chem. Int. Ed. Engl. **51**, 8708–8720 (2012)
54. E. Seemüller, A. Lupas, D. Stock, J. Löwe, R. Huber, W. Baumeister, Science **268**, 579–582 (1995)
55. H.B. Bürgi, J.D. Dunitz, E. Shefter, Nat. New Biol. **244**, 186–187 (1973)
56. M. Groll, R. Huber, B. Potts, J. Am. Chem. Soc. **128**, 5136–5141 (2006)
57. J.A. Brannigan, G. Dodson, H.J. Duggleby, P.C. Moody, J.L. Smith, D.R. Tomchick, A.G. Murzin, Nature **378**, 416–419 (1995)
58. S. Murata, K. Sasaki, T. Kishimoto, S. Niwa, H. Hayashi, Y. Takahama, K. Tanaka, Science **316**, 1349–1353 (2007)
59. M. Groettrup, C.J. Kirk, M. Basler, Nat. Rev. Immunol. **10**, 73–78 (2010)
60. M. Aki, N. Shimbara, M. Takashina, K. Akiyama, S. Kagawa, T. Tamura, N. Tanahashi, T. Yoshimura, K. Tanaka, A. Ichihara, J. Biochem. **115**, 257–269 (1994)
61. M. Groettrup, R. Kraft, S. Kostka, S. Standera, R. Stohwasser, P.M. Kloetzel, Eur. J. Immunol. **26**, 863–869 (1996)
62. E.M. Huber, M. Basler, R. Schwab, W. Heinemeyer, C.J. Kirk, M. Groettrup, M. Groll, Cell **148**, 727–738 (2012)
63. C. Cardozo, R.A. Kohanski, J. Biol. Chem. **273**, 16764–16770 (1998)
64. P.J. Bjorkman, M.A. Saper, B. Samraoui, W.S. Bennett, J.L. Strominger, D.C. Wiley, Nature **329**, 512–518 (1987)
65. P. Romero, G. Corradin, I.F. Luescher, J.L. Maryanski, J. Exp. Med. **174**, 603–612 (1991)
66. U. Tomaru, A. Ishizu, S. Murata, Y. Miyatake, S. Suzuki, S. Takahashi, T. Kazamaki, J. Ohara, T. Baba, S. Iwasaki, K. Fugo, N. Otsuka, K. Tanaka, M. Kasahara, Blood **113**, 5186–5191 (2009)
67. S. Murata, Y. Takahama, K. Tanaka, Curr. Opin. Immunol. **20**, 192–196 (2008)
68. M. Gaczynska, K.L. Rock, T. Spies, A.L. Goldberg, Proc. Natl. Acad. Sci. USA **91**, 9213–9217 (1994)
69. P. D'Arcy, S. Brnjic, M.H. Olofsson, M. Fryknas, K. Lindsten, M. De Cesare, P. Perego, B. Sadeghi, M. Hassan, R. Larsson, S. Linder, Nat. Med. **17**, 1636–1640 (2011)
70. M.A. Gräwert, M. Groll, Chem. Commun. (Camb.) **48**, 1364–1378 (2012)
71. P.G. Richardson, T. Hideshima, K.C. Anderson, Cancer Control **10**, 361–369 (2003)
72. D.J. McConkey, K. Zhu, Drug Resist. Updat. **11**, 164–179 (2008)
73. P. Bonvini, E. Zorzi, G. Basso, A. Rosolen, Leukemia **21**, 838–842 (2007)
74. B. Zheng, G.V. Georgakis, Y. Li, A. Bharti, D. McConkey, B.B. Aggarwal, A. Younes, Clin. cancer res. official j. Am. Assoc. Cancer Res. **10**, 3207–3215 (2004)
75. P. Neri, N.J. Bahlis, Expert Opin. Biol. Ther. **13**(Suppl 1), S69–S82 (2013)
76. S.T. Nawrocki, J.S. Carew, K. Dunner Jr, L.H. Boise, P.J. Chiao, P. Huang, J.L. Abbruzzese, D.J. McConkey, Cancer Res. **65**, 11510–11519 (2005)
77. P. Beck, C. Dubiella, M. Groll, Biol. Chem. **393**, 1101–1120 (2012)
78. Y. Saitoh, H. Yokosawa, K. Takahashi, S. Ishii, J. Biochem. **105**, 254–260 (1989)
79. S. Tsubuki, H. Kawasaki, Y. Saito, N. Miyashita, M. Inomata, S. Kawashima, Biochem. Biophys. Res. Commun. **196**, 1195–1201 (1993)
80. A. Vinitsky, C. Michaud, J. Powers, M. Orlowski, Biochemistry **31**, 9421–9428 (1992)
81. A.F. Kisselev, A.L. Goldberg, Chem. Biol. **8**, 739–758 (2001)
82. M.A. Gräwert, N. Gallastegui, M. Stein, B. Schmidt, P.M. Kloetzel, R. Huber, M. Groll, Angew. Chem. Int. Ed. Engl. **50**, 542–544 (2011)
83. M. Bogyo, J. McMaster, M. Gaczynska, D. Tortorella, A. Goldberg, H. Ploegh, Proc. Natl. Acad. Sci. USA **94**, 6629–6634 (1997)
84. M. Marastoni, A. Baldisserotto, S. Cellini, R. Gavioli, R. Tomatis, J. Med. Chem. **48**, 5038–5042 (2005)
85. M. Groll, C. Berkers, H. Ploegh, H. Ovaa, Structure **14**, 451–456 (2006)

86. S. Westphal, S. Hansson, G. Stelin, J. Holgersson, L. Mjornstedt, S. Friman, Transpl. Proc. **45**, 1213–1215 (2013)
87. J. Koreth, K.E. Stevenson, H.T. Kim, S.M. McDonough, B. Bindra, P. Armand, V.T. Ho, C. Cutler, B.R. Blazar, J.H. Antin, R.J. Soiffer, J. Ritz, E.P. Alyea, Third J. Clin. Oncol. Official J. Am. Soc. Clin. Oncol. **30**, 3202–3208 (2012)
88. D. Buac, M. Shen, S. Schmitt, F.R. Kona, R. Deshmukh, Z. Zhang, C. Neslund-Dudas, B. Mitra, Q.P. Dou, Curr. Pharm. Des. **19**, 4025–4038 (2013)
89. D.E. Reece, D. Sullivan, S. Lonial, A.F. Mohrbacher, G. Chatta, C. Shustik, H. Burris 3rd, K. Venkatakrishnan, R. Neuwirth, W.J. Riordan, M. Karol, L.L. von Moltke, M. Acharya, P. Zannikos, A. Keith, Stewart. Cancer Chemother. Pharmacol. **67**, 57–67 (2011)
90. P.G. Richardson, B. Barlogie, J. Berenson, S. Singhal, S. Jagannath, D. Irwin, S.V. Rajkumar, G. Srkalovic, M. Alsina, R. Alexanian, D. Siegel, R.Z. Orlowski, D. Kuter, S.A. Limentani, S. Lee, T. Hideshima, D.L. Esseltine, M. Kauffman, J. Adams, D.P. Schenkein, K.C. Anderson, N. Engl. J. Med. **348**, 2609–2617 (2003)
91. C.N. Papandreou, D.D. Daliani, D. Nix, H. Yang, T. Madden, X. Wang, C.S. Pien, R.E. Millikan, S.M. Tu, L. Pagliaro, J. Kim, J. Adams, P. Elliott, D. Esseltine, A. Petrusich, P. Dieringer, C. Perez, C.J. Logothetis, J. Clin. Oncol. **22**, 2108–2121 (2004)
92. M.J. Williamson, M.D. Silva, J. Terkelsen, R. Robertson, L. Yu, C. Xia, P. Hatsis, B. Bannerman, T. Babcock, Y. Cao, E. Kupperman, Mol. Cancer. Ther. **8**, 3234–3243 (2009)
93. R. Oerlemans, N.E. Franke, Y.G. Assaraf, J. Cloos, I. van Zantwijk, C.R. Berkers, G.L. Scheffer, K. Debipersad, K. Vojtekova, C. Lemos, J.W. van der Heijden, B. Ylstra, G.J. Peters, G.L. Kaspers, B.A. Dijkmans, R.J. Scheper, G. Jansen, Blood **112**, 2489–2499 (2008)
94. S. Arastu-Kapur, J.L. Anderl, M. Kraus, F. Parlati, K.D. Shenk, S.J. Lee, T. Muchamuel, M.K. Bennett, C. Driessen, A.J. Ball, C.J. Kirk, Clin. Cancer Res. **17**, 2734–2743 (2011)
95. P. Lawasut, D. Chauhan, J. Laubach, C. Hayes, C. Fabre, M. Maglio, C. Mitsiades, T. Hideshima, K.C. Anderson, P.G. Richardson, Curr. Hematol. Malig. Rep. **7**, 258–266 (2012)
96. M. Groll, K.B. Kim, N. Kairies, R. Huber, C.M. Crews, J. Am. Chem. Soc. **122**, 1237–1238 (2000)
97. T. Muchamuel, M. Basler, M.A. Aujay, E. Suzuki, K.W. Kalim, C. Lauer, C. Sylvain, E.R. Ring, J. Shields, J. Jiang, P. Shwonek, F. Parlati, S.D. Demo, M.K. Bennett, C.J. Kirk, M. Groettrup, Nat. Med. **15**, 781–787 (2009)
98. J. Yang, Z. Wang, Y. Fang, J. Jiang, F. Zhao, H. Wong, M.K. Bennett, C.J. Molineaux, C.J. Kirk, Drug Metab. Dispos. **39**, 1873–1882 (2011)
99. L. Meng, R. Mohan, B.H. Kwok, M. Elofsson, N. Sin, C.M. Crews, Proc. Natl. Acad. Sci. USA **96**, 10403–10408 (1999)
100. M. Hanada, K. Sugawara, K. Kaneta, S. Toda, Y. Nishiyama, K. Tomita, H. Yamamoto, M. Konishi, T. Oki, J. Antibiot. (Tokyo) **45**, 1746–1752 (1992)
101. A.R. Pereira, A.J. Kale, A.T. Fenley, T. Byrum, H.M. Debonsi, M.K. Gilson, F.A. Valeriote, B.S. Moore, W.H. Gerwick, Chembiochem **13**, 810–817 (2012)
102. K. Sugawara, M. Hatori, Y. Nishiyama, K. Tomita, H. Kamei, M. Konishi, T. Oki, J. Antibiot. (Tokyo) **43**, 8–18 (1990)
103. S. Omura, T. Fujimoto, K. Otoguro, K. Matsuzaki, R. Moriguchi, H. Tanaka, Y. Sasaki, J. Antibiot. (Tokyo) **44**, 113–116 (1991)
104. G. Fenteany, R. Standaert, W. Lane, S. Choi, E. Corey, S. Schreiber, Science **268**, 726–731 (1995)
105. R. Feling, G. Buchanan, T. Mincer, C. Kauffman, P. Jensen, W. Fenical, Angew. Chem. Int. Ed. Engl. **42**, 355–357 (2003)
106. M. Millward, T. Price, A. Townsend, C. Sweeney, A. Spencer, S. Sukumaran, A. Longenecker, L. Lee, A. Lay, G. Sharma, R.M. Gemmill, H.A. Drabkin, G.K. Lloyd, S.T. Neuteboom, D.J. McConkey, M.A. Palladino, M.A. Spear, Invest. New Drugs **30**, 2303–2317 (2012)
107. Y. Koguchi, J. Kohno, M. Nishio, K. Takahashi, T. Okuda, T. Ohnuki, S. Komatsubara, J. antibiot. **53**, 105–109 (2000)

108. J. Kohno, Y. Koguchi, M. Nishio, K. Nakao, M. Kuroda, R. Shimizu, T. Ohnuki, S. Komatsubara, J. Org. Chem. **65**, 990–995 (2000)
109. M. Groll, M. Gotz, M. Kaiser, E. Weyher, L. Moroder, Chem. Biol. **13**, 607–614 (2006)
110. M. Kaiser, C. Siciliano, I. Assfalg-Machleidt, M. Groll, A.G. Milbradt, L. Moroder, Org. Lett. **5**, 3435–3437 (2003)
111. M. Groll, Y. Koguchi, R. Huber, J. Kohno, J. Mol. Biol. **311**, 543–548 (2001)
112. S. Lin, S.J. Danishefsky, Ange. Chemie. **41**, 512–515 (2002)
113. B.K. Albrecht, R.M. Williams, Org. Lett. **5**, 197–200 (2003)
114. M. Kaiser, M. Groll, C. Renner, R. Huber, L. Moroder, Angew. Chem. Int. Ed. Engl. **41**, 780–783 (2002)
115. M. Groll, N. Gallastegui, X. Marechal, V. Le Ravalec, N. Basse, N. Richy, E. Genin, R. Huber, L. Moroder, J. Vidal, M. Reboud-Ravaux, ChemMedChem **5**, 1701–1705 (2010)
116. M. Kaiser, A. Milbradt, C. Siciliano, I. Assfalg-Machleidt, W. Machleidt, M. Groll, C. Renner, L. Moroder, Chem. Biodivers. **1**, 161–173 (2004)
117. M. Groll, B. Schellenberg, A. Bachmann, C. Archer, R. Huber, T. Powell, S. Lindow, M. Kaiser, R. Dudler, Nature **452**, 755–758 (2008)
118. U. Waspi, D. Blanc, T. Winkler, P. Ruedi, R. Dudler, Mol. Plant-Microbe Interact. **11**, 727–733 (1998)
119. M. Oka, Y. Nishiyama, S. Ohta, H. Kamei, M. Konishi, T. Miyaki, T. Oki, H. Kawaguchi, J. Antibiot. (Tokyo) **41**, 1331–1337 (1988)
120. B. Schellenberg, L. Bigler, R. Dudler, Environ. Microbiol. **9**, 1640–1650 (2007)
121. W.J. Wiersinga, T. van der Poll, N.J. White, N.P. Day, S.J. Peacock, Nat. Rev. Microbiol. **4**, 272–282 (2006)
122. D.D. Baker, M. Chu, U. Oza, V. Rajgarhia, Nat. Prod. Rep. **24**, 1225–1244 (2007)
123. H.B. Bode, R. Müller, Angew. Chem. Int. Ed. Engl. **44**, 6828–6846 (2005)
124. A.O. Brachmann, F. Kirchner, C. Kegler, S.C. Kinski, I. Schmitt, H.B. Bode, J. Biotechnol. **157**, 96–99 (2012)
125. J. Crawford, R. Kontnik, J. Clardy, Curr. Biol. **20**, 69–74 (2010)
126. M.L. Stein, P. Beck, M. Kaiser, R. Dudler, C.F. Becker, M. Groll, Proc. Natl. Acad. Sci. USA **109**, 18367–18371 (2012)
127. A. Liggett, L.J. Crawford, B. Walker, T.C. Morris, A.E. Irvine, Leuk. Res. **34**, 1403–1409 (2010)
128. M.E. Bosch, A.J. Sanchez, F.S. Rojas, C.B. Ojeda, Comb. Chem. High Throughput Screen **10**, 413–432 (2007)
129. T.H. Haverkamp, D. Schouten, M. Doeleman, U. Wollenzien, J. Huisman, L.J. Stal, Isme J. **3**, 397–408 (2009)
130. P. Thawornwiriyanun, S. Tanasupawat, C. Dechsakulwatana, S. Techkarnjanaruk, W. Suntornsuk, Appl. Biochem. Biotechnol. **167**, 2357–2368 (2012)
131. A. Khanafari, D. Khavarinejad, A. Mashinchian, Iran J Microbiol **2**, 103–109 (2012)
132. Y. Tu, C. Jeffries, H. Ruan, C. Nelson, D. Smithson, A.A. Shelat, K.M. Brown, X.C. Li, J.P. Hester, T. Smillie, I.A. Khan, L. Walker, K. Guy, B. Yan, J. nat. prod. **73**, 751–754 (2012)
133. M.E. Figueiredo-Pereira, K.A. Berg, S. Wilk, J. Neurochem. **63**, 1578–1581 (1994)
134. N. Myeku, M.E. Figueiredo-Pereira, J. biol. chem. **286**, 22426–22440 (2011)
135. E.B. Traenckner, S. Wilk, P.A. Baeuerle, EMBO J. **13**, 5433–5441 (1994)
136. M.H. Kubbutat, S.N. Jones, K.H. Vousden, Nature **387**, 299–303 (1997)
137. A.B. Meriin, V.L. Gabai, J. Yaglom, V.I. Shifrin, M.Y. Sherman, J. Biol. Chem. **273**, 6373–6379 (1998)
138. M. Basler, M. Dajee, C. Moll, M. Groettrup, C.J. Kirk, J. Immunol. **185**, 634–641 (2010)
139. V. Akimov, K.T. Rigbolt, M.M. Nielsen, B. Blagoev, Mol. Biosyst. **7**, 3223–3233 (2011)
140. N.D. Udeshi, D.R. Mani, T. Eisenhaure, P. Mertins, J.D. Jaffe, K.R. Clauser, N. Hacohen, S.A. Carr, Mol. Cell Proteomics **11**, 148–159 (2012)
141. F. Shang, A. Taylor, Free Radic. Biol. Med. **51**, 5–16 (2011)
142. S. Meiners, D. Heyken, A. Weller, A. Ludwig, K. Stangl, P.M. Kloetzel, E. Kruger, J. Biol. Chem. **278**, 21517–21525 (2003)

143. J. Clerc, B.I. Florea, M. Kraus, M. Groll, R. Huber, A.S. Bachmann, R. Dudler, C. Driessen, H.S. Overkleeft, M. Kaiser, ChemBioChem **10**, 2638–2643 (2009)
144. C.R. Berkers, H. Ovaa, Biochem. Soc. Trans. **38**, 14–20 (2010)
145. C.R. Berkers, M. Verdoes, E. Lichtman, E. Fiebiger, B.M. Kessler, K.C. Anderson, H.L. Ploegh, H. Ovaa, P.J. Galardy, Nat. Meth. **2**, 357–362 (2005)
146. C.R. Berkers, F.W. van Leeuwen, T.A. Groothuis, V. Peperzak, E.W. van Tilburg, J. Borst, J.J. Neefjes, H. Ovaa, Mol. Pharm. **4**, 739–748 (2007)
147. C.R. Berkers, Y. Leestemaker, K.G. Schuurman, B. Ruggeri, S. Jones-Bolin, M. Williams, H. Ovaa, Mol. Pharm. **9**, 1126–1135 (2012)

# Chapter 2
# Objective

Due to the silencing of many natural toxins under common growth conditions, a robust and unambiguous technique is required to screen different fermentation approaches and identify the defined molecular trigger for the secretion of metabolites that affect biological maintenance. Once a suitable condition is established, the downstream purification and characterization of the respective secondary metabolite is a straightforward process. With regard to the plentitude of identified natural proteasome inhibitor classes and the conserved character of the UPS in various species, it is likely that the application of such a technique will yield many novel and auspicious lead structures.

Therefore, the aim of this thesis was the development of a methodology to unambiguously detect proteasome-inhibiting agents in crude culture broths. In order to avoid all biochemical artifacts, the assay was intended to be based on a natural and subunit-specific proteasome substrate. With regard to the unreliability of common proteasome assays in heterogeneous mixtures, the substrate was devised to enable NMR readout by regiospecific atom labeling.

After the establishment of a suitable peptide sequence, the assay was to be verified by analyzing media of *P. syringae* containing defined quantities of the irreversible syrbactin inhibitor SylA in order to probe the detection limits and analyze the signal-to-noise ratio of the technique. In turn, the developed tool was envisioned to be applied for the analyses of cultures derived from other organisms suggested to produce syrbactins due to genetic similarities with *P. syringae*. As the group of syrbactins comprises the extremely potent GlbA, it was likely that the isolation of the respective molecules would identify other at least equally potent compounds and grant deeper insight into their binding mechanisms. From the list of potential organisms, it was intended to analyze cultures of *P. luminescens* because the S1 insect pathogen can be handled easily especially compared to the equally promising but highly virulent *Burkholderia* species. Moreover, it was described that *P. luminescens* produces intensely colorful substances and would therefore represent a case of hardship for the approval of the developed technique.

M. L. Stein, *NMR-Bioassay Guided Isolation of the Natural 20S Proteasome Inhibitors from Photorhabdus Luminescens*, Springer Theses, DOI: 10.1007/978-3-319-07914-1_2,
© Springer International Publishing Switzerland 2014

Due to the silencing of the respective gene cluster in common cultures of the bacterium, the assay was to be utilized for the identification of a suitable growth condition to trigger the biosynthesis of the toxin. The major purpose of the research project was to pave the way for the isolation and structural characterization of the proteasome inhibiting compound from natural source. Subsequently, it was aspired to investigate the molecular binding mechanism and in vivo potency of the natural compound by the means of crystallographic complex structure analysis with the 20S proteasome as well as cell culture experiments for the evaluation of cytotoxicity and intracellular pathway affection.

In summary, the introduction of an orthogonal methodology into the field of proteasome assays aimed to disclose the broad range of still undiscovered inhibitors by offering a methodology for their detection already during the fermentation procedure of the organism. Exemplifying the approach on a real-case scenario, it was envisioned to pursue the whole process from the detection to the isolation of the inhibitor and eventually characterize its in vitro and in vivo properties by performing multidisciplinary experiments.

# Chapter 3
# Materials and Methods

## 3.1 Materials

### *3.1.1 Chemicals*

All applied compounds were acquired from the following companies: Bachem (Bubendorf, SWI), Enzo Life Sciences (Lörrach, GER), Fluka (Neu-Ulm, GER), Merck (Darmstadt, GER), Santa Cruz (Heidelberg, GER), Sigma-Aldrich (Steinheim, GER), Roth (Karlsruhe, GER) and VWR (Darmstadt, GER).

### *3.1.2 Growth Media*

| | | |
|---|---|---|
| $LB_0$ | NaCl | 1 % (w/v) |
| | Peptone | 1 % (w/v) |
| | Yeast extract | 0.5 % (w/v) |
| $SRM_{AF}$ | Arbutin | 100 µM |
| | $FeCl_3$ | 10 µM |
| | Fructose | 0.1 % (w/v) |
| | Glucose | 1 % (w/v) |
| | Histidine | 0.4 % (w/v) |
| | Potassium phosphate | 0.8 mM |
| *2xTY* | NaCl | 0.5 % (w/v) |
| | Peptone | 1.6 % (w/v) |
| | Yeast extract | 1 % (w/v) |
| *TYEA* | NaCl | 1 % (w/v) |
| | Tryptone | 0.2 % (w/v) |
| | Yeast extract | 0.5 % (w/v) |

(continued)

M. L. Stein, *NMR-Bioassay Guided Isolation of the Natural 20S Proteasome Inhibitors from Photorhabdus Luminescens*, Springer Theses, DOI: 10.1007/978-3-319-07914-1_3,
© Springer International Publishing Switzerland 2014

(continued)

| | | |
|---|---|---|
| *TYEB* | Tryptone | 0.2 % (w/v) |
| | Yeast extract | 0.5 % (w/v) |
| *YPD* | Glucose | 2 % (w/v) |
| | Peptone | 2 % (w/v) |
| | Yeast extract | 1 % (w/v) |

### 3.1.3 Strains

| Organism | Strain | Genotype | Source |
|---|---|---|---|
| *S. cerevisiae* | YHei140 WCG-4a β5-T1A | MATα, ura3 leu2-3, 112 his3-11, 15 $Can^S$ GAL1 pre2Δ: HIS3, pRS315-UBI/mmpre2-T1A and propeptide PRE2 nat1Δ: KanMX4 | Heinemeyer et al. [1] |
| *S. cerevisiae* | YHei113 WCG-4a β2-T1A | MATa, ura3 leu2-3, 112 his3-11, 15 $Can^S$ GAL1 UBI/mmpup1-T1A | Heinemeyer et al. [1] |
| *S. cerevisiae* | WCG-4a, Pre1-1 | MATα, ura3 leu2-3, 112 his3-11, 15 $Can^S$ GAL Pre1-1 (S142F) | Heinemeyer et al. [2] |
| *S. cerevisiae* | YHei032 WCG-4a, β5-$(His)_6$ | MATα, ura3 leu2-3, 112 his3-11, 15 $Can^S$ GAL1 pre2Δ: HIS3 pRS425-PRE2-C-$His_6$ | Donnation from PD. W. Heinemeyer |
| *P. syringae ssp syringae* | TT01 | WT | Gross et al. [3] |
| *P. luminescens ssp laumondii* | TT01 | WT | Fischer-Le Saux et al. [4] |

### 3.1.4 Fluorogenic Substrates

| | |
|---|---|
| Suc-Leu-Leu-Val-Tyr-AMC | Enzo Life Science (Lörrach, GER) |
| Z-Leu-Leu-Glu-AMC | Enzo Life Science (Lörrach, GER) |
| Boc-Leu-Arg-Arg-AMC | Enzo Life Science (Lörrach, GER) |
| Z-Gly-Gly-Leu-AMC | Bachem (Bubendorf, SUI) |

All substrates were dissolved in DMSO at concentrations of 20 mM and stored at −20 °C.

### 3.1.5 Instruments

| | |
|---|---|
| **Balances** | |
| Analytical balance TE124S | Sartorius (Göttingen, GER) |
| Precision balance BP3100 P | Sartorius (Göttingen, GER) |
| **Centrifuges** | |
| Biofuge Pico | Heraeus instruments (Hanau, GER) |
| SIGMA 4K15 rotor 11150/13220 and rotor 11150/13350 | SIGMA Laborzentrifugen (Osterode am Harz, GER) |
| SIGMA 6–16 K rotor 12500 | SIGMA Laborzentrifugen (Osterode am Harz, GER) |
| SIGMA 8 K rotor 11805 | SIGMA Laborzentrifugen (Osterode am Harz, GER) |
| SIGMA 3–30 K rotor 12150 | SIGMA Laborzentrifugen (Osterode am Harz, GER) |
| **Crystallography** | |
| Art Robbins instruments Phoenix | Dunn Labortechnik (Asbach, GER) |
| Cooled incubator series 3000 | RUMED Rubarth Apparate (Laatzen, GER) |
| Crystal Cap HT für CryoLoop | Hampton (Aliso Viejo, USA) |
| Crystal Cap HT Vial | Hampton (Aliso Viejo, USA) |
| Foam dewar | Spearlab (San Francisco, USA) |
| Magnetic Caps, Pins and Vials | Molecular dimensions (Newmarket, UK) |
| MICORLAB STARlet | Hamilton (Reno, USA) |
| Micro Tool Box | Molecular dimensions (Newmarket, UK) |
| Mounted CryoLoop | Hampton (Aliso Viejo, USA) |
| Quick Combi Sealer Plus | HJ-Bioanalytik (Mönchengladbach, GER) |
| Siliconized Glass Cover Slides | Hampton (Aliso Viejo, USA) |
| Storing dewar HC20 | Taylor-Wharton Germany (Mildestedt, GER) |
| Super Clear Pregreased 24 Well Plate | Crystalgen (New York, USA) |
| Vial clamp | Molecular Dimensions (Newmarket, UK) |
| Zoom stereo microscope SZX10/KL1500LCD | Olympus (Tokyo, JP) |
| **Electrophoresis and Blotting** | |
| Fastblot B44 | Biometra (Göttingen, GER) |
| Gel documentation system GBOX | Syngene (Cambridge, USA) |
| Mini PROTEAN Cell | BioRad (Hercules, USA) |
| PowerPAc Basic Power Supply | BioRad (Hercules, USA) |
| **Liquid chromatography** | |
| ÄKTAprime plus | GE Healthcare (Chalfont St. Giles, UK) |
| ÄKTApurifier | GE Healthcare (Chalfont St. Giles, UK) |
| CHT Ceramic Hydroxyapatite | BioRad (Hercules, USA) |
| HiPrep 26/10 desalting column | GE Healthcare (Chalfont St. Giles, UK) |
| Ni-NTA, 5 and 1 ml | GE Healthcare (Chalfont St. Giles, UK) |
| Phenyl Sepharose 6 Fast Flow | GE Healthcare (Chalfont St. Giles, UK) |
| RESOURCE Q, 6 and 1 ml | GE Healthcare (Chalfont St. Giles, UK) |
| **Peptide Synthesis** | |
| Alpha 2-4 LD plus lyophylization device | Christ (Osterode, GER) |
| Peptide synthesizer PS3 | Protein Technologies (Tucson, USA) |
| Rotavapor R215 | Büchi (Essen, GER) |

(continued)

(continued)

| | |
|---|---|
| **HPLC and mass spectroscopy** | |
| Binary pump system 1525 | Waters (Eschborn, GER) |
| Column selector | Waters (Eschborn, GER) |
| Flex Inject Loop | Waters (Eschborn, GER) |
| Fraction collector II | Waters (Eschborn, GER) |
| HPLC system Ultimate 3000 | Dionex (Idsetin, GER) |
| LCQ Fleet MS | Thermo Fisher (Schwerte, GER) |
| Xbridge BEH C18, 10 mm × 250 mm | Waters (Eschborn, GER) |
| Xbridge BEH C18, 2.1 mm × 250 mm | Waters (Eschborn, GER) |
| **NMR** | |
| Cryo NMR Ultrashield 500 plus | Bruker (Billerica, USA) |
| NMR Ultrashield 500 | Bruker (Billerica, USA) |
| NMR Tubes 5 mm Professional | Schott (Mainz, GER) |
| **Additional equipments and materials** | |
| Cary Eclipse Fluorescence spectrometer | Varian (Darmstadt, GER) |
| Constant Cell Disruption System E1061 | Constant Systems (Northants, UK) |
| Cold trap CT 02–50 SR | Buch and Holm (Herlev, DEN) |
| Infors HAT Multitron incubator | Infors (Einsbach, GER) |
| InoLab pH 720 pH-Meter | WTW (Weilheim, GER) |
| Laboklav 195-MV | SHP Steriltechnik AG (Detzel, GER) |
| Laboklav 25-MV | SHP Steriltechnik AG (Detzel, GER) |
| MR Hei-Standard Magentic stirrer | Heidolph (Schwabach, GER) |
| NanoPhotometer | Pearl IMPLEN (München, GER) |
| Shaking incubator Multitron | Infors HT (Bottmingen, SUI) |
| Speedvac, centrifuge RVC 2–25 CO plus, | Christ, (Osterode, GER) |
| Thermomixer comfort | Eppendorf (Hamburg, GER) |
| Vortex Genie 2 | Scientific Industries (New York, USA) |
| Vacuum pump MZ 2C NT | VacuBrand (Wertheim, GER) |
| White 96 well plate NUNC | Thermo scientific (München, GER) |
| Water purification device | TCA (Niederelbert, GER) |

### *3.1.6 Computer Software and Bioinformatic Tools*

| | |
|---|---|
| Breeze | Waters (Eschborn, GER) |
| CCP4i Software Suite | www.ccp4.ac.uk [5] |
| Chemdraw | Perkin Elmer (Cambridge, USA) |
| Chromäleon | Dionex (Idsetin, GER) |
| COOT | Emsley [6] |
| CorelDRAW X5 | Corel (Ottawa, CA) |
| Endnote X4 | Thomson Reuters (New York, USA) |
| Graph Pad Prism 5 | Graph Pad Sowtware (La Jolla, USA) |
| Main | Turk [7] |
| MestReNova 7 | Mestre Lab Research S.L. (Santiago de Compostela, SPA) |
| PyMOL | Schrödinger, LLC [8] |

(continued)

(continued)

| | |
|---|---|
| Sybyl | Tripos (St. Luis, USA) [9] |
| Unicorn LC software | GE Healthcare (Chalfont St. Giles, UK) |
| Xcalibur | Thermo Scientific (Waltham, USA) |
| XDS programme package | Kabsch (Heidelberg, Germany) [10] |

## 3.2 Generation of Peptide Substrates

### *3.2.1 Solid Phase Synthesis*

Two different types of Fmoc-based resins were used to create peptides of 5 to 15 amino acids. In case of free carboxylic acid C-termini, a polystyrene polymer with a 2-chlorotrityl alcohol linker was first swollen in dry DCM for one hour in a syringe sealed with a glass frit and a PTFE stopper. After discarding the DCM, the first amino acid was coupled by adding a solution of 2 eq. of the Fmoc-protected amino acid, HCTU and DIPEA in DCM for 6 h. The reaction was quenched by first washing with DCM /MeOH /DIPEA in a 17/2/1 ratio and subsequently with DCM, which in turn was evaporated.

In order to create amide C-termini, an Fmoc-protected Rink-amine resin was used. After swelling the resin for 1 h in DMF, the protection group was removed in 20 % (v/v) piperidine in DMF for 20 min and washed in DMF. The first amino acid was then coupled by incubation again with a solution of 2 eq. of the Fmoc-protected amino acid, HCTU and DIPEA in DMF for 3 h. The reaction solution was removed by washing with DMF and DCM and the resin was then dried under vacuum.

The amino acid coupling steps were carried out on a peptide synthesizer PS3 (Peptide Technologies) on a 0.2 mmol scale. Briefly, the resin was swollen in DMF for 1 h, followed by deprotection in a solution of 20 % (v/v) piperidine in DMF for 20 min. After washing with DMF, the resin was incubated with a fresh solution of HCTU and Fmoc-amino acid in 20 % (v/vl) N-methyl morpholine for 20–40 min and washed again with DMF. Synthesis of $^{13}C$ labeled substrates used an Fmoc-$^{13}C$(O)-phenylalanine building block (Santa Cruz). Protection groups of amino acid side chains were as follows: Arg (Pbf), Asn (Trt), Gln (Trt), Thr (OtBu), Ser (OtBu), Trp (Boc), Tyr (OtBu). After repeated elongation cycles, the N-terminal Fmoc protection group was removed, followed by washing with DCM. The resins were stored at −20 °C.

### *3.2.2 Resin Separation and Purification*

Rink amide resins were treated with 10 % (v/v) TFA, 2.5 % (v/v) TIS in DCM for some minutes and washed with the same mixture. The solvent was then evaporated and the resulting yellow oil was dissolved in 95 % (v/v) TFA with 2.5 % (v/v)

TIS and 2.5 % (v/v) water. This solution was stirred for at least 9 h at room temperature and further 24 h at 4 °C in order to remove all side chain protection groups. In contrast, the more stable trityl resins could directly be treated with a highly concentrated TFA solution and was incubated under the same conditions as the cleaved amides. The resin was finally washed with the cleavage solution.

The TFA solutions were subsequently transferred to 50 ml Falcon tubes, cooled on ice, and then complemented with approximately the same volume of cold diethyl ether. The precipitate could then be separated by centrifugation at 3,000 rpm for 10 min. The supernatant was discarded, the peptide redissolved in a small amount of TFA and the precipitation repeated.

Eventually, the precipitate was dried and redissolved in 5 % (v/v) ACN in 95 % (v/v) water. This solution was applied to preparative HPLC chromatography with a gradient of 5 % (v/v) ACN to 40 % ACN (v/v) over 100 min. Depending on their size and chemical nature, peptides typically eluted between 20 and 30 % ACN (v/v).

HPLC fractions were analyzed by ESI-MS analysis with positive and negative ion detection. Fractions were pooled accordingly and the solvent was removed by lyophylization overnight. The resulting white powder was dissolved in DMSO to concentrations of 20–100 mM, which were directly used in digestion assays and soaking experiments.

## 3.3 Protein Chemistry

### *3.3.1 Purification of the 20S Proteasome*

In order to purify wild type CP from yeast, the cells were dissolved in 2 times the pellet weight of 50 mM potassium phosphate buffer (pH 7.5, supplemented with DNAse I and disrupted in a French press device. The raw lysate was centrifuged at 41,000 g for 30 min. The supernatant could be further purified by filtration through a double layer of gossamer cloth.

The proteasome was then precipitated with a cold and saturated solution of ammonium sulphate, which was poured into the protein extract under vigorous stirring until the final concentration reached 40 % (w/v), which coincided with a general clouding of the solution. This suspension was then loaded on a 100 ml column of FF phenylsepharose, which had been equilibrated with 20 mM potassium phosphate (pH 7.5) in 1 M ammonium sulfate. The CP was then eluted in a gradient to a low salt buffer of 20 mM potassium phosphate over 400 ml. Proteasome-containing fractions were identified by fluorescence assays. Hereby, 30 µl of a fraction were incubated with 300 µM of a given AMC substrate at 37 °C for 20 min. The reaction was then quenched by addition of 700 µl of 20 mM Tris/HCl buffer (pH 7.5) and measured as described under 5.4.

The fractions were pooled and applied to a 15 ml CHT ceramic hydroxyapatite column, which was then eluted with 500 mM potassium phosphate (pH 7.5) in

a gradient over 120 ml. Again, fractions were pooled according to their activity profile and finally loaded on a 6 ml Resource-Q anion exchange column.

After rinsing with 20 mM Tris/HCl (pH 7.5), a gradient to 500 mM NaCl in 20 mM Tris/HCl (pH 7.5) was applied over 30 ml, in which the protein eluted at approximately 450 mM NaCl. If the proteasome was to be used for crystallization trials, a desalting step to 20 mM Tris /HCl (pH 7.5) had to be performed on a High Prep 26/10 desalting column and the protein was concentrated to 40 mg/ml by ultracentrifugation devices with a 300 kDa cut-off.

In case of the Pre2-$(His)_6$ yeast mutant strain, the cells were disrupted in 100 mM Tris/HCl (pH 7.5), 300 mM NaCl and 20 mM imidazole. Instead of an ammonium sulfate precipitation, the crude extract was loaded on a 5 ml Ni-NTA column, washed with the same buffer, and eluted in a 50 ml gradient to 500 mM Imidazol. Positive fractions were dialyzed overnight to 20 mM Tris/HCl (pH 7.5) and then applied to anion exchange chromatography as described above.

In contrast to the preparation steps for purifications from yeast cells, proteasome from erythrocytes had to be purified under milder conditions. Hence, crude blood was centrifuged at 500 g for 5 min and washed with PBS buffer containing 1 mM EDTA. The resulting pellet was resuspended in lysis buffer (155 mM ammonium chloride, 10 mM $KHCO_3$, 37 mg/l EDTA) and the cell debris was again centrifuged as described above. All following steps were performed according to the procedure for yeast proteasome purification.

### *3.3.2 SDS-PAGE Analysis*

Beside fluorescence assays, the purification procedure was monitored by SDS-PAGE analysis. Protein samples were mixed with Laemmli buffer [11], heated to 95 °C for 5 min and then centrifuged.

The samples, as well as a protein standard (Roti-Mark Standard, Carl Roth), were applied to a 12 % (w/v) polyacrylamide gel, which was run at 25 mA until the dye reached the end of the gel. The gel chamber was opened, the stacking gel removed, and the separating gel stained in Coomassie. Destaining was performed in boiling 10 % (v/v) acetic acid.

| Substance | 12 % Separating gel | Stacking gel |
|---|---|---|
| Water (ml) | 4.5 | 2.5 |
| 40 % Acrilamide (w/v) (Acrylamid /Bisacrylamide 29/1, ml) | 3 | 0.5 |
| Separating gel buffer (ml) | 2.5 | – |
| Stacking gel buffer (ml) | – | 2 |
| 10 % (w/v) APS (µl) | 50 | 50 |
| TEMED (µl) | 5 | 5 |

| | | |
|---|---|---|
| *Buffers* | | |
| Separating gel buffer | Tris/HCl pH 6.8 | 1.5 M |
| | SDS | 0.4 % (w/v) |
| Stacking gel buffer | Tris/HCl pH6.8 | 0.5 M |
| | SDS | 0.4 % (w/v) |
| Coomassie solution | Acetic acid | 10 % (v/v) |
| | Coomassie brilliant blue | 0.05 % (w/v) |
| | Isopropanol | 15 % (v/v) |
| 10 × Laemmli solution | Tris/HCl pH 6.8 | 60 mM |
| | Glycerol | 30 % (w/v) |
| | Saccharose | 10 % (w/v) |
| | SDS | 5 % (w/v) |
| | β-mercaptoethanol | 3 % (v/v) |
| | Bromophenol blue | 0.02 % (v/v) |
| 10 × running buffer | Glycine | 1.92 M |
| | SDS | 1 % (w/v) |
| | Tris | 0.25 M |

### *3.3.3 Determination of Protein Concentrations*

In order to record the protein concentration of a crude human cell lysate, the sample was diluted 1/1000 with buffer and then mixed with a freshly prepared and filtrated Bradford solution [12] (Biorad Protein Assay) and measured at 595 nM. The resulting absorption was compared to a calibration curve, which was recorded with BSA at various concentrations.

Alternatively, a defined dilution of the crude lysate was directly measured on a Pearl Implen NanoPhotometer and the absorptions at 260 and 280 nm were determined. The protein concentration could then be calculated using the Warburg equation.

If the measurement was performed on purified protein solutions, the absorption was directly measured at 280 nm and the protein concentration was calculated with the Lambert-Beer equation by using a theoretical absorption coefficient generated by the ProtParam tool supplied by expasy.com.

## 3.4 Activity Assays

### *3.4.1 Artificial Fluorescent Probes and $IC_{50}$ Measurements*

Point measurements and $IC_{50}$ curves of inhibitory substances were usually recorded using CP concentrations between 1 and 50 µg/ml in 100 mM Tris/HCl (pH 8.0), 10 % (w/v) DMSO and 0.01 % SDS (w/v). Serial dilution of inhibitors was carried out in DMSO at equal intervals on a logarithmic scale. Incubation of

yeast CP with inhibitors or DMSO as a control usually lasted for 1 h in a volume of 30 µl. Three replicas of each sample was pipetted into a white and flat-bottomed Nunc plate. AMC-substrate solutions in DMSO were pipetted to the side of the well and then centrifuged down to start all reactions simultaneously. In order to address the different proteolytic activities of the proteasome, either Suc-Leu-Leu-Val-Tyr-AMC or Ac-Gly-Gly-Leu-AMC was used for monitoring the β5 subunit, as well as Boc-Leu-Arg-Arg-AMC and Z-Leu-Leu-Glu-AMC for β2 and β1, respectively. Fluorescence development was stopped by adding 300 µl of a 20 mM Tris /HCl (pH 7.5) buffer to the wells and the plate was measured at a Varian Cary Eclipse Fluorescence Spectrometer with excitation and emission wavelengths at 360 and 460 nm. $IC_{50}$ curves were analyzed using the Graph Pad Prism 5 software using a Dose-response inhibition fit with variable slope.

### *3.4.2 Native Gel Fluorescence Analysis*

Reversibility and inhibition of the CP by isolated small molecules and crude extracts were carried out by monitoring the proteasomal activity in native gels. For this, 5–10 µg of the CP was incubated with inhibitors for a defined period of time, mixed with a native gel loading buffer and applied to a precast 3–15 % (w/v) gradient native gel (Bio-Rad). Gels were run at 25 mA for at least 2 h in native gel running buffer. The gel was then soaked with a solution of AMC substrate (200 µM in 100 mM Tris pH 8.0) for 1 min and the fluorescence was monitored in a gel documentation system (GBOX, Syngene) at 350 nm. Fluorescent bands indicated active proteasome, whereas weak or missing bands hinted to irreversible blockage. In contrast, reversible inhibitors diffused out of the gel during electrophoresis, thus leading to a fully recovered CP activity.

| | | |
|---|---|---|
| *Native gel loading buffer (2x)* | Tris | 62.5 mM |
| | Glycerol | 25 % (w/v) |
| | Bromophenol blue | 1 % (w/v) |
| *Native gel running buffer (1x)* | Tris | 25 mM |
| | Glycine | 192 mM |

### *3.4.3 SDS-PAGE Shift Assay*

Alternatively, covalent binding was monitored using a combination of SDS-PAGE gel shift and western blot analysis. For this purpose, 10 µg of Pre2-$(His)_6$ tagged proteasome was incubated with inhibitors for one to 6 h and submitted to SDS-gel electrophoresis as described in 5.3.2. In order to estimate the position of the analyzed β5 subunit, a prestained marker (Roti-Mark Standard Prestained, Carl Roth) was used. The separated subunits were then blotted on nitrocellulose at 100 mA

for 1 h in transfer buffer and stained with Ponceau S (Sigma Aldrich). The membrane was then treated with blocking solution for 1 h, followed by incubation with a primary rabbit anit-$(His)_6$ antibody (1/5000 in blocking buffer, Sigma Aldrich) for another hour. The membrane was then washed six times with TBS-Tween for 5 min and incubated with a secondary anti-rabbit antibody (1/10,000 in blocking buffer, Sigma Aldrich) dilution for 1 h. After washing with TBS-tween and TBS three times each, the membrane was laid in AP buffer and supplemented with 33 µl BCIP and 66 µl NBT for 5 min. The reaction was quenched by exchanging the reaction solution with destilled water. Covalent and irreversible adducts with the β5 subunit resulted in a band shift of usually 500 Da, which could clearly be distinguished if compared with a standard. Moreover, the proportion of bound to free subunits could be nicely followed over a certain range of inhibitor concentrations by the appearance of double bands.

| | | |
|---|---|---|
| *Blocking buffer* | Milk powder | 5 % (w/v) |
| | 10 × TBS | 10 % (v/v) |
| | Tween 20 | 0.1 % (w/v) |
| *Transfer buffer* | Methanol | 20 % (v/v) |
| | SDS-running buffer | 80 % (v/v) |
| *10 × TBS* | Tris/HCl pH 7.4 | 500 mM |
| | NaCl | 1500 mM |
| *TBS-tween* | 10 × TBS | 10 % (v/v) |
| | Tween 20 | 0.1 % (w/v) |
| *Ponceau S solution* | Acetic acid | 5 % (v/v) |
| | Ponceau red | 0.1 % (w/v) |

### *3.4.4 Peptide Digestion and Product Cleavage Pattern Analysis*

In order to analyze either the cleavage pattern of a peptide or assess the proteasomal activity, 50 µg/ml of yeast CP was incubated in 100 mM Tris /HCl pH 8.0, 0.01 % (w/v) SDS and 10 % (w/v) DMSO in which the respective peptide was dissolved to a final concentration of 1 mM. The mixture was incubated at 37 °C for 1–3 h, whereupon the reaction was stopped by removal of the enzyme. For this, the solution was filtered through a Centricon Centrifugal Filter Unit with a cutoff of 100 kDa and the filtrate was used to perform analytical HPLC runs with UV-VIS detection or LC-MS experiments. In the first case, 50–100 µl of the filtrate was applied on a 150 mm C-18 Xbridge column that was eluted with a gradient of 10–90 % buffer A (ACN plus 0.1 % TFA) in buffer B (water plus 0.1 % TFA) in 45 min. Depending on the size, peptides and peptide fragments eluted around 20 min. In order to identify the corresponding peptides, peaks of each peptide digestion were collected and measured by electron spray ionization mass spectrometry (ESI-MS) experiments. The reaction progress was then verified by

integrating the respective peaks at a wavelength of 280 nm and calculating their ratios that were corrected by the distinct extinction coefficients. Alternatively, the reaction progress could directly be determined by LC-MS runs. Due to the semi-quantitative character of the method, the concentration of the undigested peptide in the buffer solution was determined by UV-VIS spectrometry at 280 nm and the solution was then used as an external standard for all subsequent mass spectrometric measurements. At least three samples were taken from the digestion solution, quenched by filtration and applied to LC-MS. Hereby, 5 µl were injected on a C18 column (3.5, 4.6, 30 mm), which was eluted with a gradient of 10–90 % buffer A (ACN plus 0.1 % formic acid) in buffer B (water plus 0.1 % formic acid). Mass integration of the mother peptide was performed over the whole time period of the run and compared to the blank without digestion to monitor the reaction progress.

### *3.4.5 NMR Analysis of Labeled Peptide Substrates*

For all peptide digestion with NMR readout, a peptide with the sequence REEWNNFSSYPEI that was labeled with a $^{13}C$ isotope at the phenylalanine carbonyl position was used. The peptide sequence was derived from the digestion pattern of the murine JAK-1 kinase and adapted towards specificity for the yeast CP ChTL activity. Subunit specificity was confirmed in digestion experiments with the β5 specific boronic acid inhibitor MG262 Enzo Life Sciences. The peptide was either prepared by Fmoc chemistry or generously provided by Prof. Christian Becker (University of Vienna). In order to achieve maximum sensitivity for the screening of growth environments, the cleavage reaction was performed entirely in the buffered supernatant of the crude culture broth. In contrast, for tracking the progress of the purification of the metabolites, only 10 % of the reaction mixture contained the respective samples in organic solvent to prevent denaturation of the enzyme. In order to exclude any accumulation of detergent effects, no SDS was added for activation of the CP. Due to the low sensitivity of NMR spectroscopy, at least 1 mM of the $^{13}C$ labeled peptide had to be added and the concentration was verified by UV-VIS measurements at a wavelength of 280 nm. Analogous to digestion experiments with unlabeled peptides, the reaction mixture was incubated at 37 °C for 1–3 h and then ultrafiltrated to remove the proteasome and stop the digestion. A volume of 500 µl was supplemented with 50 µl $D_2O$ and inserted into an NMR vial. Samples were measured on a 500 MHz spectrometer (Bruker Topspin $^{13}C$-Cryo NMR) with a total number of scans between 500 and 1,000 and the resulting spectra were evaluated using MestReNova 7. Typically, the background signals derived from media components occurred in the range between 0 and 90 ppm with few exceptions that appeared up to 150 ppm. By contrast, the peaks originating from the $^{13}C$-labelled carbonyl amide educt and the carboxylic acid product appeared at 173 and 177 ppm, respectively. The residual proteasome

activity was then calculated by scaling the product to the educt peak compared to a blank digestion.

| Substance | Detection in culture broth | Purification analysis |
|---|---|---|
| Tris pH 8.0 (mM) | 100 | 100 |
| Peptide in DMSO (mM) | 1–2 | 1–2 |
| Supernatant/Solution in organic solvent (%) | 85 | 10 |
| Water (%) | – | 75 |
| Yeast CP µg/ml | 50 | 50 |

## 3.5 Isolation of Natural Products

### *3.5.1 Screening of Growth Conditions*

In order to elucidate a suitable molecular trigger to induce the biosynthesis of secondary metabolites in *P. luminescens*, various strategies were pursued. Bacteria were grown on $LB_0$ or 2xTY agar plates at room temperature overnight. This was then used to inoculate 3 ml cultures of various media. In one approach, standard compositions present in LB, TB or PDB media were used and the concentrations of the different ingredients were varied. Furthermore, additional triggers that have been described to be important for the development for virulence, such as iron(III)-chloride or L-proline, were added to the standardized culture broths. Moreover, different inorganic salts ranging from KCl to $MgSO_4$ were added in different amounts and both the temperature and the shaking velocities were varied. Finally, these cultures were used to inoculate a medium with altered parameters in order to simulate environmental changes.

| Media | Parameters and additives |
|---|---|
| Standard media | LB, 2xTY, CY, SRM, PDB, TYEA DSMZ media 1, 54, 220 |
| Changed parameters in these media | Sugar, casitone, peptone, yeast extract, and salt ingredients |
| Additives | Fructose, maltose, arbutin, sucrose, lactose, L-proline, L-arginine, Iron(III)-chloride, Iron(II)-chloride, soluble and insoluble magnesium and calcium salts |
| Other parameters | Temperature (18–34 °C in steps of 2 °C), rotation speed, incubation time (1–10 d), inoculation density |

### *3.5.2 Secretion and Purification of the Syrbactins CepI and GlbA*

In order to trigger the biosynthesis of the compounds, *P. luminescens* was first grown in TYEA medium at 28 °C for 3 d under continuous shaking. The culture was then used to inoculate TYEB medium at a ratio of 1:100, which was again incubated under the same conditions for further 3 d. In order to enrich the toxic

metabolites, 2 % (w/v) of hydrophobic resin beads (XAD-16) were added to the fermentation broth. After filtration, the beads were washed with water and the inhibitory compounds were eluted with EtOAc and MeOH.

The condensed extracts were then submitted to silica column purification (Silica Gel 60, Merck). After washing with cyclohexane, the column was eluted with EtOAc. All fractions were tested by proteasome assays and positive samples were combined and concentrated by evaporation. Polishing was achieved by final HPLC purification over a RP-C18 column to which a gradient from 10 % (v/v) buffer A [0.1 % (v/v) TFA in ACN] in 90 % (v/v) buffer B [water plus 0.1 % (v/v) TFA in water] to 70 % (v/v) buffer A within 60 min was applied. Fractions were again tested by NMR proteasome assays. The two active components GlbA and CepI eluted at approximately 55 % (v/v) ACN as nicely separated peaks.

### *3.5.3 LC-MS, 1D- and 2D-NMR Structure Elucidation*

After lyophylization of the solvent, the compounds were dissolved in D6-DMSO and submitted to structure analysis. In order to determine the purity of the compounds and elucidate their molecular weight, LC-MS runs were performed on a RP-C18 column using a gradient from 10 % buffer A (0.25 % formic acid in ACN) in buffer B (0.25 % formic acid in water) to 90 % buffer A in 10 min with ESI-MS detection.

As X-ray crystallographic data were not sufficient to reveal the chemical structure of the compounds, 2D-NMR experiments were performed at a concentration of 25 mM on a 500 MHz spectrometer. Proton couplings were analyzed by H,H-COSY measurements, which were combined with C-H assignments derived from decoupled C,H-HSQC analyses. Eventually, HMBC couplings were used to combine the derived fragments. Stereochemistry could then be assigned by a combination of crystallographic data and NMR analyses applying Karplus dependency.

## 3.6 Protein Crystallography

### *3.6.1 Crystallization of the Yeast 20S Proteasome*

Crystals of the yeast CP were produced in hanging drops at 20 °C using protein concentrations in the range of 40 mg/mL in Mes /NaOH (10 mM, pH 6.8) and EDTA (1 mM) as described previously [13, 14]. Drops contained a 1:1 mixture of protein to reservoir solution (30 mM magnesium acetate, 100 mM morpholinoethane-sulfonic acid (pH 6.8) and 10 % (w/v) 2-methyl-2, 4-pentanediol). Grown crystals reached their maximum size after 2 d and could directly be soaked with inhibitors in DMSO at final concentrations of 2–10 mM for at least 24 h. Subsequently, crystal droplets were supplemented with cryoprotection buffer

(30 % (w/v) 2-methyl-2,4-pentanediol, 20 mM magnesium acetate, 100 mM morpholino-ethane-sulfonic acid, pH 6.9) and supercooled in liquid nitrogen for storage.

### *3.6.2 Data Collection, Processing and Structure Determination*

Datasets were collected from the CP:CepI, the CP:GlbA and the CP:SylA-GlbA complexes with resolutions of 2.8, 3.0 and 2.8 Å, respectively, by using synchrotron radiation ($\lambda = 1.0$ Å) at the X06SA-beamline (Swiss Light Source, Villingen, Switzerland) equipped with a Pilatus 6 M detector and a 100 K nitrogen cryoprotection system. Cell parameters in the space group $P2_1$ were determined to be approximately a = 134 Å, b = 301 Å, c = 144 Å, and $\beta = 112°$. Assessment of reflection intensities and data reduction were carried out with the XDS programme package [10].

The anisotropy of diffraction was corrected by an overall anisotropic temperature factor by comparing observed and calculated structure amplitudes using the program CNS [15]. Conventional crystallographic rigid body calculations were carried out with CNS using the yeast CP structure as starting model (PDB accession code 1RYP), followed by positional and temperature factor refinements that took into account the 2-fold non-crystallographic symmetry axis. Model building was performed with the programmes MAIN [7] and COOT [6] for the overall structure, whereas the non-peptidic ligands were built with SYBYL [9]. Water molecules were automatically added with ARP/WARP and the overall quality of the structure was scrutinized using PROCHECK [5]. Figures were generated by using the programs MOLSCRIPT [16] and BOBSCRIPT [17]. The coordinates of the published structures were deposited at the PDB under the accession codes 4FZC (CepI), 4FZG (GlbA) and 4GK7 (SylA-GlbA).

## 3.7 Cell Culture Experiments

### *3.7.1 Cell Viability Assays and Kinetic Experiments*

For cytotoxicity measurements, HeLa cells were seeded on a 24-well plate to cell densities of 5,000 cells /well in DMEM medium supplemented with 10 % (v/v) FBS. After incubation for 24 h, the medium was exchanged and the inhibitors were added to various concentrations but with a final content of 1 % (v/v) DMSO. After an additional incubation period of 48 h, the medium was again exchanged and supplemented with 10 % (v/v) Alamar blue reagent (Sigma Aldrich). Assay development was accomplished after approximately 2 h and the residual cell

viability titer could be elucidated by recording the fluorescence at 575 and 585 nm excitation and emission wavelengths, respectively.

Evaluation of the time-dependent cytotoxicity of the inhibitory compounds was similarly performed by Alamar blue assays but with a uniform inhibitor concentration of 1 μM for all compounds. The cell viability was evaluated after various time intervals, ranging from 6 to 48 h and standardized against an untreated culture.

### *3.7.2 NF-κB Pathway Analysis*

For intracellular evaluation of the IκBα accumulation, HeLa cells were treated with 40 μM of the inhibitor for 6 h and then stimulated by the addition of 30 ng/mL IL-1 for 20 min. After washing with PBS, cells were trypsinized, washed again and collected by centrifugation. Cells were lyzed by the addition of 40 μl of mammalian protein extraction kit solution (M-Per). Cell debris was subsequently removed by centrifugation at 15,000 g for 5 min and protein concentration was determined by standard Bradford assays. A total amount of 10 μg of protein was separated by SDS-PAGE analysis and blotted on a PVDF membrane, which was in turn developed by the addition of IκB antibodies (Sigma Aldrich) followed by treatment with a horseradish peroxidase-coupled secondary antibody and ECL solution. Chemoluminescence was recorded at 430 nm on a BioMax® Light Films device.

For standardization of the western blot, the housekeeper protein GAPDH was co-evaluated. The PVDF membrane was stripped with Tween-20 in a solution of 5 % (w/v) milk powder overnight and treated with GAPDH antibodies. Detection was achieved by development with horseradish peroxidase and ECL reagent.

## References

1. W. Heinemeyer, M. Fischer, T. Krimmer, U. Stachon, D.H. Wolf, J. Biol. Chem. **272**, 25200–25209 (1997)
2. W. Heinemeyer, J.A. Kleinschmidt, J. Saidowsky, C. Escher, D.H. Wolf, EMBO j. **10**, 555–562 (1991)
3. D.C. Gross, J.E. DeVay, J. Appl. Bacteriol. **43**, 453–463 (1977)
4. M. Fischer-Le Saux, V. Viallard, B. Brunel, P. Normand, N. E. Boemare, Int J Syst. Bacteriol. 49 Pt 4, 1645–1656 (1999)
5. Acta Crystallogr. Sect. D—Biol. Crystallogr. 50, 486–501
6. P. Emsley, B. Lohkamp, W. G. Scott, K. Cowtan, Acta crystallographica. Section D, Biol. crystallogr. **66**, 486–501 (2010)
7. D. Turk, Ph.D. thesis, Technische Universität München, 1992
8. W.L. DeLano, *The PyMOL molecular graphics system* (DeLano Scientific, San Carlos, 2002)
9. S. H. R. SYBYL 8.0 Tripos International, St. Louis, Missouri, 63144, Usai, G
10. W. Kabsch, Acta Crystallogr. D Biol. Crystallogr. **66**, 125–132 (2010)
11. U.K. Laemmli, Nature **227**, 680–685 (1970)
12. M.M. Bradford, Anal. Biochem. **72**, 248–254 (1976)

13. M. Groll, L. Ditzel, J. Löwe, D. Stock, M. Bochtler, H. Bartunik, R. Huber, Nature **386**, 463–471 (1997)
14. M. Groll, R. Huber, Methods Enzymol. **398**, 329–336 (2005)
15. A.T. Brünger, P.D. Adams, G.M. Clore, W.L. DeLano, P. Gros, R.W. Grosse-Kunstleve, J.S. Jiang, J. Kuszewski, M. Nilges, N.S. Pannu, R.J. Read, L.M. Rice, T. Simonson, G.L. Warren, Acta Crystallogr. D Biol. Crystallogr. **54**, 905–921 (1998)
16. P.J. Kraulis, J. Appl. Crystallogr. **24**, 946–950 (1991)
17. R.M. Esnouf, J. Mol. Graph. Model. **15**(132–134), 112–133 (1997)

# Chapter 4
# Results

## 4.1 Development of a NMR-Based Proteasome Assay

### *4.1.1 Peptide Design and Digestion Analyses*

Initially, a suitable subunit-selective peptide sequence had to be established, which then served as a scaffold for the NMR-active substrate. Although the general cleavage specificities of the three proteasomal activities have been determined, it is still not possible to theoretically predict the digestion pattern of a given peptide sequence. This is not only caused by the lack of information on the primed site, but also by the complex interactions within the S1–S4 pockets. Therefore, the sequence for the peptide substrate was not designed de novo, but deferred from the cleavage pattern of the murine JAK-1 kinase, a well-characterized natural substrate of the proteasome [1]. Furthermore, the peptide was adapted for specificity towards the ChTL activity, as inhibitors of the corresponding β5 subunit exert strong cytotoxic activities and influence the adaptive immune response by attenuating the MHC-I presentation (Fig. 4.1a) [2].

In order to assess the cleavage sites and the kinetics of the substrate turnover, the digestion pattern of the peptide was determined by LC-MS analyses. Hereby, yeast wild type proteasome (50 µg/ml) was incubated with the substrate (1 mM) at 37 °C for various points of time and the reaction was stopped by ultrafiltration through a 100 kDa cut-off membrane. Subsequently, a standardized amount of the filtrate was submitted to HPLC analysis (Fig. 4.1b). Whereas fragment identification was carried out by mass spectrometry, quantifications were usually performed by integration of the UV-VIS signals at 280 nm using theoretical extinction coefficients.

As expected, the major cleavage site of the peptide appeared after phenylalanine, which was kept conserved also in the altered sequence. Interestingly, no cleavage was detected after tyrosine, thereby pronouncing the unpredictability of proteasomal hydrolysis sites in the primary structure. Additionally, and in contrast to the original peptide, cutting after tryptophan occurs as a minor side reaction that is, however, only relevant for prolonged digestion periods.

M. L. Stein, *NMR-Bioassay Guided Isolation of the Natural 20S Proteasome Inhibitors from Photorhabdus Luminescens*, Springer Theses, DOI: 10.1007/978-3-319-07914-1_4,
© Springer International Publishing Switzerland 2014

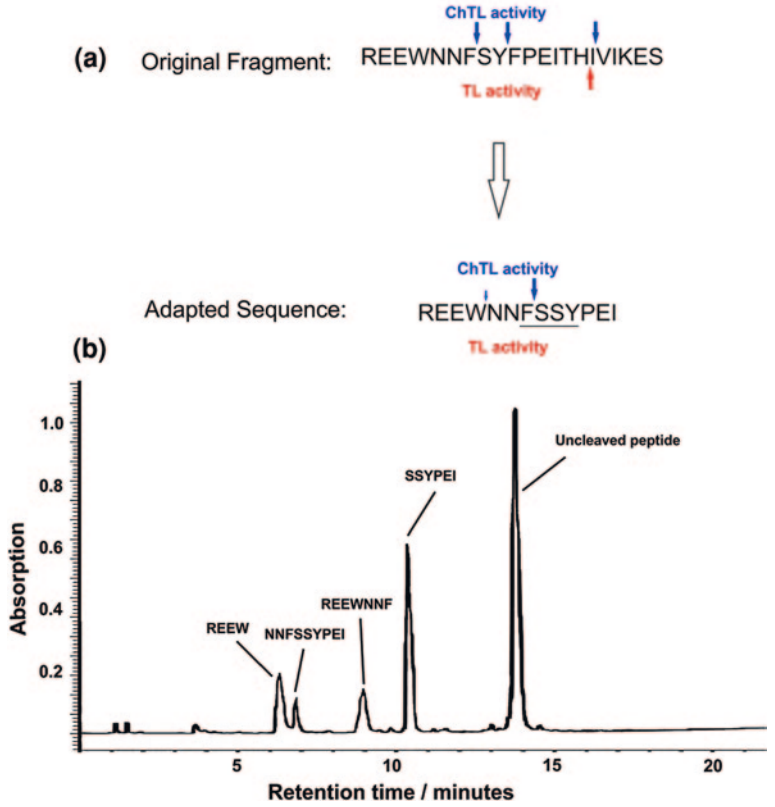


**Fig. 4.1** Peptide digestion analyses. **a** The peptide was shortened compared to the original murine fragment and its sequence altered (region underlined) to increase subunit specificity. *Blue* and *red arrows* indicate proteolytic cleavage sites of the proteasomal ChTL and TL activities, respectively. **b** Digestion experiments were evaluated by HPLC analyses and quantified by integration of the educt and product peaks. Peptides were identified by ESI-MS measurements. The main hydrolysis site is located after phenylalanine, whereas cleavage after tryptophan occurs only to a minor proportion of approximately 5 %

In order to investigate the contribution of the different proteolytic activities, the digestion was assessed with inactivated T1A mutants of both the β2 and β5 subunits. Whereas β5 harbors an intrinsic specificity for hydrophobic residues, β2 has been shown to accept a broad range of suitable substrates ranging from basic to branched hydrophobic residues. Interestingly, both the β5-T1A and the β2-T1A mutants exhibited an unchanged digestion pattern. As the T1A mutation of both mutants could be confirmed by sequencing, the observed activity of the β5-T1A mutant remains elusive.

Yet, as the corresponding yeast strain is barely viable, spontaneous mutations in the other subunits frequently occurred during fermentation, thereby possibly altering their respective substrate specificities. Moreover, substitution of the β5-T1A

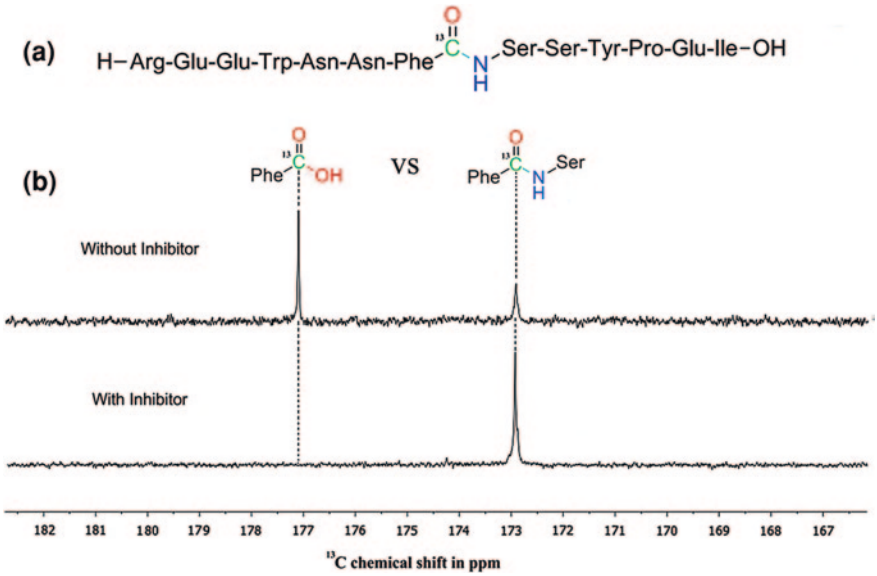


**Fig. 4.2** NMR peptide assay. **a** Primary sequence of the substrate with the scissile peptide bond and the $^{13}$C-label. **b** NMR spectrum of substrate digestions with the uncleaved educt and the carboxylic acid product at 173 and 177 ppm, respectively (*Upper*). Product peak formation is suppressed upon addition of a CP-inhibiting compound (*Lower*). Figure adopted from Stein et al. [4]

strain with the equally ChTL deprived Pre1-1 (S142F) [3] mutant completely prevented the digestion.

Due to slightly inconclusive data derived from proteasome mutants, the specificities were also evaluated chemically by using subunit selective inhibitors. Addition of 100 nm of SylA, which blocks only the ChTL and TL activities at this concentration, completely suppresses the reaction, thereby also directly excluding the β1 subunits as potential reaction participant. Eventually, digestion of the peptide is prevented in presence of the β5 specific inhibitor MG262, which carries a boronic acid as C-terminal pharmacophore on a Z–Leu–Leu–Leu backbone, thus confirming the specificity of the peptide towards the ChTL activity. Additionally, subsequent complex structure elucidation with the β5-T1A proteasome validated binding of the peptide into the β5 subunit.

### *4.1.2 NMR Analysis of the Cleavage Reaction*

In order to allow for an NMR based readout, the substrate was then atom-selectively labeled with a $^{13}$C-probe at the scissile peptide bond (Fig. 4.2a). Thus, the reaction progress can be qualitatively and quantitatively evaluated by a peak shift from 173 to 177 ppm corresponding to the amide educt and the carbonic acid

product, respectively. Due to the enrichment with the $^{13}$C-isotope, the background-to-noise ratio is extraordinary high and the downfield range of the chemical shift prevents interference with compounds present in the matrix (Fig. 4.2b). Large scale chemical synthesis of the peptide could be achieved by standard Fmoc- or Boc-based peptide solid phase chemistry using the labeled amino acid precursor (Sigma Aldrich) with yields ranging between 30 and 50 %.

Despite the undisputed insensitivity of NMR, peptide concentrations could be kept below 5 mM, thereby limiting the consumption of isotope-labeled material. Digestion experiments were performed within few hours and the recording time on a 500-MHz NMR spectrometer, equipped with an auto-sampler, was only around 15 min per sample, thereby allowing the analysis of a typical number of 96 samples per day. Eventually, the small required volume of only 500 µl enabled the screening of a large number of growth conditions and fermentation strategies.

### *4.1.3 Primary Sequence Optimization*

Aiming at simplifying the sequence and accelerating the catalytic turnover of the substrate, the peptide was further optimized by truncation and site-directed mutagenesis. As the interactions of the proteasomal binding channels with peptide extend from the P1 to the P4 residue of both substrates and inhibitors, the N-terminus was shortened accordingly. On the other hand, the C-terminus was reduced to three residues to avoid detrimental contributions by the proline residue. By this size reduction from a 13-meric peptide to a heptamer, the synthesis yield was considerably improved. Moreover, the catalysis rate was increased by a factor of 2–3, which may be attributed to the improved diffusion properties of the shortened construct.

Additionally, single-site mutagenesis was applied to improve binding to the β5 substrate channel. Preliminary, only the unprimed positions were altered, as these sites have been described as the major determinants for selectivity and kinetics. However, no significant improvements could be achieved, as the peptide sequence obviously ranged within the previously determined optimum [5]. Interestingly, however, further truncation of the N-terminus to three residues substantially slowed down the digestion progress.

In contrast, mutations of the primed-site residues enhanced proteolysis both with regard to kinetics and cleavage site selectivity (Fig. 4.3a).

Especially the P1’ position turned out to be crucial for both aspects. Trying to increase the hydrophobic character of P1’ and thus enhance interactions with the lipophilic binding channel, S1’F and S1’M mutations were introduced. However, these led to a significant proteolytic frame shift to a cleavage after P1’. Contrary, a size reduction of P1 to alanine accelerated the catalytic turnover and even prevented the minor hydrolysis after tryptophan present in the untruncated substrate. Mutations in P2’, however, did not alter the regioselectivity, but still substantially influenced the reaction kinetics. Generally, hydrophobic residues such as leucine or tyrosine were preferred over small hydrophilic amino acids (Fig. 4.3b).

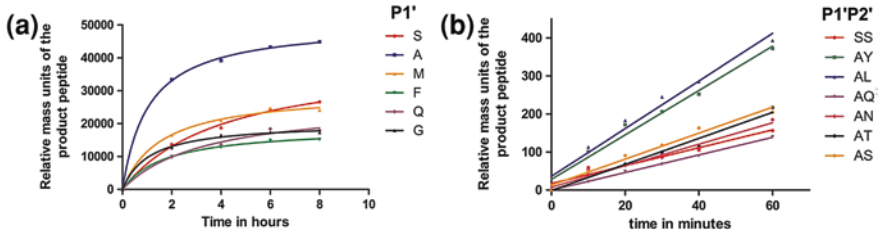


**Fig. 4.3** Kinetic measurements of substrates. The digestion progress was evaluated by LC-MS analysis. Due to the semi-quantitative character of the technique, the produced N-terminal peptide was used as a standard. **a** Mutagenesis of the first primed site (P1') has a massive impact on substrate turnover. Especially small amino acids like alanine are favored. Bulky side chains as in methionine, phenylalanine or glutamine lead to a plentitude of side products as they change the proteolytic frame. The final concentrations of the detected N-terminal peptides differ considerable due to these side reactions that yield alternative fragments. **b** Alteration of the P2' residue also influences the kinetics, but has no effect on the regioselectivity of the cleavage. Therefore, only the initial turnover rates were monitored. The experiment clearly shows that P1' has a greater influence on the reaction than P2'. However, also the latter has a direct and substantial impact on cleavage kinetics

The results gained by these experiments were surprising, as only the non-primed sites have been described to determine the regioselectivity and kinetics of the proteolytic cleavage. On the other hand, complex structures of the proteasome with belactosin C have hinted at the presence of primed site binding pockets, which can be addressed to generate considerable binding strengths of the corresponding ligands [6].

## 4.2 Assay Verification in a Real-Case Scenario

### *4.2.1 Detection of SylA in Cultures of P. syringae by Orthogonal Methodologies*

For evaluation of the assay by a positive control, culture media of *P. syringae*, the well-known producer of the potent proteasome inhibitor SylA [7], were analyzed. The plant pathogenic bacteria were grown in $SRM_{AF}$ medium containing the phenolic sugar arbutin present in the leaves of its host organisms for induction of the pathogenic phase [8, 9]. In order to pre-assess the concentration of SylA by independent and orthogonal methods, the fermentation broth was initially tested by in-gel fluorescence and western blot analyses.

Therefore, a native PAGE followed by subsequent fluorescence staining was performed. In detail, 5 µg of WT proteasome were mixed with different concentrations of the crude growth medium and submitted to a native gel. The gel was run for several hours and developed by addition of a solution of the Suc–Leu–Leu–Val–Tyr-AMC fluorescent substrate in 100 mM Tris /HCl pH 8.0. The gel was

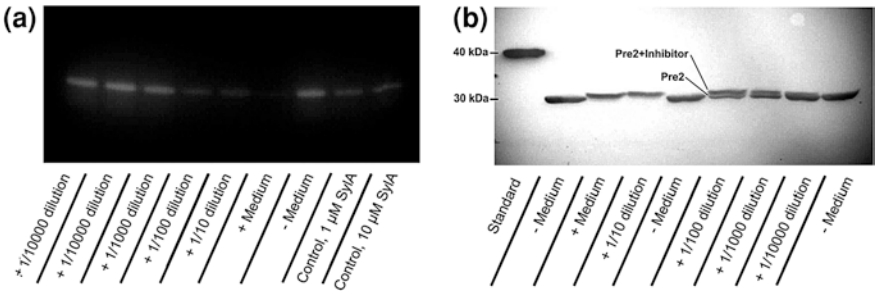


**Fig. 4.4** Orthogonal gel assays. **a** Native gel with fluorescent dye development. Increasing concentrations of SylA suppresses fluorescence. Comparison with standardized concentrations reveals that the medium contains SylA in the micromolar range. **b** Gel shift assay in denaturing SDS-PAGE using a Pre2-$(His)_6$ mutant. The β5 subunit is selectively stained in a western blot by $(His)_6$-antibodies. The gel shift confirms the covalent attachment of SylA to the β5 subunit and the extent of the shift hints at an inhibitor size of approximately 0.5 kDa

incubated for 1 min and scanned with a fluorescence detection device (Fig. 4.4a). Due to the high affinity and covalent attachment of SylA to the proteasomal subunits, the inhibitor stays bound to the protein during electrophoresis and suppresses fluorescence development. Moreover, the intensity of the bands can directly be correlated to the residual proteasome activity, thereby permitting an estimation of the $IC_{50}$ value that ranges at an approximate dilution of 1/100 of the crude fermentation broth. Alternatively, different dilutions of the growth medium were incubated with a proteasome mutant carrying a C-terminal β5-$(His)_6$ tag and submitted to a denaturing SDS-gel. After blotting to a nitrocellulose membrane and immunostaining with $(His)_6$-antibodies, a clear band shift was visible (Fig. 4.4b).

Staying attached to the denatured subunit even during electrophoresis demonstrates the irreversible character of the inhibitor, which forms a stable ether adduct to Thr-1$O^{\gamma}$. Interestingly, a second band corresponding to the unaltered β5-subunit appeared at higher dilutions, thereby also allowing a semi-quantitative evaluation of the $IC_{50}$ value, which is in good agreement with the gel fluorescence technique. As SylA inhibits the proteasome at low micromolar values, the inhibitor concentration in the fermentation broth could be determined to be in the high micromolar range. This was confirmed by isolation and subsequent quantification of the inhibitor to approximately 130 µM in the lab of Prof. R. Dudler (University of Zürich) as described previously by Wäspi et al. [7].

### *4.2.2 Analysis of SylA Concentrations by NMR Assays*

Subsequent to the determination of the SylA concentration in the medium of *P. syringae*, the NMR assay was utilized to analyse the sample in order to assess the sensitivity and reproducibility of the newly developed technique (Fig. 4.5a).

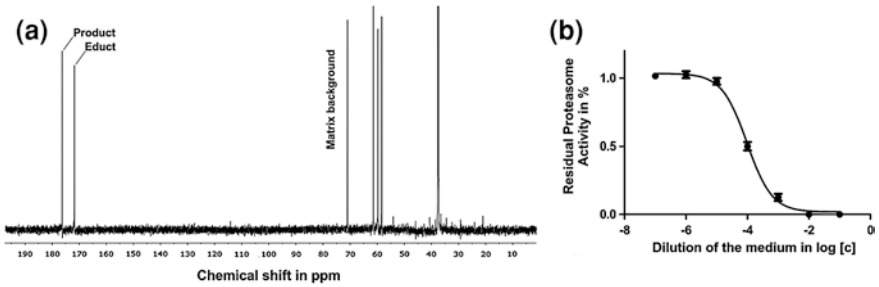


**Fig. 4.5** Analysis of *P. syringae* extracts by the NMR assay. **a** Full $^{13}$C-NMR spectrum of an exemplary digestion. The signal-to-noise ratio of the product and educt peaks (*extreme left*) is very high and no interference occurs with components of the medium or the buffer (*peaks on the right*). **b** The serial dilution of the medium demonstrates that the assay is able to detect even trace amount of the inhibitor in the crude matrix

Therefore, the sterile-filtrated culture broth was added to the assay mixture containing yeast CP and pre-incubated for only ten minutes. Subsequently, $^{13}$C-labeld substrate was added and the digestion was again incubated at 37 °C for few hours and quenched by ultrafiltration.

Notably, the signal-to-noise ratio is very high even in the presence of huge concentrations of the raw fermentation broth. Signals derived from buffer components or the crude sample matrix appear in the upfield region of the spectrum between 20 and 80 ppm, thereby avoiding interference with the spectral range of the educt and the product peak. Unlike commonly applied UV-VIS-based techniques, the readout unambiguously confirmed the presence of a strong inhibiting substance by the complete suppression of product peak formation.

Owing to the low enzyme content of only 50 µg/ml, even final inhibitor dilutions of $1/10^4$ were nicely detectable compared to $1/10^2$ for the orthogonal techniques, thereby enabling an extremely sensitive readout. By integration of the respective peaks and standardization to a blank sample, the assay result could be easily quantified and the $IC_{50}$ value was determined (Fig. 4.5b). In contrast to the gel shift assays, whose execution is rather tedious and time consuming, the performance of the NMR technique reliably yielded an unambiguous result.

Interestingly, the strong inhibition cannot be solely explained by the presence of SylA, but might hint at the presence of other inhibiting compounds, such as SylB, which lacks an electrophilic Michael system and would hence not be detectable by the techniques describe above. This was supported by the defined addition of SylA to *P. syringae* medium containing no inhibitors and the subsequent analysis of the mixture by the NMR assay, which resulted in a higher $IC_{50}$ value.

The direct comparison of the NMR technique with the gel fluorescence and the western blot analysis therefore pronounces the high sensitivity and robustness of the assay, which is able to detect both reversible and irreversible compounds in extremely diverse mixtures that may contain a plethora of other substances, which often substantially interfere especially with UV-VIS based methods.

## 4.3 Induction of Proteasome Inhibitor Secretion in *P. luminescens*

### *4.3.1 Triggering the Pathogenic Phase in Photorhabdus*

Next, the NMR assay was applied for the analysis of growth media of the insect pathogen *Photorhabdus luminescens*. The bacterium was grown in $SRM_{AF}$ medium that induces the pathogenic phase and in turn inhibitor secretion in *Pseudomonas syringae*. Harbouring a similar gene cluster as required for SylA production, *Photorhabdus* had been argued to produce a member of the syrbactin family and was suggested to react to the same molecular stimulus for the induction of its biosynthesis. However, no inhibitor secretion could be detected by applying the established NMR assay on *P. luminescens* cultures treated with $SRM_{AF}$ medium. Moreover, also the application of the previously described conditions for the isolation of GlbA from *Burkholderia* strain K481-B101 did not result in the secretion of an inhibitory molecule, thereby hinting at the divergent evolution of the sensory systems of these species to adapt to their respective host organisms, as well as the differing chemical environments during their life-cycles.

*Photorhabdus* obviously required a different molecular trigger present in insects to spark off its pathogenic phase. Therefore, numerous fermentation strategies were performed and the supernatants were evaluated by the NMR assay. Hereby, the bacteria were grown in a variety of standard media, such as 2xTY, TB or PDB, and incubated for different time intervals at various temperatures. Furthermore, additives that have been described to confer virulence to other pathogenic organisms, such as Fe(III)-chloride, as well as L-proline, which had been shown to influence to pattern of secondary metabolites in *Photorhabdus* [10] were added.

Surprisingly, no secretion of any CP-inhibiting compounds could be detected by the NMR-based assay. Comparison with standard absorption or fluorescence assays, however, again demonstrated the robustness of the assay especially against pigments, whose colour ranged from dark red to marine blue (Fig. 4.6a).

Thus, successive combinations of the growth conditions described above were analyzed with regard to the biphasic life-cycle of the bacterium. *Photorhabdus* was grown for 3 d in liquid medium, whereupon this culture was used to inoculate a second vial with a ratio of 1/100. This fermentation was incubated for another 3 d, centrifuged, sterile-filtrated and analysed by the NMR assay. Eventually, this approach proved to be successful by the identification of an osmotic shock from high to low salt concentrations, which sufficiently mimicked the intrusion into the insect body and consequently induced inhibitor secretion. Interestingly, the bacteria also started the excretion of red pigments, which have been described in literature as warning signal against other scavenging organisms to deter them from the consumption of the killed insect larvae [11, 12].

Peptide digestion was completely suppressed in the assay even at higher dilutions, thereby hinting at the presence of extremely powerful inhibitory components. Inhibitor secretion was detectable already few hours after the inoculation of the low salt medium and rose to a constant value after few days.

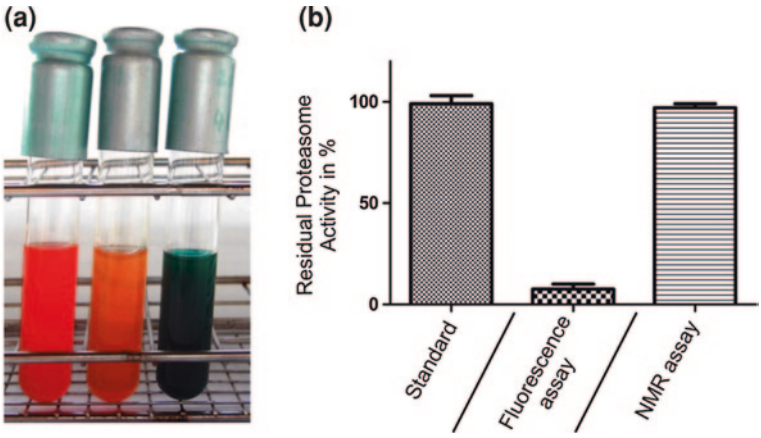


**Fig. 4.6** Quenching of conventional proteasome assays. **a** *Photorhabdus* produces a whole variety of intensely coloured pigments, which quench the chromogenic molecules detected in these assay techniques [4]. **b** The NMR assay demonstrates its superiority over these methods by avoiding the plenitude of false positive assay results

### *4.3.2 Isolation and Structure Elucidation of the Natural Proteasome Inhibitors*

The CP-inhibiting compounds were identified by establishing a procedure for their isolation from liquid broth [13]. Despite attempts to further optimize the fermentation strategy, the CP inhibitors were only secreted in low concentrations, which never rose above nanomolar values. Hence, a solid adsorber resin (XAD-16) was added to the growth medium directly after the osmotic shock. Thereby, the inhibitors were considerably enriched and could be easily regained by filtration of the medium, followed by washing of the resin beads with water and elution of the hydrophobic adsorbates with EtOAc and MeOH. The concentrated extracts were then applied to a silica column (Silica Gel60 by Merck).

The column was washed with cyclohexane and eluted with EtOAc. Due to the co-adsorption of many pigments, all fractions had to be tested by the NMR assay (Fig. 4.7a). Active fractions were pooled and submitted to preparative HPLC purification (RP-C18, 150 mm, 1 cm i.d., 3.5 µm) with a gradient of 10–70 % (v/v) ACN within 60 min.

Again, fractions were tested by the NMR assay. Intriguingly, two inhibiting compounds of equal amount could be separated, which eluted at approximately 55 % ACN (Fig. 4.7b) and whose yield could be augmented by the solid adsorption approach to 10 mg from 3 L culture broth each. Mass spectrometrical analyses showed that the compounds exhibited masses of 520 and 534 g/mol, respectively.

In order to reconfirm the accuracy of our NMR assay, LC-MS runs of an induced culture were recorded in direct comparison with a culture that was continuously grown at high salt conditions. These demonstrated that the compounds are only secreted if the osmotic trigger is applied (Fig. 4.8). Moreover, the elution

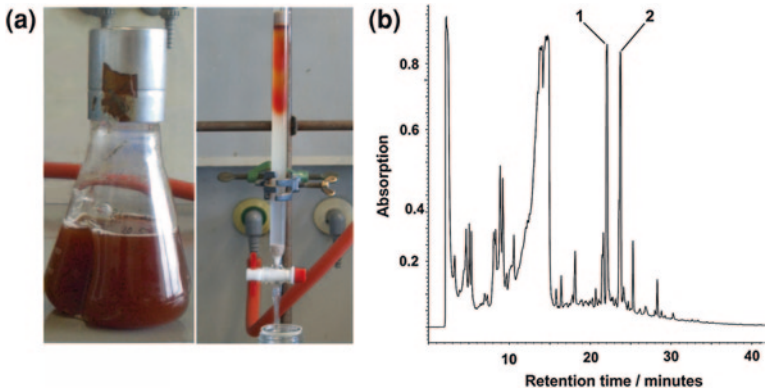


**Fig. 4.7** Column purification of the inhibiting substances. **a** The growth medium of *Photorhabdus* occurs as non-transparent and extremely colourful suspensions. Silica column chromatography of the solid resin extract displays the variety of pigments produced by the bacterium, thereby making the NMR-based assay an indispensable tool for fraction analysis [13]. **b** HPLC polishing of the active fractions. Two highly potent and lipophilic substances could be separated, which corresponded to the masses 520 and 534 g/mol. Figure adapted from Stein et al. [13]

profiles display an altered spectrum of secondary metabolites in the area between 20 and 40 min, thus reflecting a complete switch of the life-cycle of the bacterium and the induction of the virulent phase.

The LC-MS runs verify that the proteasome inhibitors are only produced in trace amounts compared to other compounds in the medium. Although the natural products were previously enriched by the solid phase adsorption method and purified by silica column purification, their detection by mass spectrometry is extremely difficult, whereas the NMR assay is already able to unambiguously determine their content in the crude culture broth.

In conclusion, although a high number of growth conditions were analysed, only an osmotic shock was able to trigger the shift from quiescence to pathogenicity, thus demonstrating the rigidity and strict regulation of inhibitor production and secretion. Furthermore, as there is no consensus between *Burkholderia*, *Pseudomonas* and *Photorhabdus* with regard to their respective environmental stimuli, their sensory systems reflect the adaptation of these bacteria to their different environments.

## 4.4 Functional and Structural Characterization of CepI and GlbA

### *4.4.1 Structure Elucidation by 2D-NMR Spectroscopy*

After the successful isolation of the compounds, their respective structures were elucidated by 2D-NMR spectroscopy. A 25 mM solution of both inhibitors in $D_6$-DMSO was prepared and the H,H-COSY, H,C-HSQC and H,C-HMBC spectra were

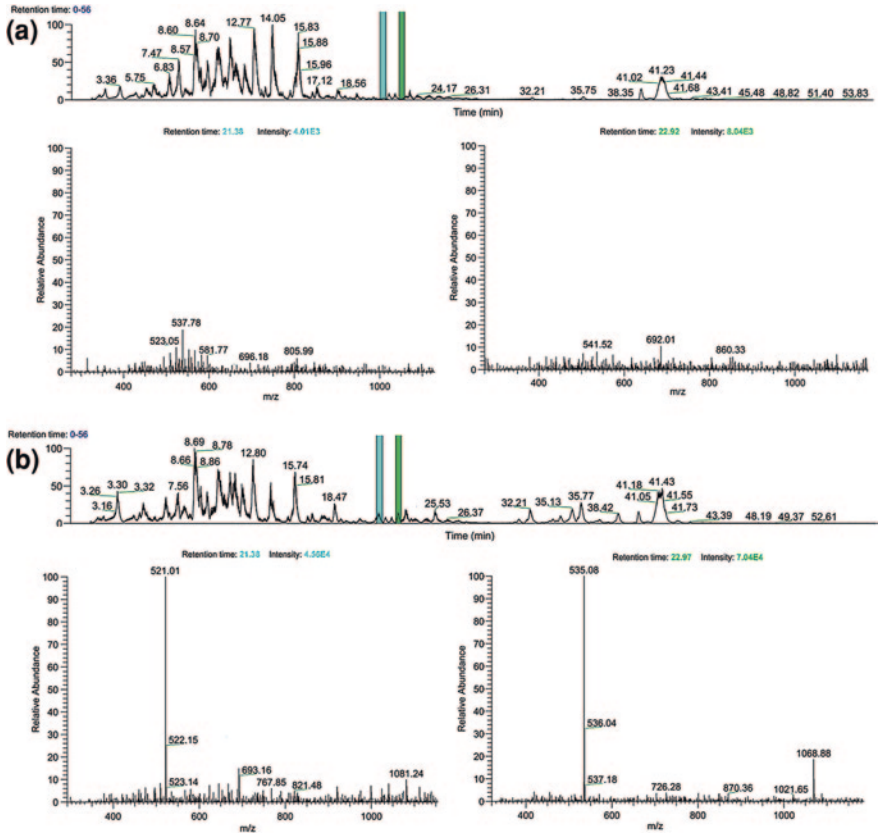


**Fig. 4.8** Mass spectrometrical analyses of *P. luminescens* cultures. **a** Under normal growth conditions, inhibitor secretion can be detected neither by the NMR assay nor by the downstream accumulation and LC-MS analysis. **b** After the induction by a suitable environmental stimulus, *Photorhabdus* starts to dramatically change its spectrum of secondary metabolites. Whereas the range between 0 and 20 min stays unaltered in the chromatogram, a whole array of additional substances can be visualized in the area between 20 and 40 min retention time. Among these, the highly potent proteasome inhibitors are also produced in trace amounts (*blue* and *green* interval corresponding to the masses of 521 and 535 g/mol). Even by LC-MS analysis, the compounds can only be visualized after their enrichment by the solid resin and silica column purification step, whereas the NMR assay is able to already detect them in the highly heterogeneous culture broth. Figure adopted from Stein et al. [4]

recorded on a 500 MHz spectrometer. This resulted in the identification of glidobactin A, which had been described to be one of the most powerful proteasome inhibitors, as well as a molecule that has been named cepafungin I in literature (Fig. 4.9a) [14–16]. NMR peak assignments of both molecules are listed in Table 4.1.

Although the inhibitors differ in only one methyl moiety, CepI has never been characterized with regard to its CP-modulatory activities. Both CepI and GlbA share the macrolactam cycle typical for syrbactin compounds, which carries the electrophilic Michael system required for the reaction with Thr-1O$^{\gamma}$. Adjacent to

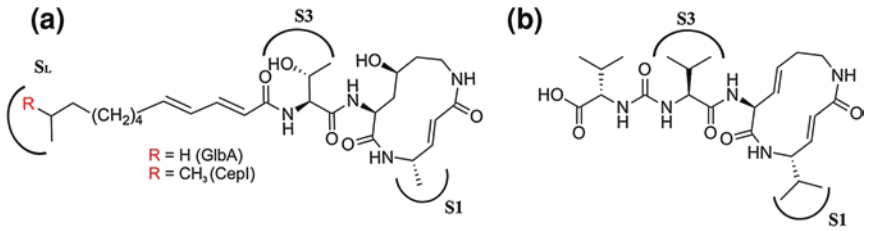


**Fig. 4.9** Structural comparison between the isolated molecules with SylA. **a** GlbA and CepI share the macrolactam cycle of syrbactin compounds containing an electrophilic Michael system. Bot molecules only differ in their fatty acid moiety, which carries a branched terminus in the case of CepI, whereas it is linear in GlbA. **b** In contrast to the molecules produced by *Photorhabdus*, SylA displays a highly hydrophilic carbonic acid tail, which is connected to the macrolactam moiety by a urea link. Eventually, its decoration pattern slightly differs, especially with regard to the moieties that interact with the S1 and S3 pockets. Figure adopted from Stein et al. [13]

this moiety, they carry a threonine residue, which links the macrolactam ring to a fatty acid chain that is strained by two conjugated double bonds. In fact, the inhibitors only differ in one methyl group situated at the far end of the fatty acid tail. Whereas this chain is linear in GlbA, it is terminally branched in CepI, thereby increasing the hydrophobic surface area. In contrast, the structure of SylA displays a highly hydrophilic carboxylic acid terminus (Fig. 4.9b). Moreover, it features a urea moiety that links the two valine residues head-to-head in its tail. Eventually, the decoration pattern of both the macrolactam cycle and the adjacent amino acid differs slightly, especially with regard to the crucial interactions with the proteasomal S1 and S3 binding pockets.

In conclusion, although the three molecules are produced by bacteria with very different habitae, their virulence relies on the same molecular lead structure, which, however, is fine-tuned to match the respective biochemical requirements. Interestingly, *Photorhabdus* has slightly shifted the product spectrum present in the *Burkholderiales* strain K481-B101 towards a more hydrophobic fatty acid tail, though still producing GlbA as well.

### *4.4.2 Reversibility Assays, Selectivity and $IC_{50}$ Measurements*

Aiming to investigate the inhibitory potential of the compounds, $IC_{50}$ measurements were performed for all proteasomal activities. As the purified inhibitors formed colourless solutions and therefore were not prone to produce any artefacts by quenching or autofluorescence, the experiments could be carried out by utilizing the standard fluorescence AMC substrates. For direct comparison with the new NMR technique, the residual ChTL activity was also evaluated with the labelled natural peptide substrate. Both assay variants resulted in almost

**Table 4.1** NMR spectroscopic data ($D_6$-DMSO) for CepI (a) and GlbA (b)

| | $\delta_H$, mult. [J (Hz)] | $\delta_C$ | Type | COSY | HMBC |
|---|---|---|---|---|---|
| 1a, 2a | 0.84, d, (3.25) | 23.03 | $CH_3$ | 3a | 1a, 2a, 3a, 4a |
| 3a | 1.50, m | 27.82 | CH | 1a, 2a, 4a | 1a, 2a, 4a 5a |
| 4a | 1.15, m | 38.86 | $CH_2$ | 3a, 5a | 1a, 2a, 3a, 5a, 6a |
| 1b | 0.86, t (7.0) | 14.46 | $CH_3$ | 3 | 3b, 4b |
| 3b | 1.26, m | 31.68 | $CH_2$ | 1b | 1b |
| 4b | 1.26, m | 26.21 | $CH_2$ | | |
| 5 | 1.26, m | 27.08 | $CH_2$ | 4a | |
| 6 | 1.26, m | 29.21 | $CH_2$ | | |
| 7 | 1.39, m | 28.81 | $CH_2$ | 8 | 5, 6, 8 |
| 8 | 2.13, m | 32.76 | $CH_2$ | 7, 9 | 7, 9, 10 |
| 9 | 6.11, m | 142.68 | CH | 8, 10 | 7, 8, 10, 11 |
| 10 | 6.19, m | 129.49 | CH | 9, 11 | 8, 9, 11 |
| 11 | 7.00, dd (15.0, 10.0) | 140.24 | CH | 10, 12 | 9, 10, 12, 13 |
| 12 | 6.13, m | 123.49 | CH | 11 | 11, 13 |
| 13 | – | 165.88 | C(O) | | 11, 12 |
| 14 | 7.91, d (9.0) | – | NH | 15 | 13, 15 |
| 15 | 4.29, m | 58.49 | CH | 14, 16 | 16, 17, 18 |
| 16 | 3.97, m | 67.18 | CH | 15, 17 | |
| 17 | 1.0, d (10) | 20.46 | $CH_3$ | 16 | 15, 16 |
| 18 | – | 169.86 | C(O) | | 15, 19 |
| 19 | 7.76, d (7.0) | – | NH | 20 | 18, 20, 21 |
| 20 | 4.34, m | 51.66 | CH | 19, 32 | |
| 21 | – | 171.44 | C(O) | | 19 |
| 22 | 8.69 | – | NH | | 23 |
| 23 | 4.37, m | 45.21 | CH | 22, 24, 25 | |
| 24 | 1.22, m | 19.05 | $CH_3$ | 23 | 23 |
| 25 | 6.41, d (15.0) | 143.56 | CH | 26 | |
| 26 | 6.19, m | 140.23 | CH | 25 | 26 |
| 27 | – | 168.09 | C(O) | | 25, 29 |
| 28 | 7.44, t (5.5) | – | NH | 29 | 26, 29, 30 |
| 29 | 3.02, m | 40.4 | $CH_2$ | 28, 30 | 27, 28, 30 |
| 30 | 1.45, m | 40.07 | $CH_2$ | 29, 31 | 29 |
| 31 | 3.58, m | 67.57 | CH | 30, 32 | 30 |
| 32 | 1.85, m | 42.93 | $CH_2$ | 31, 32, 20 | |
| | 1.58, d (11.5) | | | | |

The peak assignments refer to the atom numbering in Fig. 4.10
δ: Chemical shift in ppm
d: duplet
m: multiplet
t: triplet

identical $IC_{50}$ values, thereby again pronouncing the equivalency of the NMR- and the UV-VIS-based approach (Fig. 4.11a). Remarkably, the ChTL activity was inhibited with an $IC_{50}$ value of 4 nm, which was five times lower compared with GlbA (19 nm). This is especially noteworthy with regard to the high

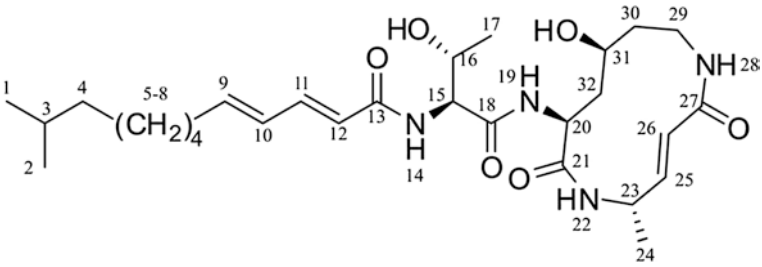


**Fig. 4.10** Structure of CepI with atom labeling

chemical similarity of both molecules. Analysis of the stoichiometry between CepI and proteasome molecules in the assay mixture reveals that a complete shut-down of the enzymatic activity occurs already at a ratio of 2:1, thereby reaching the detection limit of the assay due to the 2-fold symmetry of the proteasome particle [4].

The results gained for the ChTL activity were analogous for the TL activity, which was inhibited by CepI and GlbA to 24 and 193 nm, respectively (Fig. 4.11b). In contrast, the proteasomal CL was unaffected by both molecules up to concentrations of 100 μM. The inhibition pattern can be explained by the small hydrophobic P1 and P3 moieties of the inhibitors, which perfectly suit the binding channel formed on the interface of β5 and β6. Furthermore, as β2 has been shown to exhibit a wide range of acceptable substrates covering basic and small hydrophobic residues, the inhibitors are also able to bind to this active subunit. In contrast, β1 has a rather narrow substrate spectrum focused on acidic P1 residues and therefore rejects both GlbA and CepI.

The results gained for the ChTL and TL activities were surprising, because the only minor change of an additional methyl moiety distant to the actual coupling reaction to the active subunits influence the inhibition profile to that extent.

In order to reconfirm the binding mode of the inhibitors, gel shift experiments were performed with both compounds using the Pre2-$(His)_6$ mutant (Fig. 4.12). These verified their irreversible mechanisms by a clear increase of the mass of the β5 subunit to the approximate extent of the size of the inhibitors. Interestingly, no second band corresponding to the unbound subunit appeared at the range of the $IC_{50}$ value, thereby contrasting the findings of SylA (Fig. 4.4b).

The broad transition from the bound to the unbound state displayed by SylA reflects a different kinetic behaviour. Although the proteasomal binding sites are blocked by the inhibitor, thus preventing substrate turnover in catalytic measurements, SylA does not instantly undergo an irreversible reaction. In crystal structure analyses, however, the long reaction time allows for the complete coupling reaction to take place, hence yielding only the bound adduct.

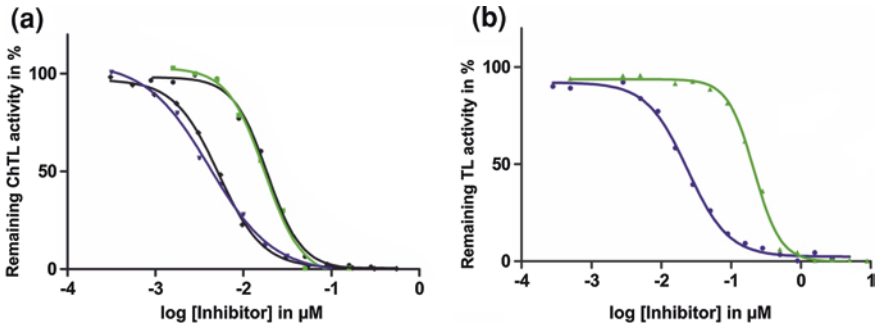


**Fig. 4.11** $IC_{50}$ curves of GlbA (*green*) /CepI (*blue*) with yeast CP. **a** Evaluation of the ChTL activity shows that CepI is far more potent than GlbA, sporting $IC_{50}$ values of 4 and 19 nm, respectively. Comparison between the data produced with fluorescence and NMR (*black*) assays underlines the equivalency of both techniques also with regard to sensitivity. Error bars are too small to be visible. **b** The inhibitory properties of both compounds can also be observed for the TL activity, despite their binding preference for the β5 subunit. The $IC_{50}$ value of CepI (22 nm) is even ten times decreased compared to GlbA (214 nm)

By contrast, even the small incubation time of few min previous to SDS gel analysis are sufficient for CepI and GlbA to form the stable ether bond to the β5 subunit, thereby again reflecting the optimization of the inhibitors.

### *4.4.3 Analysis of the Yeast 20S Proteasome: Ligand Complex Structures*

Aiming at elucidating the molecular background for the inhibitory properties of the compounds, crystal structure analyses of CepI and GlbA in complex with the yeast 20S proteasome were performed. CP crystals were grown as described previously and soaked with the inhibitors at final concentrations of 10 mM [17, 18]. Data for both CepI and GlbA were recorded to resolutions of 2.8 and 3.0 Å, respectively, by using synchrotron radiation at the SLS (Paul-Scherrer Institut, Villingen, Switzerland).

Molecular replacement was carried out by using the 20S yeast proteasome structure (1RYP) as a starting model for rigid body minimization, which was followed by translation-liberation-screw refinements under consideration of the 2-fold NCS symmetry. Ligands were built and minimized with the molecular modelling programme SYBYL and model building was achieved by cyclic density averaging in MAIN, which resulted in $R_{free}$ values of 24.3 % for the CepI and 22.7 % for the GlbA structure (Table 4.2).

Analysis of the electron densities clearly shows the covalent attachment of the macrolactam moiety to Thr-1$O^{\gamma}$ typical for syrbactin compounds, thus confirming

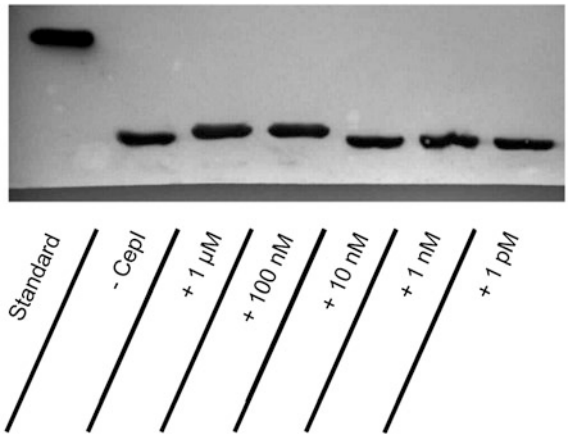


**Fig. 4.12** Reversibility experiment by western blot analysis of the β5 subunit using the Pre2-$(His)_6$ mutant. A clear increase of the molecular mass of the active subunit is visible down to nanomolar concentrations, thereby verifying the irreversible attachment of the inhibitor. In contrast to analogous experiments with SylA, no double band occurs at the transition between the completely bound and the uninhibited state, thereby hinting at enhanced kinetic properties compared to SylA

the results gained by the gel shift assays and the kinetic experiments (Fig. 4.13). Just as SylA, the inhibitors form an antiparallel β-sheet with the proteasomal subunits via their peptidic backbone. Interestingly, the compounds occupy the oxyanion hole formed by Gly-47 N by their intracyclic carbonyl moiety adjacent to the active Michael system. Structural comparison between the syrbactin compounds reveals that the P1 moiety of CepI /GlbA is diminished to a methyl moiety. Hereby, they are able to bind into the S1 pocket without dislocating Met-45 out of its original state, which, however, is necessary in the case of SylA to meet the spatial requirements of the i-propyl group.

Furthermore, both CepI and GlbA exhibit a threonine residue that links the macrolactam ring to their fatty acid chain via two peptide bonds. Thereby, they are able to undergo tight hydrogen bond interactions with Asp-114$O^{\gamma}$ both by their Thr-$O^{\gamma}$ and main chain carbonyl moieties. By contrast, SylA carries a hydrophobic valine residue in its P3 position and is only capable to exploit one hydrogen bond of Asp-114 with its urea moiety. Eventually, whereas SylA harbours a second valine residue in P4 and a free carboxylic acid terminus, GlbA and CepI possess a highly lipophilic unsaturated fatty acid chain (Fig. 4.14).

Due to the conjugated π-electron system formed by the peptide bond and the adjacent double bonds, the fatty acid tail adopts a linear arrangement that is stabilized and pre-oriented by van-der-Waals interactions with a forceps-like setup formed by Pro-115 and Val-116. Thus, the aliphatic termini of CepI and GlbA point directly towards a lipophilic patch in β6 adjacent to the catalytically active β5 subunit formed by Tyr-(-5), Pro-94 and Tyr-96. Due to the flexibility of the distal part of the fatty acid chains, they are able to perfectly bend and interact with this site that

**Table 4.2** Crystallographic data and refinement statistics

| Crystallographic data | CP: CepI[a] | CP: GlbA[a] |
|---|---|---|
| *Crystal parameters* | | |
| Space group | $P2_1$ | $P2_1$ |
| Cell constants (Å/°) | a = 135.7 | 134.8 |
| (dataset was collected from 1 crystal/1 CP per AU | b = 301.0 | 300.4 |
| | c = 144.8 | 144.5 |
| | β = 112.9 | 112.7 |
| *Data collection* | | |
| Beamline | X06SA, SLS | 1.0 |
| Wavelength, Å | 1.0 | 15–3.0 |
| Resolution range, Å[b] | 25–2.8 | 724,190 |
| No. observations | 837,332 | 209,581 |
| No. unique reflections[c] | 256,455 | 99.3 (99.7) |
| Completeness, %[b] | 97.8 (99.0) | |
| $R_{merge}$[b, d] | 7.7 (61.4) | 6,7 (47.2) |
| I/σ (I)[b] | 13.0 (2.4) | 15.2 (3.2) |
| *Refinement* | | |
| Resolution range, Å | 15–2.8 | 15–3.0 |
| No. reflections working set | 242,408 | 197,883 |
| No. reflections test set | 12,718 | 10,363 |
| No. nonhydrogen | 49,548 | 49,548 |
| No. of ligand atoms | 140 | 136 |
| Water | 1,320 | 1,290 |
| $R_{work}/R_{free}$ % | 21.3/24.3 | 19.8/22.7 |
| Rmsd bond (Å)/(°)[e] | 0.007/1.32 | 0.007/1.32 |
| Ramachandran plot, %[f] | 95.0/4.7/0.3 | 94.7/4.8/0.5 |

Despite the existing structural information of the CP:GlbA complex (PDB ID code 3BDM), we performed crystal structure analysis also with the isolated natural compound from *Photorhabdus* for direct comparison because the crystallization conditions were slightly modified

[a]Dataset has been collected on a single crystal

[b]Values in parentheses of resolution range, completeness, Rmerge, and I/σ (I) correspond to the last resolution shell

[c]Friedel pairs were treated as identical reflections

[d]Rmerge $(I) = \Sigma_{hkl}\Sigma_j |[I(hkl)_j - I(hkl)]|/\Sigma_{hkl} I_{hkl}$, where $I(hkl)_j$ is the measurement of the intensity of reflection hkl and < I(hkl) > is the average intensity

$R = \Sigma_{hkl}||F_{obs}| - |F_{calc}||/\Sigma_{hkl}|F_{obs}|$, where $R_{free}$ is calculated without a sigma cut off for a randomly chosen 5 % of reflections, which were not used for structure refinement, and $R_{work}$ is calculated for the remaining reflections

[e]Deviations from ideal bond lengths/angles

[f]Number of residues in favored region/allowed region/outlier region

resides at the end of a concave proteasomal setup (Fig. 4.13a). The increased hydrophobic surface area of the branched i-propyl side chain present in CepI enhances the interactions exploited by GlbA, thereby explaining the surprisingly differing in vitro inhibition properties of the chemically highly similar molecules (Fig. 4.13b).

Inspection of the other subunits reveals that CepI /GlbA only occupy the β2 subunit, whereas β1 is completely empty, thus confirming the results gained by the

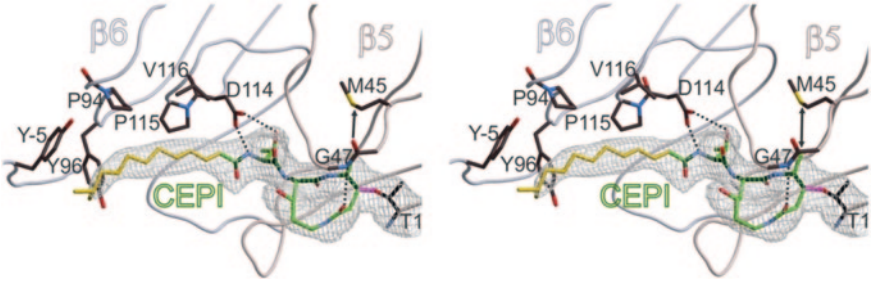


**Fig. 4.13** Stereo view of the $2F_O$-$F_C$ omit electron density map (*grey mesh*, 1σ) of CepI in complex with the proteasomal ChTL active site. Hydrogen bonds are indicated by *dashed lines*, whereas the arrow underlines the accurate fitting of the P1 methyl moiety into the binding pocket without displacing Met-45 out of its original state. CepI is able to occupy the oxyanion hole formed by Gly-47 N via its intracyclic peptide carbonyl moiety. Due to the rigidity of their fatty acid tails and the alignment by Asp-114, the termini of the inhibitors point towards a hydrophobic patch formed by the β6 subunit. The increased hydrophobic surface of CepI compared to GlbA enhances the van-der-Waals interactions with this groove and are thus responsible for the improved binding properties of CepI. Figure adopted from Stein et al. [4]

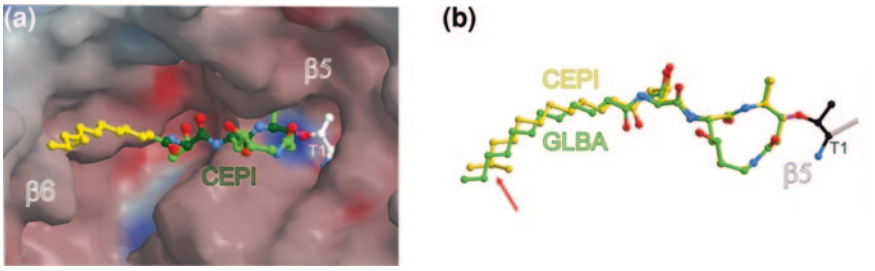


**Fig. 4.14** **a** Surface representation of CepI in the binding channel formed by β5 and β6. Surface colours indicate the positive (*red*) and negative (*blue*) electrostatic potential contoured from −30 kT/e to +30 kT/e. The aliphatic tail follows the curvature formed by β6 and tightly interacts with the hydrophobic patch at its distal end. **b** Superposition of GlbA and CepI derived from their respective complex crystal structures to the yeast CP. The structures perfectly match with the exception of the additional methyl moiety in CepI, which is indicated by a *red arrow*. Figure adopted from Stein et al. [4]

inhibition assays. Interestingly, the β1 binding channel does not contain an Asp-114 residue from the adjacent subunit and is thus not able to stabilize CepI and GlbA. In contrast, SylA binds to all proteasomal subunits as it does not benefit from the additional hydrophobic interactions at the distant pocket and in turn does not necessarily require the additional interaction with the Asp-Pro-Val (DPV) motive for binding.

As a conclusion, CepI displays the most sophisticated and in turn most powerful binding mechanism of all syrbactin inhibitors. However, despite originating from very different species, all compounds have conserved their macrolactam lead structures and only display altered decoration patterns, which arguably enhance binding to their respective host organisms.

### 4.4.4 Target Specific Adaptations of Syrbactins

Aiming to understand the different functionalization of the syrbactin compounds, the β5 and β6 subunit sequences of *Saccharomyces cerevisiae*, *Homo sapiens*, *Phaseolus vulgaris* (bean plant) and *Drosophila melanogaster* were aligned to allow a direct comparison of the interacting loops and residues within the proteasomal binding channel (Fig. 4.15). Although belonging to different biological kingdoms, both subunits are highly conserved between the species with regard to the catalytically active residues. Intriguingly, however, they differ exactly at the crucial positions that interact with the syrbactin inhibitors.

First, the S1 binding site in yeast, human and bean plants contains a Met-45 residue lining the bottom of the hydrophobic grove, which directly interacts with Ile-35 and confers a considerable degree of plasticity to the size of the binding pocket. Insects, however, display both an M45L as well as a I35 V exchange. Although the exact biochemical implications of the displacement of Met-45 are not yet fully understood, this variance is highly interesting with regard to the differently sized P1 residues of the corresponding inhibitors CepI and GlbA that consist of only a small methyl moiety. SylA with its i-propyl side chain on the other hand side is still able to affect the plant proteasome that contains the flexible Met-45 residue equally present in yeast and human. Therefore, the evolutionary adaptation of CepI /GlbA may originate from the lack of structural plasticity of the S1 pocket in insects host organisms.

Apart from the P1 side group, the second major difference between SylA and CepI /GlbA is the exchange of valine to threonine adjacent to the macrolactam scaffold, which is able to bind to the Asp-114 residue in a loop of the β6 subunit. Both the loop and Asp-114 are conserved in yeast, human and insects, thus enabling the hydrogen bonds and also the hydrophobic interactions between Pro-115, Val-116 and the fatty acid chain. By contrast, the loop is truncated in bean plants, thus possibly explaining the reduction of threonine to valine in SylA.

The hydrophobic patch formed by β6 is conserved in all target species. Therefore, the biochemical background for the carbonic acid tail of SylA remains elusive. Yet, a possible explanation might be that only the stabilization conferred by the DPV motive enables the alignment of the fatty acid chain in order to stretch out and reach the hydrophobic patch. Hence, the exchange of a highly hydrophobic tail in favour of a charged carbonic acid in SylA enhances the solubility of the compound whereas the inhibition properties against the plant proteasome arguably stay unaffected. By contrast, CepI and GlbA are perfectly suited to bind to the structurally similar human and yeast CP, as the inhibitors are able to engage in all major interactions present in their natural target particles.

Yet, as the human proteasome is endowed with a flexible S1 pocket, it remains an open and highly interesting question whether a human pathogen such as *B. pseudomallei* sports a methyl moiety in P1 or has conserved the i-propyl group in SylA due to the lack of evolutionary selection. As shown in the complex crystal

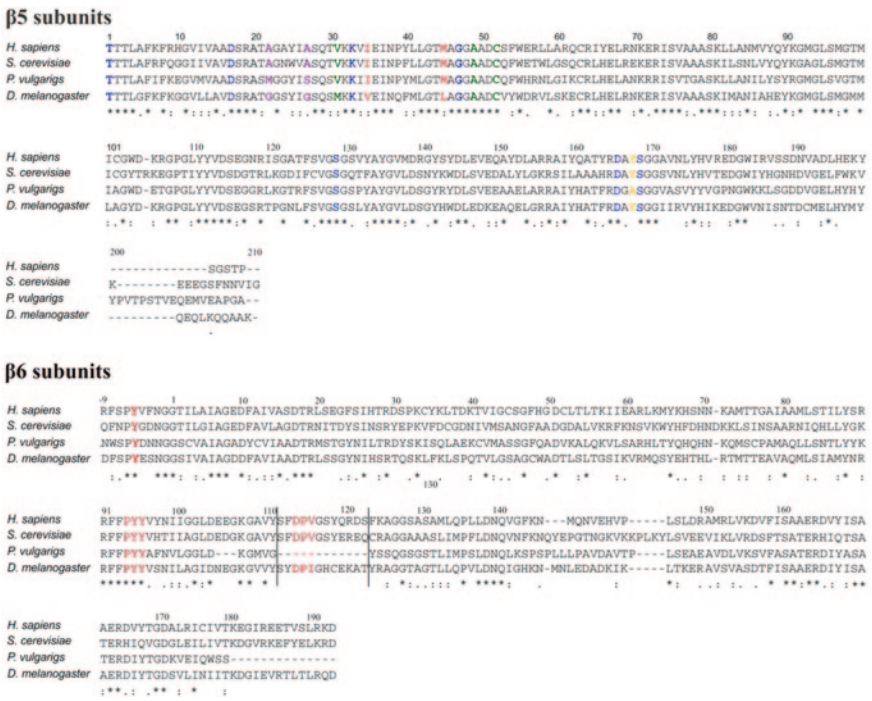


**Fig. 4.15** Sequence alignment of different syrbactin target organisms: *Homo sapiens*, *Saccharomyces cerevisiae* (baker's yeast), *Phaseolus vulgaris* (bean plant) and *Drosophila melanogaster* (fruit fly). Residues that are necessary for the proteolytic activity are coloured in *blue*, whereas amino acids that form the proteasomal binding pockets are displayed in *green* (S1), *violet* (S3) and *yellow* (S1'). Amino acids that are crucial for interaction with CepI /GlbA are shown in *red*. Interestingly, insects possess an alternative S1 pocket with an M45L and a I35 V exchange, thereby explaining the reduction of the P1 residue in CepI /GlbA. Although the lipophilic patch is conserved in all β6 subunits (Tyr-(-5), Pro-94 to Tyr-96), the loop region Ser-111 to Glu-123 (*black bars*) is deleted in bean plants, thus arguably preventing the stabilization and pre-orientation of the inhibitor towards this binding site. The amino acid numbering is according to the *Thermoplasma acidophilum* proteasome [19]

structure of the murine iCP and cCP with the immunoproteasome-specific inhibitor PR-957, both particles and consequently the related pathways can be selectively addressed by the spatial requirements of an altered P1 residue. This might also be exploitable by *Burkholderia* in order to directly and specifically affect the human secondary defence system by a down regulation of the MHC I presentation.

In order to chemically analyse the effect of the P1 side group exchange, a hybrid of SylA and GlbA was synthesized and evaluated with regard to its inhibitory strength towards the human CP (Fig. 4.16) [20].

Furthermore, crystallographic measurements of the inhibitors in complex with the yeast proteasome were performed to investigate the structural implications. Datasets were recorded at a final resolution of 2.8 Å and refined similarly

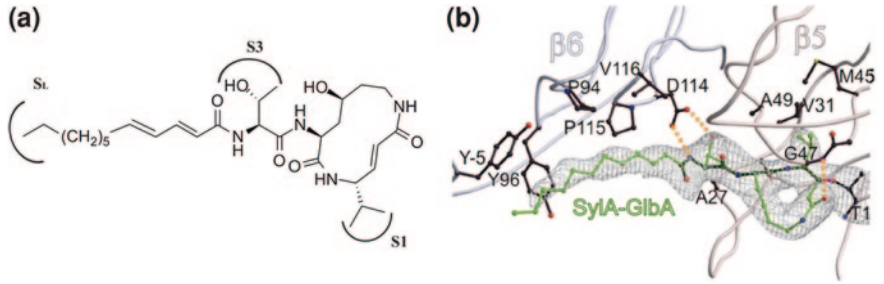


**Fig. 4.16** SylA-GlbA hybrid molecule. **a** The chimera of SylA and GlbA is mostly derived from GlbA, but carries an i-propyl moiety in P1. **b** Electron density map (1 σ) of the inhibitor in complex with the proteasomal β5 and β6 subunits. Hydrogen bonds are indicated by *dashed lines*. All interactions present in the structure of GlbA can also be observed in case of the chimera. Due to the higher spatial requirements of the i-propyl moiety, M45 is dislocated to enlarge the S1 pocket [21]

as described for the complex structure elucidation of the natural inhibitors to yield an $R_{free}$ value of 24.4 % (Table 4.3) [22]. The molecule is mainly based on GlbA, but carries the SylA P1 side group. In vitro evaluation of the compound had previously shown that the inhibitory potency of the SylA-GlbA chimera is slightly diminished compared to GlbA [20].

Crystal structure analysis reveals that the inhibitor binds to the β5 subunits analogous to GlbA and exploits all interactions present in the original inhibitor. However, the i-propyl moiety forces Met-45 out of its native state to extend the binding pocket in the yeast proteasome structure. Therefore, the energy required for this dislocation is directly responsible for the deteriorated $IC_{50}$ value of the compound.

As a conclusion, the three natural inhibitors reflect a directed evolution of the syrbactin inhibitors. Albeit perfectly suited for plant proteasomes, both the charged and highly polar carbonic acid tail as well as the unfavourable decoration pattern in SylA had to be optimized to enable binding to mammalian or insect proteasomes. By contrast, GlbA is able to exploit the distant lipophilic patch and displays enhanced interactions with the P1 and P3 binding pockets. The gradual optimization yielded CepI with increased binding affinities due to the enhanced hydrophobic interactions.

## 4.5 Cell Viability and Pathway Specific Protein Accumulation Assays

### *4.5.1 Cell Cytotoxicity Measurements*

In order to assess the in vivo effects of the inhibitors, their inhibition properties were evaluated in cell culture assays using HeLa tumor cells. Initially, their cytotoxicities were evaluated by standard Alamar blue assays (Fig. 4.17a). In short,

**Table 4.3** Crystallographic data and refinement statistics

| Crystallographic data | CP:SylA-GlbA[a] |
|---|---|
| *Crystal parameters* | |
| Space group | $P2_1$ |
| Cell constants (Å/°) | 134.9 |
| (dataset was collected from 1 crystal/1 CP per AU | 298.4 |
| | 145.3 |
| | 112.6 |
| *Data collection* | |
| Beamline | SLS, X06SA |
| Wavelength, Å | 1.0 |
| Resolution range, Å[b] | 15–2.8 |
| No. observations | 961, 261 |
| No. unique reflections[c] | 255, 488 |
| Completeness, %[b] | 97.7 (89.8) |
| $R_{merge}$[b, d] | 12.5 (61.2) |
| I/σ (I)[b] | 8.6 (2.0) |
| *Refinement* | |
| Resolution range, Å | 15–2.8 |
| No. reflections working set | 241,310 |
| No. reflections test set | 12,662 |
| No. nonhydrogen | 49,548 |
| No. of ligand atoms | 228 |
| Water | 1,333 |
| $R_{work}/R_{free}$ % | 21.3 /24.4 |
| Rmsd bond (Å)/(°)[e] | 0.007 /1.3 |
| Ramachandran plot, %[f] | 94.7/4.5/0.8 |

[a]Dataset has been collected on a single crystal

[b]Values in parentheses of resolution range, completeness, Rmerge, and I/σ (I) correspond to the last resolution shell

[c]Friedel pairs were treated as identical reflections

[d]Rmerge $(I) = \Sigma_{hkl}\Sigma_j |[I(hkl)_j - I(hkl)]|/\Sigma_{hkl} I_{hkl}$, where $I(hkl)_j$ is the measurement of the intensity of reflection hkl and $< I(hkl) >$ is the average intensity

$R = \Sigma_{hkl}||F_{obs}| - |F_{calc}||/\Sigma_{hkl}|F_{obs}|$, where $R_{free}$ is calculated without a sigma cut off for a randomly chosen 5 % of reflections, which were not used for structure refinement, and $R_{work}$ is calculated for the remaining reflections

[e]Deviations from ideal bond lengths/angles

[f]Number of residues in favored region/allowed region/outlier region

cells were seeded on a 24 well plate to final densities of 5000 cells per well and left to attach for 24 h. Subsequently, the medium was exchanged and the inhibitors were added at various concentrations. After another 48 h, the residual cell viability was assessed by adding Alamar blue reagent to the medium. Development of the assay was finished after approximately 2 h and the fluorescence could be recorded and standardized to a blank sample.

For comparison with a standard proteasome inhibitor, the highly potent peptide aldehyde MG132 was added as a control compound. Intriguingly, both syrbactin inhibitors display strongly increased cytotoxicity compared to the synthetic aldehyde.

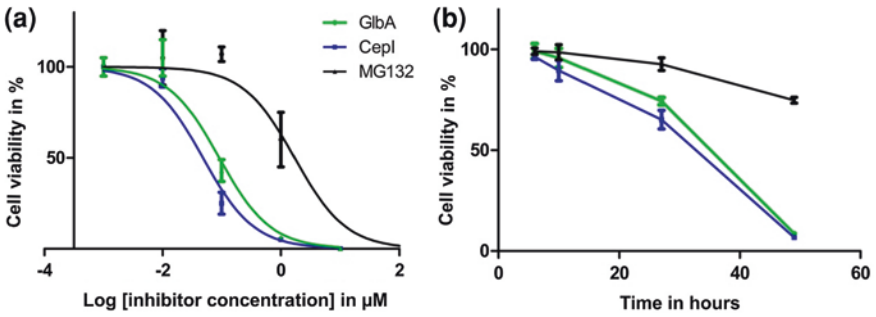


**Fig. 4.17** Cytotoxic properties of CepI and GlbA towards HeLa cancer cells in comparison with the standard aldehyde inhibitor MG132 (Z–Leu–Leu–Leu–al). **a** $LD_{50}$ curves were recorded after approximately 48 h, when the inhibitors reached their maximum cytotoxicity. Both natural compounds are far more potent than MG132 with CepI being even slightly stronger than GlbA. **b** The kinetic evaluation of the inhibitors was performed at final inhibitor concentrations of 1 µM. Whereas MG132 almost does not have any effect on lethality in accordance with the $LD_{50}$ measurements, the syrbactin inhibitors quantitatively kill the cells within 48 h. Again, CepI is slightly more efficient than GlbA, thus reflecting their in vitro characterization. Figure adapted from Stein et al. [4]

Although MG132 has been shown to inhibit a whole array of nucleophilic enzymes and inhibits the proteasomal ChTL activity in vitro with a nanomolar $IC_{50}$ value [23], it is not able to compete with the far less reactive but highly optimized natural products. Notably, the results gained in vitro can be confirmed by the cell culture measurements, as CepI is also slightly more effective in vivo than GlbA featuring $LD_{50}$ values of 48 and 90 nm, respectively.

For evaluation of the temporal dependence of cytotoxicity, HeLa cells were alternatively treated with 1 µM of all inhibitors and the residual cell titre was determined after various time intervals by Alamar blue assays (Fig. 4.17b). Hereby, the natural products achieved complete depletion of all cancer cells already after 48 h even at this low compound concentration. Compared to the synthetic aldehyde inhibitor MG132, the natural products exert their cytotoxic properties far quicker, with slight advantages for CepI over GlbA. Therefore, the rather unreactive Michael system in syrbactins is perfectly able to compete and even surpass the chemically reactive aldehyde compound. In consequence, the electrophilic moiety may not be the crucial determinant for biological activity, but can be outperformed by superior binding affinities of the whole molecule.

Both experiments nicely reflect the results gained by the in vitro measurements, thereby demonstrating that even a small change such as an additional methyl moiety results in altered in vivo properties. Furthermore, although it has been shown that inhibition of only the ChTL activity is sufficient to cause cell cytotoxicity, it is decisively enhanced if also a second subunit is affected [24]. As both CepI and GlbA effectively inhibit the ChTL and the TL activity, this explains their impressively enhanced effects against cancer cells.

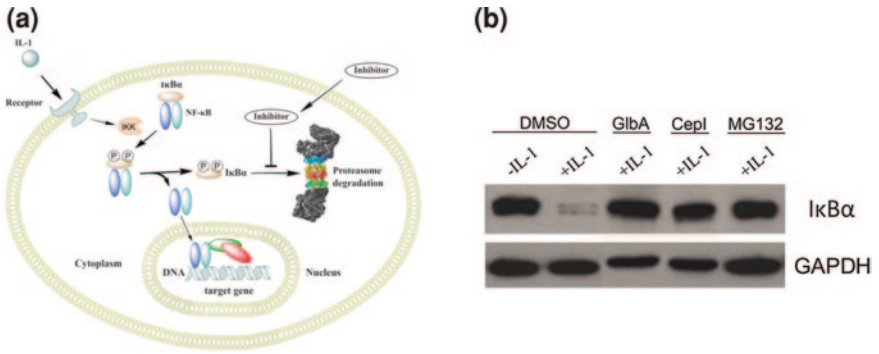


**Fig. 4.18** Intracellular accumulation assay. **a** The NF-κB signalling cascade is triggered by extracellular signals such as IL-1 and leads to the proteasomal degradation of IκBα, which inactively sequesters NF-κB in the cytosol of quiescent cells [25]. **b** Western blot analysis of IκBα accumulation upon treatment with 40 μM of the inhibitors followed by IL-1 stimulation. Both the standard inhibitor MG132 and the natural products successfully prevent IκBα degradation in the cytosol, thus demonstrating their cell permeability as well as the intracellular proteasome inhibition. Figure adapted from Stein et al. [13]

### *4.5.2 Pathway Selective Accumulation Assay*

For assessment of the intracellular CP inhibition, the accumulation of the natural proteasomal substrate protein IκB upon treatment of the cells with the proteasome inhibitors was monitored. In quiescent cells, the inflammatory transcription factor NF-κB is inactively sequestered in the cytosol by binding to the inhibitory protein complex IκB (Fig. 4.18a). Upon recognition of extracellular signalling factors such as TFNα, IL-1 or bacterial lipopolysaccharides by various receptors, IκB is phosphorylated by the activated IκB kinase.

Subsequently, IκB is ubiquitinated and subjected to proteasomal degradation, thereby ceasing the inhibition of NF-κB. The latter is then translocated into the nucleus to start transcription of a whole array of genes that are linked to immune response and cancer development.

In order to evaluate the affection of this pathway, cells were treated with a surplus of 40 μM of the inhibitors for 6 h, followed by stimulation with IL-1 for further 20 min. Quantification was achieved by western blot analysis towards IκBα and the protein concentration was standardized by co-staining of the housekeeper protein GAPDH (Fig. 4.18b). Again, MG132 was introduced as standard proteasome inhibitor. Both the natural syrbactin compounds and the artificial MG132 inhibitor prevented the degradation of IκBα, thereby demonstrating their cell permeability and intracellular CP inhibition. Since the blockbuster drug bortezomib also received its primary admission by the FDA for the inhibition of the NF-κB signalling cascade, this experiments underlines the high pharmaceutical potential of GlbA and CepI and the applicability of the class of syrbactin compounds with regard to inflammatory and cancerous diseases in general.

## References


1. T.P. Dick, A.K. Nussbaum, M. Deeg, W. Heinemeyer, M. Groll, M. Schirle, W. Keilholz, S. Stevanović, D.H. Wolf, R. Huber, H.G. Rammensee, H. Schild, J. Biol. Chem. **273**, 25637–25646 (1998)
2. M. Gaczynska, K.L. Rock, T. Spies, A.L. Goldberg, Proc. Natl. Acad. Sci. USA **91**, 9213–9217 (1994)
3. W. Heinemeyer, J.A. Kleinschmidt, J. Saidowsky, C. Escher, D.H. Wolf, EMBO J. **10**, 555–562 (1991)
4. M.L. Stein, P. Beck, M. Kaiser, R. Dudler, C.F. Becker, M. Groll, Proc. Natl. Acad. Sci. USA **109**, 18367–18371 (2012)
5. T. Nazif, M. Bogyo, Proc. Natl. Acad. Sci. USA **98**, 2967–2972 (2001)
6. M. Groll, O. Larionov, R. Huber, A. de Meijere, Proc. Natl. Acad. Sci. USA **103**, 4576–4579 (2006)
7. U. Waspi, D. Blanc, T. Winkler, P. Ruedi, R. Dudler, Mol. Plant-Microbe Interact. **11**, 727–733 (1998)
8. U. Waspi, P. Schweizer, R. Dudler, Plant Cell **58**, 167–174 (1985)
9. D.C. Gross, J. Appl. Bacteriol. **58**, 167–174 (1985)
10. J. Crawford, R. Kontnik, J. Clardy, Curr. Biol. **20**, 69–74 (2010)
11. N.R. Waterfield, T. Ciche, D. Clarke, Annu. Rev. Microbiol. **63**, 557–574 (2009)
12. D.J. Clarke, Cell. Microbiol. **10**, 2159–2167 (2008)
13. M.L. Stein, P. Beck, M. Kaiser, R. Dudler, C.F. Becker, M. Groll, Proc. Natl. Acad. Sci. USA **109**, 18367–18371 (2012)
14. M. Oka, Y. Nishiyama, S. Ohta, H. Kamei, M. Konishi, T. Miyaki, T. Oki, H. Kawaguchi, J. Antibiot. (Tokyo) **41**, 1331–1337 (1988)
15. J. Shoji, H. Hinoo, T. Kato, T. Hattori, K. Hirooka, K. Tawara, O. Shiratori, Y. Terui, J. Antibiot. (Tokyo) **452**, 755–758 (2008)
16. M. Groll, B. Schellenberg, A.S. Bachmann, C.R. Archer, R. Huber, T.K. Powell, S. Lindow, M. Kaiser, R. Dudler, Nature **452**, 755–758 (2008)
17. M. Groll, L. Ditzel, J. Löwe, D. Stock, M. Bochtler, H. Bartunik, R. Huber, Nature **386**, 463–471 (1997)
18. M. Groll, R. Huber, Methods Enzymol. **398**, 329–336 (2005)
19. J. Löwe, D. Stock, B. Jap, P. Zwickl, W. Baumeister, R. Huber, Science **268**, 533–539 (1995)
20. J. Clerc, N. Li, D. Krahn, M. Groll, A.S. Bachmann, B.I. Florea, H.S. Overkleeft, M. Kaiser, Chem. Commun. (Camb.) **47**, 385–387 (2011)
21. C.R. Archer, D.L. Koomoa, E.M. Mitsunaga, J. Clerc, M. Shimizu, M. Kaiser, B. Schellenberg, R. Dudler, A.S. Bachmann, Biochem. Pharmacol. **80**, 170–178 (2010)
22. C.R. Archer, M. Groll, M.L. Stein, B. Schellenberg, J. Clerc, M. Kaiser, T.P. Kondratyuk, J.M. Pezzuto, R. Dudler, A.S. Bachmann, Biochemistry **51**, 6880–6888 (2012)
23. D.H. Lee, A.L. Goldberg, Trends Cell Biol. **8**, 397–403 (1998)
24. M. Screen, M. Britton, S.L. Downey, M. Verdoes, M.J. Voges, A.E. Blom, P.P. Geurink, M.D. Risseeuw, B.I. Florea, W.A. van der Linden, A.A. Pletnev, H.S. Overkleeft, A.F. Kisselev, J. Biol. Chem. **285**, 40125–40134 (2010)
25. P.A. Baeuerle, T. Henkel, Annu. Rev. Immunol. **12**, 141–179 (1994)

# Chapter 5
# Discussion

## 5.1 Development of a Tool for the Identification of CP Inhibitors from Natural Sources

The present thesis has led to the establishment of a new tool for the detection of proteasome inhibitors in highly heterogeneous matrices. Due to the NMR-based nature of the assay, it is not prone to common artefacts caused by quenching or autofluorescence that are responsible for the plenitude of false positive and equally negative results in high-throughput screenings conducted with UV-VIS assays. Contrary to artificial probe molecules, the assay relies on a natural proteasomal substrate peptide, whose sequence was adapted to generate both high enzyme affinity as well as subunit specificity. Despite the insensitivity of NMR in general, the assay requires only very limited amounts of the peptide, which can be easily prepared by standard solid phase chemistry. Furthermore, comparison with routine fluorescence assays confirms its equivalence to common techniques for the analysis of isolated compounds. Due to the strong affinity of the peptide to the proteasomal β5 subunit, the catalytic turnover is extremely high even in correlation to the optimized fluorescent substrates. Therefore, only a small amount of proteasome is necessary, which in turn is responsible for the low response limits that are crucial for the detection of trace amounts of toxins.

By the atom-selective $^{13}$C-isotope labelling of the peptide, the novel methodology features a high signal-to-noise ratio even in crude mixtures. Furthermore, its robust character, high sensitivity and unambiguous readout qualify the technique for the detection of natural product inhibitors already during the fermentation process as well as in raw extracts and secretions. Once the presence of an inhibitor is confirmed, its subsequent isolation and characterization is a straightforward process as demonstrated by the purification of CepI and GlbA from cultures of *Photorhabdus luminescens*.

Therefore, the developed methodology represents a valuable tool to extend the range of natural product discovery to the vast pool of hitherto undiscovered compounds whose biosynthesis is silenced under common fermentation techniques.

M. L. Stein, *NMR-Bioassay Guided Isolation of the Natural 20S Proteasome Inhibitors from Photorhabdus Luminescens*, Springer Theses, DOI: 10.1007/978-3-319-07914-1_5,
© Springer International Publishing Switzerland 2014

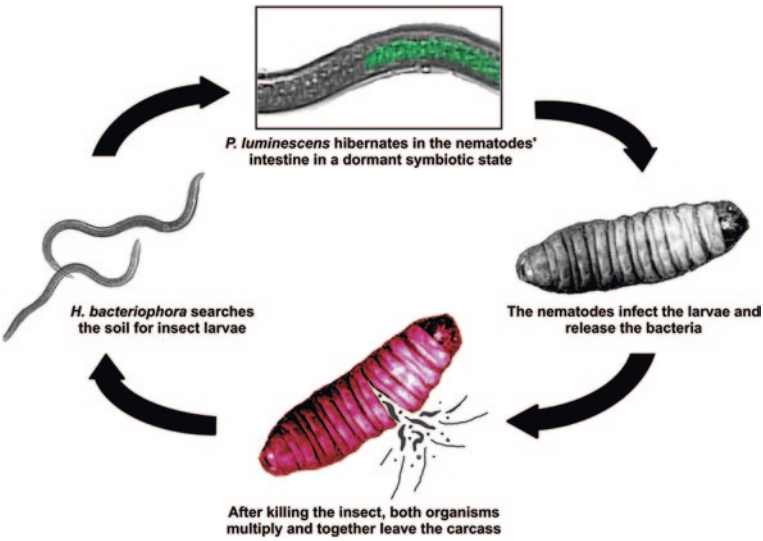


**Fig. 5.1** The bipolar life-cycle of *P. luminescens* is separated into a symbiotic phase during which the bacterium inactively abides in the intestine of a nematode (*H. bacteriophora*) and a pathogenic phase in the insect larva where it secretes toxic compounds as well as colourful pigments to deter other scavenging organisms. After killing the insect and multiplying in its carcass, the nematodes again swallows the bacteria and both leave the insect body to search for more prey

Hereby, it can be utilized for the screening of different cultivation approaches to eventually unveil the molecular triggers that are able to stimulate the crucial transition to the relevant life stage of the organism. This was exemplified by the identification of an osmotic shock in the case of *P. luminescens* that initiates the virulent phase in the life-cycle of the insect pathogenic bacterium.

As shown by the extensive screening of growth conditions, only a very defined molecular trigger is suitable to mimic the natural environmental changes during the life-cycle of the bacterium and lead to its transition to the virulent phase. This again pronounces the significance of the new methodology, as the extraction of commonly grown cultures would have been without any chances of success. Notably, the growth conditions that are suitable to initiate the secretion of SylA from *P. syringae* or GlbA from cultures of *Burkholderiales* strain K481-B101 were not able to induce inhibitor biosynthesis in *Photorhabdus*. Thus, the three organisms have adapted their sensory system towards their respective host organisms, whereas they have conserved the lead motive and inhibition mechanisms of their virulence eliciting small molecules.

Interestingly, *Photorhabdus* displays a highly complicated biphasic life-cycle, which, is typical for many pathogenic microorganisms (Fig. 5.1).

In its stationary phase, it populates the intestine of the nematode *Heterorhabditis bacteriophora,* which is closely related to the model organisms *C. elegans*. The worm searches the soil for insect larvae and, once detected, penetrates into the body

of its prey, where it regurgitates the symbiotic bacteria [1, 2]. Whereas *Photorhabdus* is rather inactive in its hibernating symbiotic stage, it immediately starts with the biosynthesis and secretion of antibiotic agents as well as toxins after the release into the insect lumen, thereby killing it in a concerted action with the nematodes [3–5]. Both organisms then feed on its tissue and multiply within its carcass [6].

Apparently an osmotic shock sufficiently simulates the environmental shift from the nematode intestine to the insect body to initiate the pathogenic phase in *Photorhabdus*. In order to then deter other scavenging organisms from the dead larvae, the bacteria start to produce a whole array of intensely colourful pigments [3, 7]. After the complete consumption of the insect tissue, the nematodes finally reabsorb the bacteria and both organisms eventually leave the insect to search for new prey. This biphasic life-cycle, which consists of a symbiotic and an aggressive pathogenic phase, can also be observed in vitro cultures, but especially the production of coloured secretions has thwarted previous attempts to isolate the syrbactin compounds that were expected from comparative genetic analyses.

Due to the high potency of the inhibitors, their secretion is strictly controlled in order to selectively address the insect host while leaving the symbiotic nematodes unharmed. In conclusion, due to the strict biosynthetic regulation of inhibitor production, the elucidation of the osmotic shock stimulus was only feasible by the new NMR technique. The straightforward detection of both inhibitors and a suitable fermentation strategy demonstrates that the developed assay holds a great potential for the analysis of other organisms and also in high-throughput screenings. With regard to the versatility of already identified natural CP inhibitors as well as to the biological conservation of the UPS in general, it is likely that the novel tool will identify a plethora of other interesting lead structures with novel binding mechanisms. Due to the easy adaptability of the assay also to other proteases and more remote enzymes, it can also be applied for the target directed search of other secondary metabolites. Therefore, its establishment is going to have an impact on natural product discovery also in other fields of research.

## 5.2 Isolation and Characterization of CepI and GlbA

Besides the establishment of the novel technique, the purification, structure elucidation and biochemical characterization of the elicitor molecules from *Photorhabdus* could be accomplished. Hereby, the NMR-based methodology again proved to be a valuable tool for the assay-guided optimization of the isolation process, as the inhibitors are only produced in trace amounts that can even hardly be detected by mass spectrometry after the penultimate purification step. The NMR structure elucidation surprisingly showed that both molecules differ only in their fatty acid tail distant from the electrophilic warheads, which bind to the proteasomal active sites.

Unexpectedly, however, this minor modification proved to efficiently influence the inhibition properties of the compounds. Although GlbA has been listed as one

of the most potent proteasome inhibitory compounds described to date with and $IC_{50}$ value ranging in the low nanomolar region, the closely related homologue CepI turned out to be even four to five times more effective. Structure elucidation of both compounds with the yeast CP led to the identification of a hydrophobic patch formed by the catalytically inactive subunits adjacent to the proteasomal active sites. This finding once again pronounces the unpredictability of complex biological systems. Despite the available structural data, it is hardly imaginable that a computational approach could have predicted the extent of the effect or even identified the additional binding motive.

Furthermore, although *P. luminescens* is genetically sequenced and even the gene clusters responsible for the synthesis of the inhibitors are assigned, it is still not possible to reliably predict the small molecule produced by the huge and complex non-ribosomal peptide synthetases and fatty acid synthase clusters. Yet, the results gained by the comparative analysis of the syrbactins also emphasizes that even though the lead structure is conserved between the species, the decoration pattern has a major influence on the binding properties of the molecule and is obviously optimized for the target enzyme. Despite the similarity of the respective gene clusters, it is therefore of crucial importance for natural product research to eventually isolate and characterize the respective secondary metabolites by conventional chemical and biochemical methods. As a consequence, the isolation of the small molecule toxins from the human pathogen *Burkholderia pseudomallei*, as well as the elucidation of the molecular trigger for its secretion would be a necessary and substantial leap forward for the understanding of the biological involvement of the compound in virulence and may even yield a molecule that has been further optimized for the human proteasome particles.

Although CepI could be shown to be the most effective CP inhibitor, it has essentially been fine-tuned for the insect CP in terms of subunit selectivity and interactions with the binding channel. Especially alterations in the P1 site, however, are likely to influence the specificities towards the distinct human cCP, iCP as well as tCP and therefore convey differing biological implications. Notably, *Photorhabdus* has been shown to produce CepI and GlbA to the same quantity, whereas the other syrbactin producing organisms only secrete one compound. This ambivalence again demonstrates the slight adaptational shifts in the decoration pattern, but may also explain the flexibility and broad spectrum of host organisms of the genus *Photorhabdus*.

However, after the successful characterization of SylA, the isolated compounds are among the first proteasome inhibitors to which a biological function could be assigned. Importantly, they are also the first examples of CP inhibitors, which are not only applied to debilitate the host organism but also to foster the next generation of symbionts. Furthermore, the conservation of the lead structure over the species barrier, ranging from plants over nematodes to men, emphasizes the universal applicability of this group of natural products also in terms of pharmaceutical applications.

After the in vitro characterization of the compounds, the inhibition properties of CepI and GlbA could also be observed in cell culture experiments. Both

substances displayed extreme cytotoxicity against cancerous cells even in comparison with established standard proteasome inhibitors. Intriguingly, the pathway-specific inhibition of the NF-κB signalling cascade could be confirmed. As this is also the primary reason for the admission of the first FDA-approved proteasome inhibitor bortezomib, this thesis will further promote the pharmaceutical implementation of the hitherto unexploited group of the syrbactins. Furthermore, the elucidation of the new binding motive will contribute to the rational design of novel synthetic compounds. After the successful introduction of the natural product derivatives of the epoxyketones for the next generation of medically applied CP inhibitors and immunoproteasome modulating agents, the highly promising syrbactins are likely to join the group of medically utilized agents and may contribute to expand the range of proteasome inhibitors to other diseases as well.

## References

1. J. Crawford, R. Kontnik, J. Clardy, Curr. Biol. **20**, 69–74 (2010)
2. D.J. Clarke, Cell. Microbiol. **10**, 2159–2167 (2008)
3. A.O. Brachmann, F. Kirchner, C. Kegler, S.C. Kinski, I. Schmitt, H.B. Bode, J. Biotechnol. **157**, 96–99 (2012)
4. S.A. Joyce, L. Lango, D.J. Clarke, Adv. Appl. Microbiol. **76**, 1–25 (2011)
5. C.M. Theodore, J.B. King, J. You, R.H. Cichewicz, J. Nat. Prod. **75**, 2007–2011 (2012)
6. N.R. Waterfield, T. Ciche, D. Clarke, Annu. Rev. Microbiol. **63**, 557–574 (2009)
7. H. Goodrich-Blair, D.J. Clarke, Mol. Microbiol. **64**, 260–268 (2007)